



# UNIVERSITÀ DI TRENTO

Master's Degree in  
Quantitative and Computational Biology

## COMPUTATIONAL MODELLING AND SIMULATION OF THE HONEYBEE ANTENNAL LOBE TO REVEAL NEURAL CORRELATES OF SLEEP

Supervisor:  
Albrecht Haase

Graduant:  
Giacomo Fantoni

Department of Cellular, Computational and Integrative Biology - CIBIO  
Università degli studi di Trento

Academic year: 2022/2023  
Discussion date: 18/11/2023



# Contents

<b>Abstract</b>	<b>3</b>
<b>1 Introduction</b>	<b>5</b>
1.1 Sleep . . . . .	5
1.1.1 Common features of sleep across organisms . . . . .	5
1.1.2 Sleep in humans . . . . .	5
1.1.3 The honey bee as a model for sleep . . . . .	6
1.2 The olfactory system of the bee . . . . .	7
1.2.1 Neuroanatomy . . . . .	7
1.2.2 Odor reception . . . . .	7
1.2.3 Antennal lobe . . . . .	8
1.3 Modelling neuronal circuitry . . . . .	9
1.3.1 Functional representation of a biological neuron . . . . .	10
1.3.2 Modelling neurons - the leaky integrate and fire model . . . . .	11
1.3.3 Interacting neurons - spiking neural networks . . . . .	13
1.4 Code availability . . . . .	14
<b>2 Objectives</b>	<b>15</b>
2.1 Revealing neural correlates of sleep in the olfactory system of the honey bee . . . . .	15
2.2 Developing a computational model of the antennal lobe . . . . .	15
<b>3 Materials and methods</b>	<b>17</b>
3.1 The model . . . . .	17
3.1.1 Architecture . . . . .	17
3.1.2 Olfactory receptors . . . . .	17
3.1.3 Neurons . . . . .	21
3.1.4 Synapses . . . . .	22
3.2 Data analysis . . . . .	24
3.2.1 Extracting data from a simulation . . . . .	24

---

3.2.2	Neuron's activity . . . . .	24
3.2.3	Spike density matrix . . . . .	24
3.2.4	Correlation matrices . . . . .	25
3.2.5	Feature extraction . . . . .	25
<b>4</b>	<b>Results</b>	<b>29</b>
4.1	Behavior of the components . . . . .	29
4.1.1	Olfactory receptors . . . . .	29
4.1.2	Neurons . . . . .	31
4.1.3	Synapses . . . . .	36
4.2	Response to odours . . . . .	39
4.3	Awake state . . . . .	40
4.3.1	Adding the Poisson trains . . . . .	40
4.4	Asleep state . . . . .	45
4.5	Comparison between awake and asleep states . . . . .	47
<b>5</b>	<b>Discussion</b>	<b>61</b>
5.1	Deep learning in neuroscience . . . . .	61
5.1.1	Spiking neural networks . . . . .	61
5.1.2	Spiking neural networks in neuroscience . . . . .	62
5.2	The honey bee as a model for human sleep . . . . .	62
5.2.1	Sleep in the antennal lobe . . . . .	63
5.3	Neuronal correlates of sleep . . . . .	63
5.3.1	Features of the system . . . . .	64
5.4	Putative biological mechanisms . . . . .	66
5.4.1	Reduction of inhibitory synapses' strength . . . . .	66
5.4.2	Introduction of a correlated input . . . . .	66
<b>6</b>	<b>Conclusions and future perspectives</b>	<b>69</b>
6.1	Conclusions . . . . .	69
6.2	Future perspectives . . . . .	69
<b>7</b>	<b>Bibliography</b>	



# Abstract

Sleep is a naturally recurring, reversible state of reduced consciousness and sensory perception characterized by altered brain wave patterns and distinctive physiological and behavioural changes. It is a vital physiological process for cognitive functioning, emotional regulation and overall health in many organisms. Despite its importance, the function of sleep needs further investigation. Invertebrates such as the honey bee (*Apis mellifera*) have recently seen a surge in interest as a model organism for sleep research. Despite the absence of a typical mammalian EEG signal in insects, the honey bee has been shown to exhibit sleep-like behaviour with the presence of a specific body posture, an increased threshold to arousing stimulation and the presence of a rebound in the sleep-like state that occurs as a consequence of sleep deprivation. The honey bee and other insects offer several advantages as models: their nervous system is relatively simple, they are easy to maintain, have a short life cycle and are equipped with a genetic toolbox [5].

The work presented in this thesis focuses on the dynamics of the antennal lobe, a part of the olfactory system of the honey bee which will be modeled as a recurrent spiking neural network to reveal what happens in this brain region during sleep. The antennal lobe of the honey bee is composed of three populations of neurons: the olfactory receptor neurons (ORN), the input of the system, the projection neurons (PN), which communicate with higher-order brain regions and the local neurons (LN), which inhibit the activity of the PNs [42]. As previous experimental results showed, there is no significant difference in the firing rate of the PNs between the sleep-like state and the awake state. However, changes can be seen at a network level [24]. This seems to support that the connectivity of the antennal lobe changes during sleep, increasing the correlation between glomeruli, the functional units of the antennal lobe responsible for processing odour information.

Recent advances in the field of computational neuroscience have allowed the development of biologically realistic models of the brain [9]. The antennal lobe is modeled using a spiking neural network [34] with noisy leaky integrate and fire neurons [12] and conductance-based synapses, expanding on a previous work which explored with success the odour response of the system [48]. The computational system is built such that it replicates the biological behaviour, avoiding some limitations of experimental methods, allowing to record neuronal activity at a higher frequency and to observe the dynamics of the whole antennal lobe.

The major change in the network's activity during sleep is an increase of correlation in the activity of projection neurons of different glomeruli with respect to the awake state [24]. The flexibility of the computational model has allowed to explore what could be the cause of this increase in correlation. In particular, I propose that this increase in correlation is due to a combination of two factors. Firstly there is a reduction in the synaptic strength of the inhibitory synapses both between local neurons and between local and projection neurons. This decrease decouples the system and causes the activity of the projection neurons to be less dependent on the activity of the local neurons, increasing their correlation. This decrease in inhibition is consistent with other studies: GABAergic synapses are known to be involved in the regulation of sleep and their strength to be reduced during this state [60]. Moreover, it appears that during sleep a correlated input is fed to the antennal lobe. This input is not present during the awake state and could be analogous to the slow wave synchronization observed in the mammalian brain during sleep [23]

In conclusion, this thesis takes advantage of new computational techniques to propose a mechanism that regulates the change of activity in the antennal lobe of the honey bee during sleep.



# **Chapter 1**

## **Introduction**

### **1.1 Sleep**

Sleep is a naturally recurring, reversible physiological state of reduced consciousness, sensory perception, and voluntary motor activity characterized by altered brain wave patterns, diminished responsiveness to external stimuli and distinctive physiological and behavioral changes [16]. It is crucial for cognitive functioning, emotional well-being and overall health in humans and many other organisms. There is an extensive overlap between sleep mechanisms and the neurophysiology of learning and memory processes, which provides a strong rationale for theories supporting a functional link between sleep and learning systems [44].

#### **1.1.1 Common features of sleep across organisms**

Sleep can be considered as a vulnerable state that is incompatible with behaviors that nourish and propagate species. Because of this sleep must fulfill some universal vital function [50]. It can be considered as a state that increases the efficiency of behavior by regulating its timing and by reducing energy use. It reduces activity and body and brain metabolism while allowing a high level of responsiveness to external stimuli with respect to hibernation or torpor. For example, the human brain can continuously process sensory signals and trigger complete awakening to significant stimuli within a few milliseconds.

#### **1.1.2 Sleep in humans**

In humans and other mammals, sleep is characterized by a reduction of voluntary motor activity and decreased responsiveness to external stimuli and is composed of two alternating phases: rapid eye movement (REM) sleep and non-REM (NREM) sleep [26]. REM sleep is characterized by Ponto-genicul-o-occipital PGO waves, theta synchrony, increased acetylcholine, reduced levels of monoamines and increased transcription of plasticity-related genes, which together contribute to freely occurring bidirectional plasticity long-term potentiation LTP and depotentiation in the hippocampal complex. During NREM sleep this is extended to the neocortex, where orderly neuronal reactivation events in phase with slow wave delta activity facilitate the events that convert early LTP to long-lasting LTP.

##### **1.1.2.1 REM sleep**

REM sleep is necessary for strong, lasting improvements and its effects on memory consolidation are circuit-specific [3]. Synaptic gains are specific to circuits involved in a learning task and do not transfer to other

## 1.1. SLEEP

---

processing fields. Moreover, spontaneous increases in REM sleep follow training and precede large increases in performance during learning. However, it is not the total REM sleep time that is fundamental for learning, but rather its relative augmentation after a task is performed that allows for better learning.

A characteristic signature of REM sleep is PGO waves, which are generated in the pons and travel to the lateral geniculate nucleus and the occipital cortex. They increase in density during intensive learning, and their density is correlated with task retention. They are hypothesized to be a potent regulator of synaptic plasticity in the hippocampus and amygdala, and they are comprised of large, synchronous excitatory waves of glutamate that terminate directly on forebrain targets.

The hippocampus is fundamental for the formation of new memories, in fact, memory consolidation is the transfer of hippocampal plasticity to long-term storage sites in the neocortex. Long-term potentiation is easily induced during sleep in this area, facilitating task retention.

Active neurons during waking are reactivated during sleep with an increased firing rate with respect to ones that were not activated. These neurons have an increased co-activation during hippocampal large irregular activity LIA which occurs during NREM and a structured replay of the waking running sequences during REM sleep. This happens in a theta-specific pattern concordant with the induction of LTP and its reversal during the REM sleep state. Place cells in the hippocampus fire dependent on the electroencephalographic (EEG) theta rhythm during active waking. This suggests that LTP could be induced with physiologically feasible stimuli if timed to the naturally occurring theta activity.

### 1.1.2.2 NREM sleep

NREM sleep is characterized by a slow wave activity (SWA) in the electroencephalogram [13]. Learning during waking amplifies slow waves which allow for a reactivation of neurons that were involved in learning or encoding during theta states on accelerated and condensed time scales. This increase in slow waves is associated with increased waking task requirements demanded from the same area neocortex. The function of these reactivations is memory consolidation: it strengthens memory circuits, facilitating LTP in the hippocampus and neocortex. The fact that slow wave-dependent processing affects synaptic weights is subject to further study, but the best evidence of this effect is a rise in the amplitude of slow waves after extended waking experience that becomes attenuated again after a period of slow wave activity ensues and the decline in evoked potentials across sleep. These results support the role of slow wave processing in reducing the strength of synapses. The work presented here will try to build a model to explain how this reduction in synaptic strength and slow wave activity can be used to explain changes in the activity patterns of neurons in the olfactory system of the honey bee during sleep.

### 1.1.3 The honey bee as a model for sleep

Insects are emerging as a model for sleep research: they have a simple nervous system, they are easy to manipulate, they have a short life cycle and they are equipped with a genetic toolbox [5]. Sleep seems to be of fundamental importance also for insects: in the honey bee sleep deprivation at night impairs the precision of waggle dance signaling [32] and the probability of successfully returning to the hive the following day [7]. In the honey bee no typical mammalian EEG signal is present, so the identification of sleep-like states in insects is based on behavioral criteria like inactivity and the presence of a specific body posture, an increased threshold to arousing stimulation and a rebound in the sleep-like state as a consequence of sleep deprivation.

Bees are the organism of choice for this work because of their highly developed brain with a 10-fold increased number of neurons with respect to Drosophila. They can fulfill complex navigation and communication tasks. The effect of sleep on a memory task seems to focus on extinction learning. Extinction learning refers to the process of learning that a previously learned association is no longer valid. Sleep promoted in the bees the formation of extinction memories [28]. Acquisition of a classical conditioned response is thought to occur at the level of the antennal lobe [22]. Other networks like the mushroom bodies might specifically support extinction memory, but their role has still to be scrutinized.

## 1.2. THE OLFACTORY SYSTEM OF THE BEE

---

### 1.1.3.1 Sleep in the honey bee

In the honey bee long-term, extracellular, single-unit recordings from optomotor intraneurons in the optic lobes show oscillations in their sensitivity to moving visual stimuli that display properties typical of a circadian rhythm [29]. In fact, the sensitivity of neurons to light of a given wavelength varies according to the time of day with a sigmoid response-log intensity function with positive slope shifts towards higher intensities in the evening. This fluctuation in sensitivity represents an endogenous circadian oscillation. The circadian changes in neuronal sensitivity are related to the sleep-wakefulness rhythm of the honey bee, showing increased sensitivity during the subjective day (when the animal's motor activity is high).

Moreover, arousal stimuli restore the neurons' sensitivity, making the existence of a general arousal system plausible, with a mechanism similar to the one found in cats. During sleep the bee can let parts of their sensory systems become largely insensitive, provided that they can be reactivated quickly.

Honey bees display a deep-sleep stage, where antennae become immobile. Repeated presentations of an odor for which the bees already learned a representation resulted in a better performance in retention tests [64].

After the deep-sleep state, spontaneous antennal activity can be observed, with a function that still needs to be explored [47]. However, it can be noted how the spontaneous activity of individual neurons in the visual system correlates with the time-courses of the antennal movement.

## 1.2 The olfactory system of the bee

As the antennal lobe is considered the site of memory acquisition, the focus of this work will be to build a model of this part of the olfactory system of the honey bee and explore the effects of sleep on it.

The olfactory system is a complex neuronal network organized in multiple highly interconnected neuropils organized hierarchically. Each of these neuropils is a complex circuit comprising thousands of neurons with feedback and feed-forward interaction within and across them [42]. The local interaction within neuropils and the global interaction between them results in the neural correlates of an olfactory stimulus.

### 1.2.1 Neuroanatomy

A schematic representation of the olfactory system of the honey bee is shown in figure 1.1. Four antennal nerve (AN) tracts (T1 to T4) compose the axon of the olfactory receptor neurons ORNs that innervate the first olfactory neuropil of the bee brain, the antennal lobe (AL). Each ORN innervates a single glomerulus. All ORNs expressing the same olfactory receptor converge to the same of the 160 glomeruli of the AL. After processing in the AL the information is relayed to higher-order processing centers via the medial and lateral antennal lobe tracts (m- and l-ALT), two antiparallel tracts projecting to the ipsilateral mushroom body and lateral horn.

### 1.2.2 Odor reception

The peripheral olfactory organs of the bee are the antennae, where the ORNs are located. Each antenna is composed of a scapus, a pedicel and a flagellum, the last of which hosts the sensilla, structures containing several olfactory receptor neurons. Volatile molecules reaching the honey bee antennae enter the sensillar pores and diffuse until they reach the ORNs' dendritic membrane. The sensillar lymph in this area contains olfactory binding proteins and odorant degrading enzymes. The former facilitates the transition of the odorant into a liquid environment and transports it toward the olfactory receptors, while the latter has a role in the degradation of odorants, promoting signal termination by limiting the time an odorant is present in the sensillar lymph and preventing olfactory receptors' saturation.

The olfactory receptors ORs are located in the dendritic membrane of the ORNs and they are the main drivers for the molecular receptive response of the system. They are C-terminus-out seven-transmembrane-domain proteins

## 1.2. THE OLFACTORY SYSTEM OF THE BEE

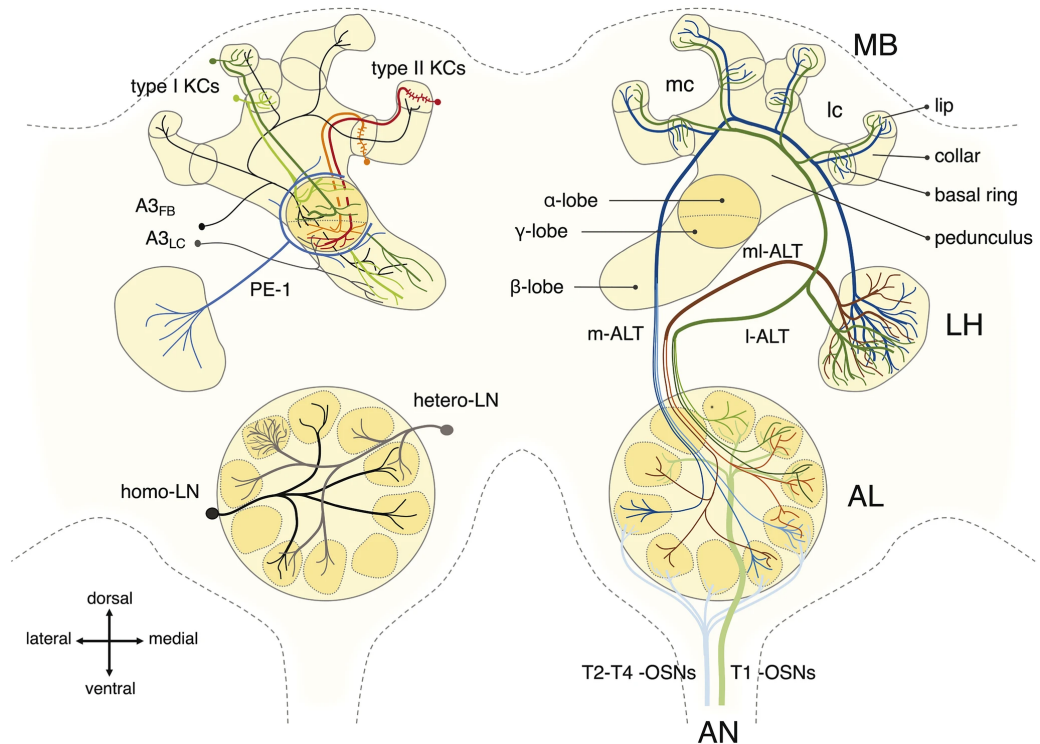


**Figure 1.1:** Schematic representation of the olfactory system of the honey bee, image taken from [42].

containing a ligand-binding domain, which are active as heterodimers with the co-receptor. Their expression level varies during the honeybee development and they are influenced by experience. Olfactory coding initiates with the biochemical interaction between the ligand and the olfactory receptor, starting odor signal transduction. The specificity varies between receptors, allowing for a limited number of receptors to encode a great number of olfactory combinations. Moreover, the specific affinity of a receptor for a particular odorant allows for a concentration-dependent response so that minute variations in stimulus nature and concentration can produce significant changes in odor representation.

### 1.2.3 Antennal lobe

The antennal lobe is the first olfactory neuropil of the bee brain and its organization can be seen in figure 1.2. It is composed of about 160 glomeruli, spherical structures of about 30 micrometers in diameter. The glomerulus is the functional unit of the AL, where the ORNs expressing the same olfactory receptor converge. An odorant creates a stereotypical map of activity in the AL, activating a subset of glomeruli. The neurons of the antennal lobe can be classified into two species: the local interneurons (LN) and the projection neurons (PN) [17]. Within a glomerulus sensory afferents form synapses with local interneurons and projection neurons. The olfactory receptor neurons convey odor, mechanosensory and gustatory information to the rest of the antennal lobe. They enter the AL through the antennal nerve and terminate in the glomeruli. Furthermore, each antenna innervates only the ipsilateral side and innervation is antennotropic: afferents originating in the distal flagellomeres occupy the external margin of the glomerular cortex, while proximal segments the inner one.

#### 1.2.3.1 Local interneurons

Local interneurons arborize through the whole glomerular volume and form synapses with the projection neurons [18]. They can present a similar density of arborization among all innervated glomeruli, or a dense

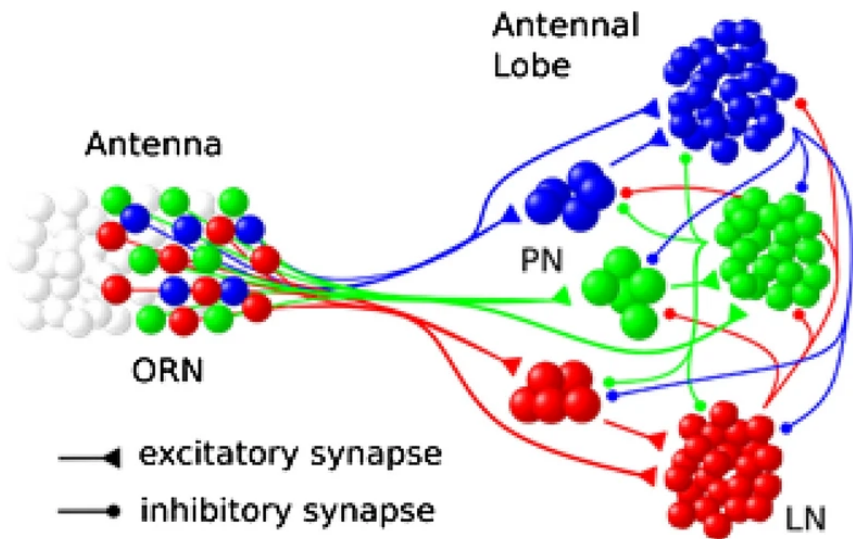


**Figure 1.2:** Schematic representation of the antennal lobe of the honey bee, image taken from [48].

arborization in one particular glomerulus. Their activity is odor-specific, they receive input from the glomerulus and deliver a mostly inhibitory output to other glomerulus. Their inhibitory activity is towards glomeruli in a spatial discontinuous pattern mediated by GABAergic synapses. This inhibitory effect of the LN produces a reduction in response intensity and a spatial and temporal increase in the representation power of the projection neurons' activity.

### 1.2.3.2 Projection neurons

Projection neurons are responsible for relaying the processed olfactory information to higher-order processing centers. Most of them receive input from individual glomeruli. The reduction in population size from the olfactory receptor neurons increases sensitivity and improves signal-to-noise ratio [20]. Their dendrites occupy the glomerular inner volume, only partially overlapping with the ORNs' pre-synaptic terminal which occupies the glomerular cortex. They innervate the mushroom body and the lateral protocerebrum, in particular the lateral horn. Axons leave the LA in five AL tracts ALTs. Fibers in these tracts differ in response latency, concentration coding and odorant specificity, suggesting that they may code for different properties of the stimulus [11].

## 1.3 Modelling neuronal circuitry

The study of the brain is a complex task, due to the high number of neurons and their interactions and it requires the use of different techniques and a system-level approach. The brain is composed of a large number of neurons, each of which is a complex system on its own. Recent advances in neuroscience have allowed for the study of the brain at a finer scale, but the complexity of the system still poses a challenge. The work proposed here involves the creation of a spiking recurrent neural network model of the antennal lobe, which will be fine-tuned to replicate the activity of the biological system.

This computational model has several advantages over an experimental approach, allowing for a more detailed data collection and study of the system, both in areas where data is available and in the frequency at which data is collected from the system.

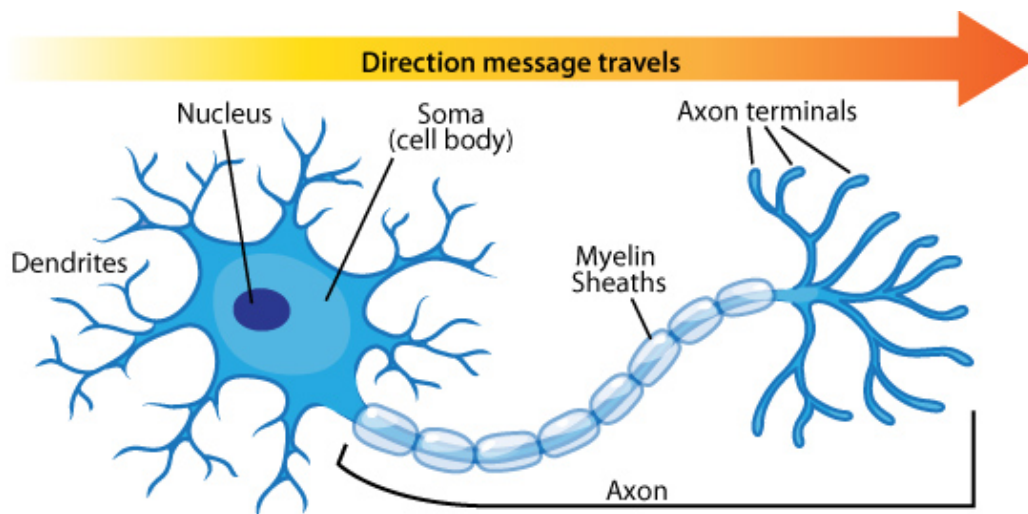


**Figure 1.3:** Schematic representation of the neuron, image taken from [2].

### 1.3.1 Functional representation of a biological neuron

A biological neuron is a complex system that can be functionally divided into three parts: the dendrites, the soma and the axon (see figure 1.3).

The dendrites are the input part of the neurons, that collects signals from others and transmits them to the soma. The soma is the “central processing unit” of the neuron, where the signal is transformed in a non-linear way: if the total input exceeds a certain threshold an output signal is generated. The output signal is then in turn taken over by the axon, which delivers it to other neurons [21].

#### 1.3.1.1 Spike trains

The neuronal signal consists of short electrical pulses, which are called action potentials or spikes. These spikes have an amplitude of around  $100\text{mV}$  and a duration in the order of a few milliseconds. The form of the pulse is constant when it travels along the axon and it tends to be similar among different neurons. Spikes can be fired at regular or irregular intervals in a neuron, depending on the input signal. From this information, it can be safely inferred that it is the number and timing of spikes that carry the information representation power in the brain and that a single action potential is the elementary unit of transmission.

#### 1.3.1.2 Synapses

Synapses are the places where two neurons come in contact: the axon of a neuron (called pre-synaptic) reaches the dendrites or soma of another (called post-synaptic). The most common type of synapse in the brain is the chemical synapse. In this type of synapse the axon terminal of the pre-synaptic neuron leaves only a tiny gap with the post-synaptic cell membrane, the synaptic cleft. When an action potential arrives at a synapse, it triggers a chain of biochemical processing steps that results in the release of neurotransmitters in the synaptic cleft. As soon as the neurotransmitter reaches the post-synaptic membrane it will bind to specific receptors, which will in turn open ion channels causing a change in the membrane potential of the post-synaptic neurons. Synapses then have a two-fold function: they transmit the signal between neurons and convert it from electrical to chemical and back to electrical, possibly causing another set of non-linear transformations to it.

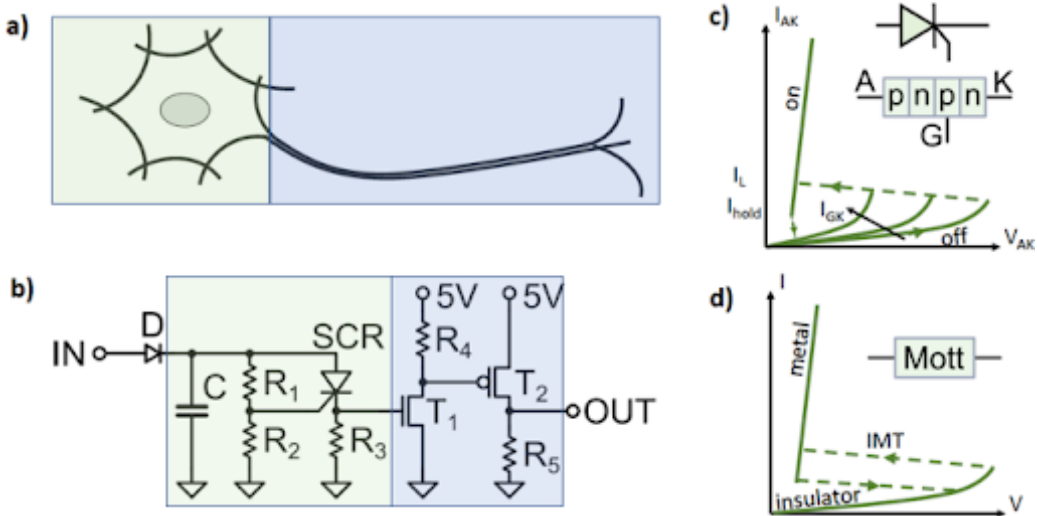


**Figure 1.4:** Modelling a neuron as a integrate and fire model, image taken from [45].

### 1.3.2 Modelling neurons - the leaky integrate and fire model

One of the most widely used models for analyzing the behavior of neural systems is the leaky integrate-and-fire model. The membrane potential of a neuron is described in terms of the synaptic inputs and the injected current that it receives [12]. An action potential is generated when the membrane potential reaches a threshold. In a sense, a neuron is an integrator of the incoming current and is equated to a capacitor-resistance electric circuit, as seen in figure 1.4. This is a point-neuron model: the spatial structure of the neuron associated with the dendrites is neglected.

The input can modelled as either injected currents (current synapses model, summation is linear) or as changes in the membrane conductance (conductance synapses model, summation is non-linear), weighted by the respective synaptic strength.

The model is leaky because the summed contributions to the membrane potential decay with a characteristic time constant.

The neuron generates a spike (or fires) when the membrane potential reaches a fixed threshold value. When this happens the membrane potential is reset to a standard resting value and, in some cases, it becomes refractory for a certain period of time. The generation of an action potential is generally not considered an intrinsic part of the model: it is usual in the description of this model to model only sub-threshold behavior.

It can be seen how the fundamental variable describing the dynamics of the neuron is the membrane potential, which evolves in time according to:

$$C_m \frac{dV(t)}{dt} = I_{leak}(t) + I_{syn}(t) + I_{inj}(t) \quad (1.1)$$

Where  $C_m$  is the membrane capacitance and is related to the time constant of decay,  $I_{leak}(t)$  is the current due to the passive leak of the membrane  $I_{syn}(t)$  is a current describing the effect of the synaptic input to the neuron and  $I_{inj}(t)$  is a current injected into the neuron. The behavior of the simplest iteration of a leaky integrate and fire neuron can be seen in figure 1.5.

The input currents can be further described as:

$$I_{leak}(t) = -\frac{C_m}{\tau_m} [V(t) - V_{rest}] \quad (1.2)$$

Where  $V_{rest}$  is the resting potential of the neuron and  $\tau_m = R_m C_m$  is the membrane time constant, the product

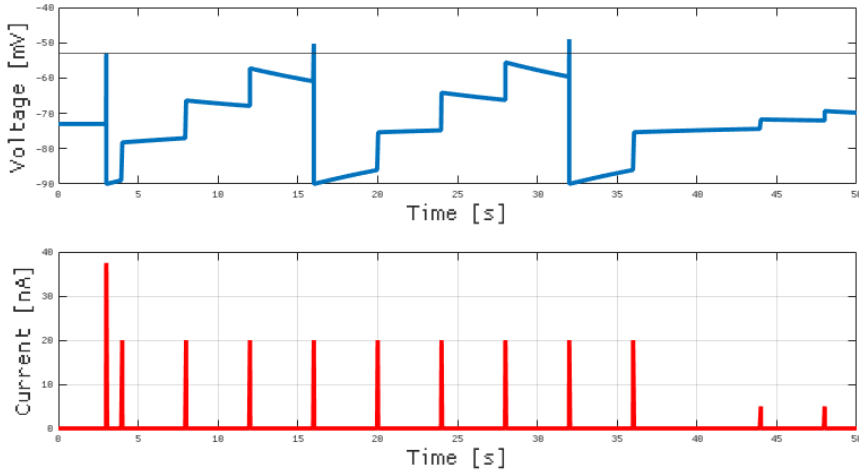


**Figure 1.5:** Behavior of the simplest leaky integrate and fire neuron:  $\begin{cases} \frac{dV(t)}{dt} = -\frac{V(t)}{\tau_m} + I_{inj} \\ V(t) = V_{reset} \text{ if } V(t) \geq V_{th} \end{cases}$ , generated with MatLab [36].

of the membrane capacitance and the leak resistance.

Although not necessary the spiking mechanism can be included in the model in terms of a spiking current:

$$I_{spike}(t) = C_m \left[ \frac{dV(t)}{dt} \right]_{v=V_{th}}^{-1} (V_{reset} - V_{th}) \delta[V(t) - V_{th}] \quad (1.3)$$

This equation describes a spike when the membrane potential reaches the spike generating threshold  $V_{th}$ , which is followed by a reset of the membrane potential to  $V_{reset}$ .  $\delta$  denotes the Dirac delta function. The membrane potential begins to evolve again according to equation 1.1 after an absolute refractory period, which can be 0 for certain applications.

### 1.3.2.1 Current synapses

The synaptic current for a current synapse is independent of the membrane potential and is described by:

$$I_{inj}(t) = C_m \sum_{k=1}^{N_E} a_{E,k} S_{E,k}(t) + C_m \sum_{k=1}^{N_I} a_{I,k} S_{I,k}(t) \quad (1.4)$$

Where  $a_{E,k} > 0$  and  $a_{I,k} < 0$  are the change in potential due to a single synaptic event and when multiplied by  $C_m$  form the associated charge delivered to the neuron by an excitatory and inhibitory input respectively.  $S_{E,k}(t)$  and  $S_{I,k}(t)$  describe the spike train:

$$S_{E,k}(t) = \sum_{t_{E,k}} \delta(t - t_{E,k}) \quad S_{I,k}(t) = \sum_{t_{I,k}} \delta(t - t_{I,k}) \quad (1.5)$$

Where  $t_{E,k}$  and  $t_{I,k}$  are the spike times of the  $k$ -th excitatory and inhibitory synapses respectively.

### 1.3.2.2 Conductance synapses

Conductance synapses offer a more biologically accurate description of synaptic current. They are modeled as:

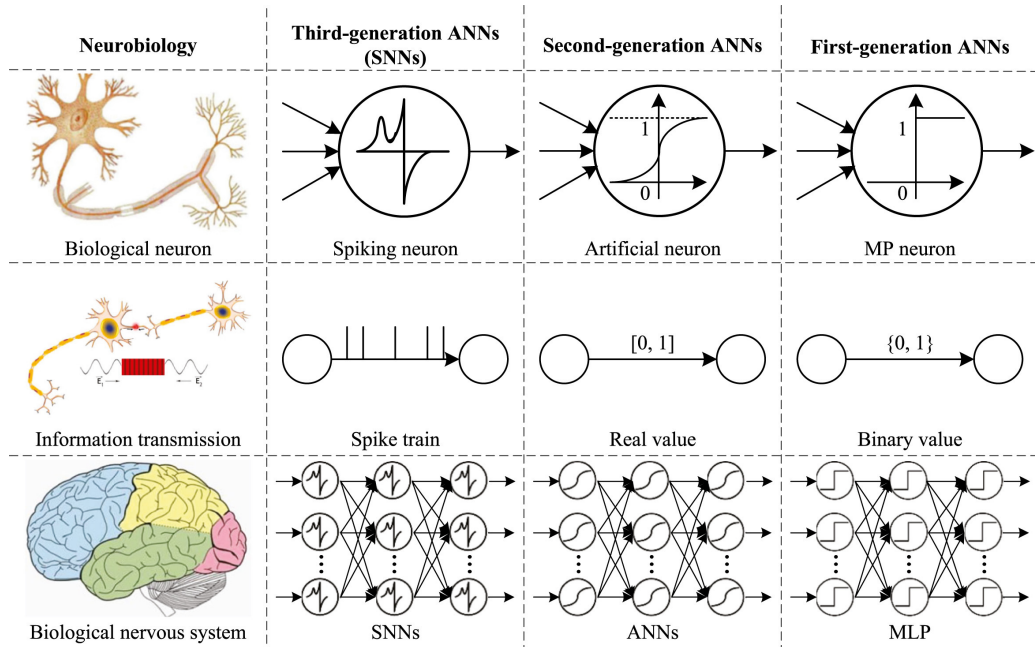


**Figure 1.6:** Schematic representation of the major differences between ANNs and SNNs. Image taken from [56].

$$I_{syn}(t) = C_m [V_E - V(t)] \sum_{k=1}^{N_E} g_{E,k} S_{E,k}(t) + C_m [V_I - V(t)] \sum_{k=1}^{N_I} g_{I,k} S_{I,k}(t) \quad (1.6)$$

Where  $V_E$  and  $V_I$  are the reversal potentials, which arise from the equilibrium potentials of the ion channels. The direction of the associated current flow switches when the membrane potential crosses the reversal potential. They introduce a non-linear factor into the summation of the individual synaptic inputs.  $g_{E,k} \wedge g_{I,k} > 0$  are the integrated conductances over the time course of the synaptic events divided by the neural capacitance (so they are dimensionless).

### 1.3.3 Interacting neurons - spiking neural networks

A collection of leaky integrate and fire neurons can be aggregated into a network. In this way, a spiking neural network (SNN) is formed. Spiking neural networks offer a different perspective on machine learning with respect to classical artificial neural networks (ANN) [34]. Data is encoded in a series of discrete time spikes, which mimics a biological brain more closely than ANNs, introducing several layers of complexity. First of all, information is no longer coded as a continuous function but as a series of discrete events (the spike train): it is the frequency of spikes and their precise timing that becomes the information carried along the network. The leaky integrate and fire (LIF) neurons become the fundamental unit of the network. Both classical artificial units and LIF units perform a non-linear transformation of the input, but the LIF unit holds a state (the membrane potential), introducing a sort of memory at a unit's level. Memory is also introduced at a system level: a biological brain is rich in recurrent connections, disrupting the classical layer structure of classical ANNs. A summary of the differences between classical ANNs and SNNs can be seen in figure 1.6.

This is interesting because biological brains are striking in how much more predictive power and efficiency they have with respect to ANNs: despite the potentially massive parameter space, the human brain only consumes about 20W.

It's this massive superiority that makes biological networks so riveting to study and model and why spiking neural networks are becoming more and more popular in machine learning. This impressive space and energy

## 1.4. CODE AVAILABILITY

---

efficiency is due to the fact that most neurons are usually inactive, meaning that the brain is highly sparse. SNNs attempt to combine more biologically plausible inputs, learning methods and architectures in order to match ANNs' performance while achieving the energy efficiency and robustness of the human brain.

From an optimization point of view, SNNs pose a unique challenge as they lack interpretable models, straightforward gradient calculation and methods that leverage the inherent advantages of SNNs. It's because of this lack of methods that observing biological networks is so important: it can provide insight into the inner workings of the brain and can be used to develop new methods for SNNs.

The work presented here is an attempt to open the “black box” of SNNs and try to understand their dynamics and how they can be used to solve problems. To do so a combination of mathematical analysis and numerical simulation will be used together with system neuroscience methods to investigate the dynamics of a specific SNN. The availability of experimental data will allow to fine-tune the model and to compare the results of a simulation with them, offering a way to validate the model, while still allowing to change it to try to understand the effect of the single elements of the system on its behavior.

## 1.4 Code availability

All the code used to generate the results presented in this work is available at <https://github.com/giacThePhantom/genn-network-model>.

# **Chapter 2**

## **Objectives**

### **2.1 Revealing neural correlates of sleep in the olfactory system of the honeybee**

The main objective of this work is to reveal the neural correlates of sleep in the olfactory system of the honeybee. To do so a computational system of the antennal lobe will be developed and used to simulate the activity of the antennal lobe in both sleep and awake states. The model will be built based on the work performed on [48] and [39]. The parameter of the model will be fine-tuned to match the activity of the antennal lobe recorded in [24]. The fine-tuned model will then be used to generate neuronal-like data and the results analyzed to reveal what are the molecular, structural and functional changes that occur in the antennal lobe between the sleep and awake states.

The experimental data recorded from [24] seems to indicate that there is no change in overall activity between the sleep and awake states: the average firing rates remain mostly unchanged across the states. The difference in between the states is found in the temporal structure of the activity and in system-wide features. As it can be seen in figure 2.1 the most striking difference is the increase in the correlation of the activity of projection neurons averaged across glomeruli during sleep.

The main hypothesis is that these changes are due to changes in connectivity between neurons and due to brain-wide changes in the structure of neurons' activity. In particular, during sleep inhibitory GABAergic synapses reduce their strength [60]. The computational model will be used to investigate this as it allows to artificially change synapses' conductances and observe the effect on the activity of the system. Moreover, currents with different shapes will be injected into the model to see whether they are able to generate the observed effect.

### **2.2 Developing a computational model of the antennal lobe**

Developing a computational model of the antennal lobe is a necessary step to achieve the main objective of this work. The model is a recurrent spiking neural network with a structure similar to the one of the biological antennal lobe. Developing such a model presents several challenges, due to the complexity of the biological system and the length of the simulation necessary to collect meaningful data.

This complexity will be tackled in a number of ways. The spatial complexity of the model will be addressed by developing a modular system, facilitating the manipulation of its parameters systematically. The computational complexity of the problem is tackled by using genn [14], a GPU-accelerated simulator, which allows to run the simulation in a reasonable amount of time. Recent development in GPU architecture has made it possible to run large-scale simulations taking advantage of the parallelism potential of GPUs. The library genn allows to transpile Python code into CUDA [40] code, which is then compiled and run on the GPU, allowing for fast development and deployment times without loss of performance. The developed code is then wrapped in a

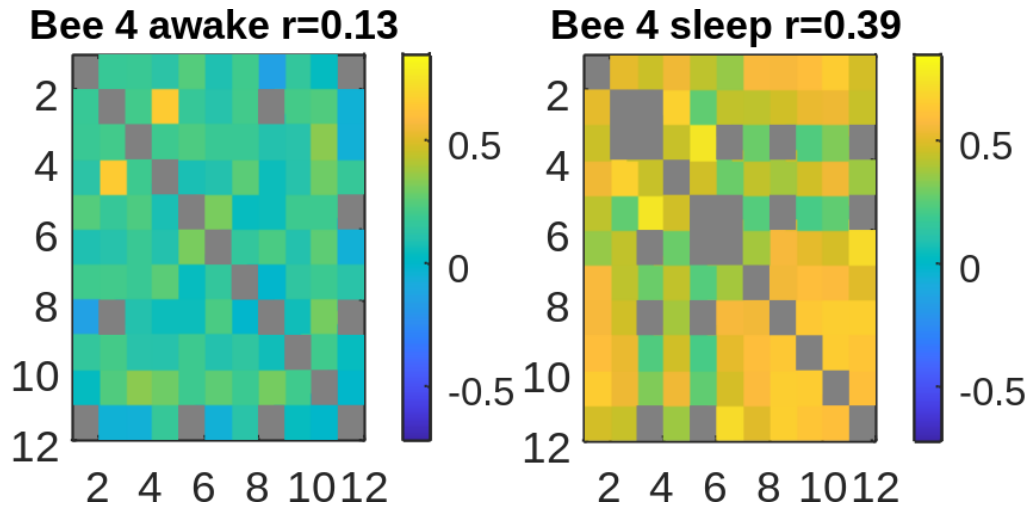


**Figure 2.1:** Correlation change between the activity of projection neurons activity averaged over glomeruli. Image from [24].

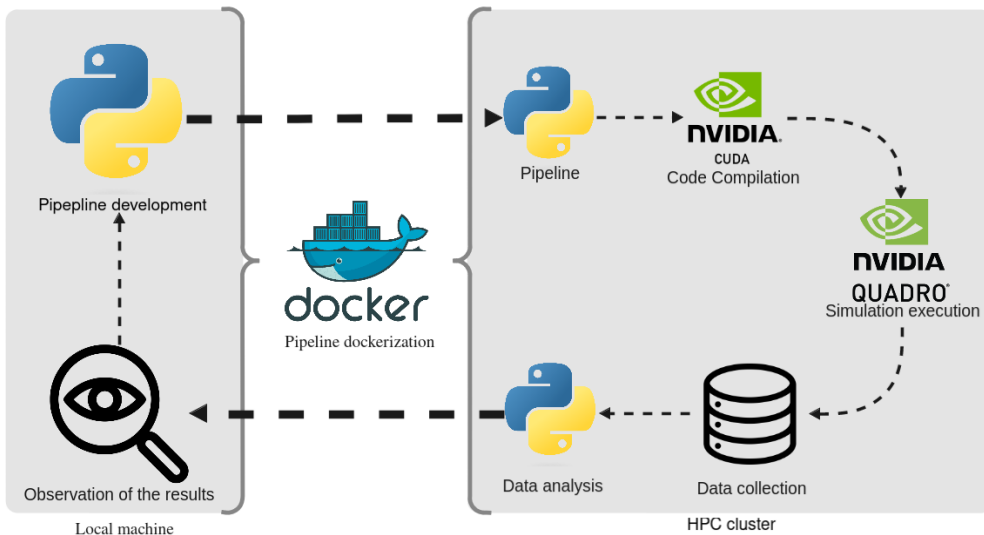


**Figure 2.2:** Visual representation of the development pipeline.

Docker container [38] and deployed to an HPC cluster, where it is transpiled and the simulation is run in a high-performance environment. The data collected is then stored in a compressed binary form and used for a later analysis pipeline. The entire pipeline is represented in figure 2.2. This approach allows to run the simulation and the data analysis pipeline in a reasonable amount of time while maintaining the flexibility of Python code.

The data analysis pipeline will allow to extract the relevant features from the data and to compare them with the experimental data. In particular, the focus will be on the activity pattern of the neurons of the antennal lobe, their correlation and how changes in the strength of the synapses and in the shape of the input will affect the neuronal computation undergoing in the olfactory system.

# Chapter 3

## Materials and methods

### 3.1 The model

The antennal lobe of the honey bee will be modeled as a recurrent spiking neural network. Its architecture is based on anatomic data from the honey bee brain and modeled extending the work done on [39] and [48]. The implementation of the model is done in Python using the library GeNN [14], a GPU-enhanced neural network environment based on NVIDIA CUDA [40] technology. GeNN offers a high-level interface to define the network architecture, the neuron and synapse models and the simulation parameters. The Python API allows for fast development times and easy integration with other Python libraries for data analysis and visualization. Its main advantage is the fact that the low-level CUDA code is generated automatically from a mixture of Python and C++ code, allowing it to fully exploit the power of modern GPUs without having to deal with memory management.

#### 3.1.1 Architecture

A schematic representation of the architecture of the resulting spiking neural network can be seen in figure 3.1.

The model is composed of 160 glomeruli, the functional unit of the antennal lobe, which are connected to each other by the local interneurons.

Each glomerulus is composed of:

- 1 olfactory receptor (OR).
- 60 olfactory receptor neurons (ORN).
- 5 projection neurons (PN).
- 25 local interneurons (LN).

Each glomerulus is a hierarchical structure in which the OR is connected to each neuron in the ORN population, which in turn forms excitatory synapses with PNs and LNs. Each neuron in the ORN population forms an excitatory synapse with a random neuron in the PN and LN populations in the same glomerulus. Each neuron in the PN population forms an excitatory synapse with each neuron in the LN population in the same glomerulus. The neurons in the LN are densely connected to each other and to neurons in the PN via inhibitory synapses. Communication between glomeruli is done via dense inhibitory synapses between LNs.

The resulting model is a recurrent spiking neural network composed of 14 560 neurons and 19 220 000 synapses.

#### 3.1.2 Olfactory receptors

The olfactory receptors are the input of the model and are implemented as in [48]. Biologically olfactory receptors are G-coupled protein receptors (GPCR) that bind to odorant molecules. They are transmembrane

### 3.1. THE MODEL

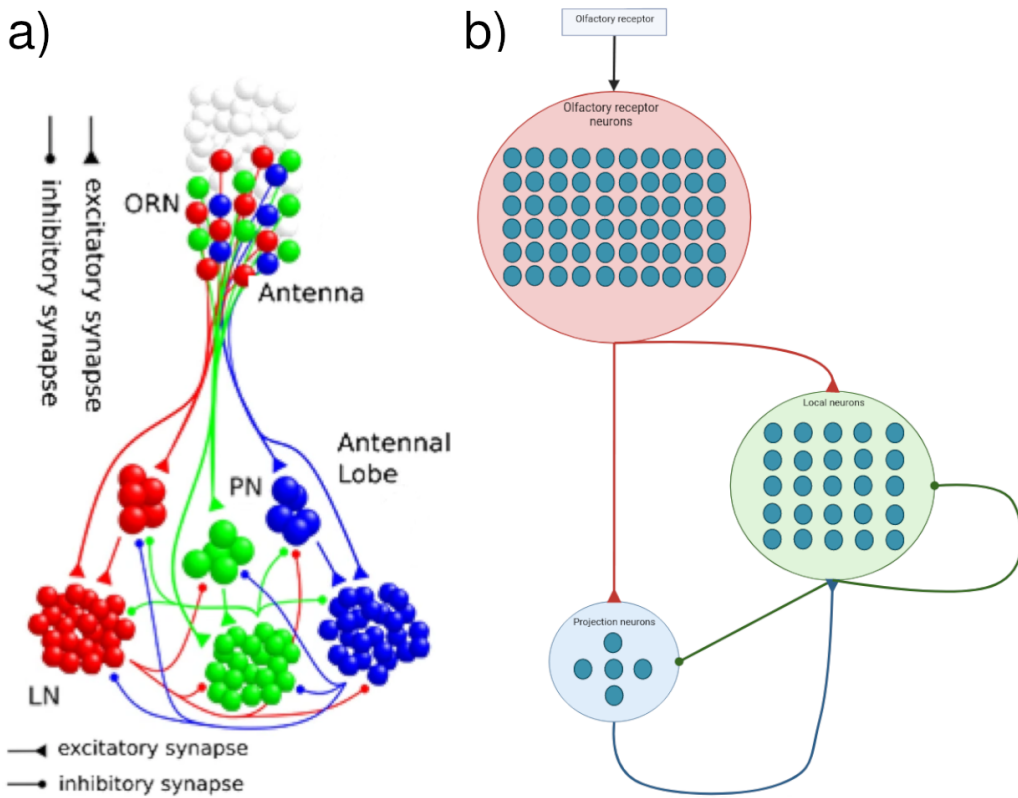


**Figure 3.1:** a) Schematic representation of the architecture of the antennal lobe model. b) Schematic representation of the connections between neurons in a singular glomerulus.

proteins located in the dendrites of the olfactory receptor neurons. When an odorant molecule binds to the receptor, it activates a G-protein which in turn activates an ionic channel, causing an increase in the membrane potential of the neuron. Each of the receptors is modeled to have three odor channels, so one neuron is able to be activated by three different odorants at the same time. Different odorants can activate the same channel, with a strength depending on their affinity to the receptor. The activation of the neuron is a two-step process, each of which is modeled by a differential equation. The first step is the binding of the odorant to the receptor:

$$\frac{dr_{bound}^{(i)}(t)}{dt} = (k_{binding}^{(i)} c_i)^n r(t) - k_{unbinding}^{(i)} r_{bound}^{(i)}(t) + k_{deactivating}^{(i)} r_{active}^{(i)}(t) - k_{activating}^{(i)} r_{bound}^{(i)}(t) \quad (3.1)$$

Where:

- $r_{bound}^{(i)}(t)$  is the fraction of channels bound by an odorant  $i$ ,
- $k_{binding}^{(i)}$  is the binding rate of odorant  $i$  to the receptor,
- $c_i$  is the concentration of odorant  $i$  receptor pair.
- $k_{unbinding}^{(i)}$  is the unbinding rate of the odorant  $i$  receptor pair.
- $k_{deactivating}^{(i)}$  is the deactivation rate of the odorant  $i$  receptor pair.
- $k_{activating}^{(i)}$  is the activation rate of the odorant  $i$  receptor pair.

And, in particular, the fraction of unbound receptors is computed as:

### 3.1. THE MODEL

---

$$\frac{dr(t)}{dt} = \sum_j k_{unbinding}^{(j)} r_{bound}^{(j)}(t) - \sum_j (k_{binding}^{(j)} c_j)^n r(t) \quad (3.2)$$

The fraction of receptors that are bound and then activated is described by:

$$\frac{dr_{active}^{(i)}(t)}{dt} = k_{activating}^{(i)} r_{bound}^{(i)}(t) - k_{deactivating}^{(i)} r_{active}^{(i)}(t) \quad (3.3)$$

All the constants can be specific to the odors and receptor types. In this work the unbinding and deactivating rates were chosen constant and equal for all types, the binding rates were specific to the odor-receptor pair, while the activation rates were odor-specific.

The total fraction of active channels can be computed as:

$$r_{active}(t) = \sum_j r_{active}^{(j)}(t) \quad (3.4)$$

#### 3.1.2.1 Odors

Odors are described by their bonding and activation rates. In particular, they were chosen as Gaussian profiles, as done in [48]:

$$k_{binding}^{(i)}(j) = 10\eta^i e^{-\frac{\pi^2(j)}{2*\sigma^2}}, \quad j = 1, \dots, N_{glo} \quad (3.5)$$

Where:

- $\pi(\cdot)$  is a randomly chosen permutation of  $1, \dots, N_{glo}$ .
- $N_{glo}$  is the number of glomeruli in the model.
- $\eta \sim \mathcal{N}(1.5, 0.5^2)$  is a normally distributed random variable truncated within 0 kHz and 4 kHz.
- $\sigma \sim \mathcal{N}(3, 0.5^2)$  is the standard deviation of the odor profile truncated to values greater than 1.5 kHz.

The activation constant  $k_{activating}^{(i)}$  was sampled from a normal distribution  $\mathcal{N}(0.02, 0.02^2)$  truncated within [0.0028 kHz, 0.2 kHz].

From a biological perspective,  $\eta$  describes how sensitive a receptor is to an odorant, while  $\sigma$  describes how broadly an odorant activates the system.

#### 3.1.2.2 Noise

Bees tend to decrease their body temperature as they sleep, and this could explain the difference in the antennal lobe's activity in this state. To include the effects of temperature white noise has been added to the olfactory receptors, with an equation described in [51]:

$$\sigma_j^{(i)} = \sqrt{D_j^{(i)} \cdot T \cdot \alpha} \quad \alpha \sim \mathcal{N}(0, 1) \quad (3.6)$$

Where  $T$  is the temperature of the system and  $D_j^{(i)}$  is the Q10 coefficient, chosen ad hoc so the activity of the system resembles experimental data.  $D_j^{(i)}$  is computed as:

### 3.1. THE MODEL

---

$$D_j^{(i)} = \frac{k(T+10)}{k(T)} \quad k(T) = A \cdot e^{-\frac{E_a}{R \cdot T}} \quad (3.7)$$

Where:

- $A$  is a scaling factor.
- $E_a$  is the activation energy, defined by Arrhenius equation as the minimum energy required to activate a receptor.
- $R$  is the gas constant.

So the new equations for the activation and binding of the odorant become:

$$\frac{dr_{bound}^{(i)}(t)}{dt} = (k_{binding}^{(i)} c_i)^n r(t) - k_{unbinding}^{(-1)} r_{bound}^{(i)} + k_{deactivating}^{(i)} r_{active}^{(i)}(t) - k_{activating}^{(i)} r_{bound}^{(i)} \quad (3.8)$$

$$\frac{dr_{active}^{(i)}}{dt} = k_{activating}^{(i)} r_{bound}^{(i)} - k_{deactivating}^{(i)} r_{active}^{(i)} + \sigma_{activating}^{(i)} + \sigma_{deactivating}^{(i)} \quad (3.9)$$

#### 3.1.2.3 Effect of other brain regions

The fact that an increase in correlated activity can be seen across the whole brain during sleep [23], suggested the possibility to add an additional correlated input into this region during sleep. This was done by generating for each olfactory receptor a Poisson train that will be added to the activity generated by the odor receptor following the work done in [19]. A different Poisson train was generated for each of the glomeruli via the modified next reaction method [35] algorithm (see algorithm 1).

---

#### Algorithm 1: Modified Next Reaction Method (MNRM) ()

---

**Input:** A spike probability event accompanied by the state change variable  $V_\mu$ , the propensity  $a$ , then the initial state  $V_0$  and the simulation ending time  $T_{max}$ .

**Output:** a trajectory of the membrane potentials, which is a collection of states  $X(t)$  for time

$$0 \leq t \leq T_{max}$$

$$t = 0$$

$$V = V_0$$

$$T = 0$$

generate a random number  $r \sim norm(0, 1)$

$$P = \ln \frac{1}{r}$$

compute  $a$

**while**  $t < T_{max}$  **do**

$$\tau = \frac{1}{a}(P - T)$$

$$V = V + V_\mu$$

$$t = t + \tau$$

generate a random number  $r \sim norm(0, 1)$

$$P = P + \ln \frac{1}{r}$$

compute new  $a$

---

The parameters of this algorithm were chosen to obtain biologically plausible results.

After having built the Poisson trains for each of the glomeruli, a template Poisson process was generated with the same method to increase the correlation between the different glomeruli. Each event in the resulting trajectory

### 3.1. THE MODEL

---

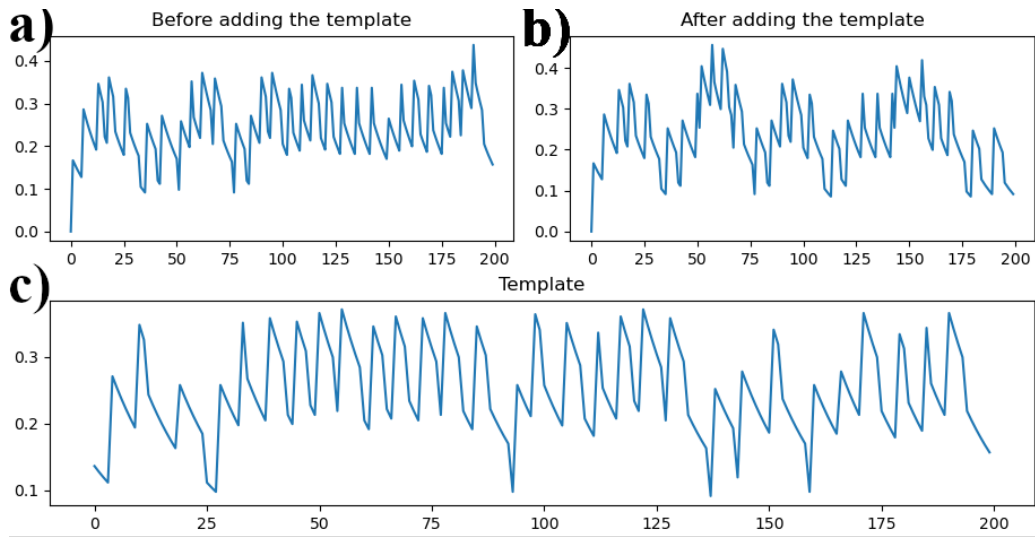


**Figure 3.2:** Example of the generation of a Poisson train. **a)** A Poisson train before adding the template. **b)** The same Poisson train as in **a** after adding the template. **c)** The template that is added to the other Poisson trains.

of the template process was added with a probability  $P_{add}$  to the Poisson train of each glomeruli and an event was removed from those latter with a probability  $P_{remove}$ .

Each of the resulting membrane potentials was then convolved with an  $\alpha$  function to obtain the final input current. An example of the resulting Poisson trains and the effect of adding a template can be seen in figure 3.2.

Calling the resulting poisson train  $poi$  the final activity of an olfactory receptor is computed as:

$$\frac{dr_{bound}^{(i)}(t)}{dt} = (k_{binding}^{(i)} c_i)^n r(t) - k_{unbinding}^{(-1)} r_{bound}^{(i)} + k_{deactivating}^{(i)} r_{active}^{(i)}(t) - k_{activating}^{(i)} r_{bound}^{(i)} \quad (3.10)$$

$$\frac{dr_{active}^{(i)}}{dt} = k_{activating}^{(i)} r_{bound}^{(i)} - k_{deactivating}^{(i)} r_{active}^{(i)} + \sigma_{activating}^{(i)} + \sigma_{deactivating}^{(i)} + poi^{(i)} \quad (3.11)$$

#### 3.1.3 Neurons

The neurons in this model are described by a noisy adaptive leaky integrate and fire model. This model expands the classic leaky integrate and fire model by adding an adaptive term to the membrane potential:

$$I_{adapt}(t) = g_{adapt} \alpha(t) (V(t) - V_{adapt}) \quad (3.12)$$

This current is called adaptive because it depends on the spike train coming into the neuron. In particular the variable  $\alpha(t)$  increases with the frequency of spikes according to:

$$\frac{d\alpha(t)}{dt} = 0.5 \sum_{t_{spike}} \delta(t_{spike} - t) - \frac{\alpha}{\tau_{adapt}} \quad (3.13)$$

Where:

### 3.1. THE MODEL

---

- $\delta$  is the Dirac delta function.
- $\tau_{adapt}$  is the time constant of the adaptation.

Other than the adaptive part the other difference from the classic leaky integrate and fire model is the noise term. A Gaussian noise is added to the membrane potential with the following equation:

$$noise(t) = A\sigma(t) \quad (3.14)$$

Where  $\sigma(i) = \mathcal{N}(0, 1) \forall i = 0, \dots, T$  and  $A$  is a constant chosen so that the noise is biologically plausible. The final equation of the membrane potential is then:

$$C \frac{dV(t)}{dt} = -I_{leak} - I_{adapt} + kI_{external} + noise(t) \quad (3.15)$$

$$= -g_{leak}(V(t) - V_{leak}) - g_{adapt}\alpha(t)(V(t) - V_{adapt}) + kI_{external} + A\sigma(t) \quad (3.16)$$

Where:

- $C$  is the capacitance of the neuron.
- $g_{leak}$  is the conductance of the leak current.
- $V_{leak}$  is the reversal potential of the leak current.
- $g_{adapt}$  is the conductance of the adaptive cur-
- rent.
- $V_{adapt}$  is the reversal potential of the adaptive current.
- $kI_{external}$  is the current arriving from other neurons scaled by a factor  $k$ .

This equation was then solved numerically using the Euler method:

$$V(t + \Delta t) = V(t) + \Delta t \frac{dV(t)}{dt} \quad (3.17)$$

$$= V(t) + \Delta t \frac{-g_{leak}(V(t) - V_{leak}) - g_{adapt}\alpha(t)(V(t) - V_{adapt}) + kI_{external} + A\sigma(t)}{C} \quad (3.18)$$

And implemented in GeNN to be used in the model.

#### 3.1.3.1 Temperature

The effect of temperature has been included also in the neurons. The same  $Q10$  formalism has been used to change the conductances of the leak and adaptive currents:

$$g_{leak}(T) = g_{leak, 0}(T_{ref}) Q_{10}^{\frac{T-T_{ref}}{10}} g_{adapt}(T) = g_{adapt, 0}(T_{ref}) Q_{10}^{\frac{T-T_{ref}}{10}} \quad (3.19)$$

#### 3.1.4 Synapses

To facilitate model implementation, the olfactory receptor, besides being a membrane protein channel, was modeled as neurons to exploit GeNN API. Because of this, the model presents three types of synapses:

1. Synapses between olfactory receptors and olfactory receptor neurons.

### 3.1. THE MODEL

---

2. Excitatory synapses between:

- Olfactory receptor neurons and projection neurons (intra-glomerulus).
- Projection neurons and local neurons (intra-glomerulus).

3. Inhibitory synapses between:

- Local neurons and projection neurons (intra-glomerulus and inter-glomerulus).
- Local neurons and local neurons (intra-glomerulus and inter-glomerulus).

#### 3.1.4.1 Connection between olfactory receptors and olfactory receptor neurons

Each olfactory receptor is connected to all the 60 olfactory receptor neurons in the same glomerulus. The connection between them is modeled as a simple current injection. An increase in current in the olfactory receptor causes an increase in current in the olfactory receptor neuron scaled by a factor  $k$ :

$$I_{post\ synaptic} = kr_{active}(t) \quad (3.20)$$

Where  $r_{active}(t)$  is the fraction of active olfactory receptors as defined in equation 3.4.

#### 3.1.4.2 Excitatory synapses

Each olfactory receptor neuron is connected to a random projection neuron in the same glomerulus by an excitatory synapse. The same is true for the connection between projection neurons and local neurons.

These synapses are modeled according to a static pulse model [1]. In this model no learning rule is applied to the synapse and for each synapse the synaptic conductances are added to the postsynaptic input variable:

$$g_{post\ synaptic} = g_{post\ synaptic} + g_{synapse} \quad (3.21)$$

Where:

- $g_{post\ synaptic}$  is the postsynaptic conductance, or  $k$  in 3.16.
- $g_{synapse}$  is the conductance of the synapse, the only variable of the model.

The model is then modified with an exponential decay on the conductance  $g_{synapse}$ .  $g_{synapse}$  then evolves according to:

$$\frac{dg_{synapse}(t)}{dt} = -\frac{g_{synapse}(t)}{\tau_{synapse}}(V(t) - E) \quad (3.22)$$

Where:

- $\tau_{synapse}$  is the time constant of the synapse.
- $E$  is the reversal potential.

#### 3.1.4.3 Inhibitory synapses

Each projection and local neuron is then connected to each local neuron both in the same and in other glomeruli. These synapses are modeled with the same static pulse model with exponential decay as the excitatory synapses but with different parameters for the time constant  $\tau_{synapse}$  and the reversal potential  $E$ .

## 3.2. DATA ANALYSIS

---

Another major difference is the fact that the inhibitory synapses form dense connections: all the neurons in the source population are connected to all the neurons in the target population, instead of being connected to only one. Furthermore, these are the only synapses that cross the glomerulus, allowing them to communicate and synchronize the activity of the different glomeruli while introducing recurrence in the network.

## 3.2 Data analysis

All the data analysis was performed using Python and the following libraries:

- Pandas [41]
- Numpy [25].
- Matplotlib [27].
- Seaborn [58].

The simulation will be performed with different parameters to fine-tune the model and make it behaves like the experimental results. The final objective is to understand the property of the model and the behavior of the neurons in the network and understand the molecular mechanisms that cause the difference in the antennal lobe between the asleep and awake states.

### 3.2.1 Extracting data from a simulation

GeNN allows to record data from all the variables during a simulation. For the olfactory receptor, the data recorded is the fraction of active receptors  $r_{active}(t)$ . Then for each population of neurons, the variable recorded will be:

- The membrane potential  $V(t)$ .
- The spike train  $S(t)$ .

These data will then be stored in a compressed format to save space and then analyzed in an offline phase. The compression is performed using the Zstandard algorithm [15].

This has been chosen because it is a fast lossless compression algorithm, built specifically for real-time compression scenarios while achieving better compression ratios. This is important because the simulation will be performed on a cluster of GPU nodes and the data will be stored on a shared file system. Optimizing the space used by the data will allow to store more data and perform more simulations.

### 3.2.2 Neuron's activity

The evolution of the membrane potential  $V(t)$  of a neuron is a good indicator of the activity of the neuron. Because of this it will be recorded and then, to allow for a visualization of the activity of the network, it will be plotted using Matplotlib [27]. Because there are too many neurons to allow for a visualization of the activity of each neuron, only a random neuron in the most active glomerulus will be plotted for each population.

This type of plot will give information about the general activity of the neurons in each population and will allow to see if the network is behaving as expected.

### 3.2.3 Spike density matrix

The spike density matrix will show the average firing rates of all the glomeruli in the network. The spike train for each neuron of each population in a network is collected from the simulation and then it is convolved with a Gaussian kernel to obtain the firing rate of each neuron. The firing rates of the neurons are then averaged across population and glomeruli and plotted as a heatmap using Matplotlib [27].

## 3.2. DATA ANALYSIS

---

This type of plot will give information about the activity of the population of neurons per glomeruli, giving visual information about which glomerulus is activated by a specific odor, or how the input is transformed when it travels across the populations of neurons.

### 3.2.4 Correlation matrices

The correlation matrices are built using the spike density matrix as obtained in the previous sections. In this way, the correlation of the firing rates of neurons in the same population per glomerulus can be visualized. It is computed using the `corrcoef` function of Numpy [25] (equation 3.23).

$$R_{ij} = \frac{C_{ij}}{\sqrt{C_{ii}C_{jj}}} \quad (3.23)$$

Where  $C_{ij}$  is the covariance matrix of the input matrix:

$$C_{ij} = \frac{1}{n-1} \sum_{k=1}^n (X_{ki} - \bar{X}_i)(X_{kj} - \bar{X}_j) \quad (3.24)$$

This function takes as input the spike density matrix and returns the Pearson product-moment correlation coefficient. In particular it returns a matrix  $C$  where  $C_{i,j}$  is the correlation coefficient between the  $i$ -th and the  $j$ -th column of the input matrix such that:

- $C_{i,j} > 1$  the activity of the two glomeruli is positively correlated.
- $C_{i,j} = 0$  the activity of the two glomeruli is not correlated.
- $C_{i,j} < 0$  the activity of the two glomeruli is negatively correlated.

The resulting correlation matrix is then clustered using the `linkage` function of Scipy [54] with the `complete` method and plotted as heatmap using Seaborn [58]. Clustering is performed with a hierarchical and agglomerative algorithm and the distance used is the Farthest Point Algorithm or Voorhees Algorithm [55]. This type of plot is of fundamental importance because one of the most visible effects of sleep in experimental data is an increase in the correlation between the projection neurons across glomeruli with respect to the awake state.

### 3.2.5 Feature extraction

After having fine-tuned the model so it reproduces the experimental data obtained from observing the activity of the antennal lobe of a bee in the awake and asleep state, the model will be used to extract features from the data.

This is done because from the experimental data it was noticed that there were no significant changes in the average firing rate of the observed brain regions, but what changed was, besides the increase in correlation, network-level features.

Several features will be extracted and analyzed using the Python library bct [4]. Bct is a brain connectivity toolbox for Matlab, but it has been ported to Python and it is available as a pip package. It provides several graph theoretical measures, and it will be used to extract several connectivity features. Besides the connectivity features, other features will be extracted from the data, regarding the distribution of the activity of the neurons in the network.

The various features will be compared visually thanks to Seaborn's [58] `pairplot` function.

## 3.2. DATA ANALYSIS

---

### 3.2.5.1 Distribution features

The distribution features will be extracted using a combination of the Scipy [54], Numpy [25] and Nolds [49] libraries.

**3.2.5.1.1 Standard deviation** The standard deviation of the activity of the neurons in the network is computed as the average of the standard deviation of the activity of neurons at each timestep. For a single timestep the standard deviation is computed as:

$$\sigma = \sqrt{\frac{1}{N} \sum_{i=1}^N (x_i - \mu)^2} \quad (3.25)$$

Where:

- $N$  is the number of neurons in the network.
- $x_i$  is the activity of the  $i$ -th neuron.
- $\mu$  is the average activity of the neurons in the network.

**3.2.5.1.2 Skewness** The skewness of the activity of the neurons in the network is computed as the average of the skewness of the activity of neurons at each timestep. For a single timestep the skewness is computed as the Fisher-Pearson coefficient of skewness:

$$g_1 = \frac{m_3}{m_2^{3/2}} \quad m_i = \frac{1}{N} \sum_{i=1}^N (x_i - \mu)^i \quad (3.26)$$

Where:

- $N$  is the number of neurons in the network.
- $x_i$  is the activity of the  $i$ -th neuron.
- $\mu$  is the average activity of the neurons in the network.

**3.2.5.1.3 Kurtosis** The kurtosis of the activity of the neurons in the network is computed as the average of the kurtosis of the activity of neurons at each timestep. For a single timestep the kurtosis is the fourth central moment divided by the square of the variance:

$$\beta_2 = \frac{\mu^4}{\sigma^4} \quad (3.27)$$

**3.2.5.1.4 Sample entropy** The sample entropy of the activity of the neurons in the network is computed as the average of the kurtosis of the activity of neurons at each timestep. For a single timestep the sample entropy is the negative natural logarithm of the conditional probability that two sequences remain similar at the next point in the activity's time series. It is computed by constructing all subsequences of length  $m$  and count all different pairs distant less than a predefined threshold  $r$ . The same is done for all subsequences of length  $m + 1$ . Then the sum of similar sequence pairs with length  $m + 1$  is divided by the sum of similar sequence pairs with length  $m$ . The result is then the negative logarithm of this probability.

**3.2.5.1.5 Hurst exponent** The Hurst exponent of the activity of the neurons in the network is computed as the average of the kurtosis of the activity of neurons at each timestep. It is a measure of long-term memory of the activity time series: the long statistical dependencies in the data that do not originate from cycles. It is computed by subtracting the mean from the time series and computing the cumulative sum of the resulting time series. Then the cumulative sum is divided into  $N$  non-overlapping segments of equal length.

**3.2.5.1.6 Detrended fluctuation analysis** The detrended fluctuation analysis (DFA) is a method that will be used to find long-term statistical dependencies in the time series of the activity of neurons, similarly to the Hurst exponent. It is computed for a single timestep by dividing the time series into  $N$  non-overlapping segments of equal length. Then for each segment the trend is removed by subtracting the least squares fit of the data in the segment. Then the root mean square of the data in each segment is computed. Finally the root mean square is plotted against the length of the segment in a log-log plot and the slope of the resulting line is the DFA.

### 3.2.5.2 Connectivity features

Connectivity features focus on the network-level effect rather than on the time series of the data. These features will be extracted from the functional connectivity of the network, which depends on the activity of the neurons in the network, rather than its architecture. Functional connectivity is extracted by computing the Pearson coefficient of the time series of the activity for each pair of neurons in the network. If the coefficient is greater than a threshold a functional connection is found between the neurons, otherwise there is no functional connection.

The features will be extracted using the library bct [4] and will be:

**3.2.5.2.1 Betweenness centrality** The betweenness centrality of a node is the average fraction of all shortest paths in the network that contain a given node. It is computed through Kintali's algorithm [31].

**3.2.5.2.2 Transitivity** The transitivity is the ratio of triangles to triplets in the network. From a connectivity graph it counts the triangles and the triplets and then divides the triangles by the triplets.

**3.2.5.2.3 Degree** The degree is the average number of incoming and outgoing links connected to a node.

**3.2.5.2.4 Efficiency** The efficiency is the average of inverse shortest path length. It is inversely related to the characteristic path length.

**3.2.5.2.5 Frobenius norm** The Frobenius norm is the square root of the sum of the absolute squares of its elements. It is a measure of the size of a matrix. It is computed for the adjacency matrix of the connectivity graph as:

$$\|A\|_F = \left[ \sum_{i,j} |a_{ij}|^2 \right]^{1/2} \quad (3.28)$$

### **3.2. DATA ANALYSIS**

---

# Chapter 4

## Results

### 4.1 Behavior of the components

The first thing to do to understand how the model operates is to analyze how its singular components behave. In this section, the behavior of the neuron, synapses, olfactory receptors, the correlated input and the temperature-dependent white noise will be analyzed.

#### 4.1.1 Olfactory receptors

Olfactory receptors are the input of the model. They evolve according to equations 3.1 and 3.4. The behavior of a noisy receptor is shown in figure 4.1.

Figure 4.1 shows 6 seconds of the behavior of a receptor when it is activated by an odor. The odor is presented at the third second, causing an increase in the fraction of active receptors, which is linear with the increase in activity of the 60 olfactory receptor neurons directly bound to it.

##### 4.1.1.1 Temperature-dependent white noise

The temperature-dependent white noise (parameters found in table 4.1) causes the activity to fluctuate around an equilibrium value, which is 0 when there is no odor and 0.5 when the odor is presented.

The parameters shown in 4.1 were chosen to obtain a reasonable behavior of the receptors. In particular, the effect of the  $Q10$  formalism on the scaling coefficient  $D(t)$  of the white noise is shown in figure 4.2. It can be seen how an increase in temperature would cause an increase in the scaling factor  $D(t)$ , which in turn would cause an increase in the fluctuations of the receptors, increasing the average firing rate of the network.

##### 4.1.1.2 Correlated input

The correlated input, or Poisson trains, is another modification to the behavior of the receptors. It is introduced to simulate the effect of the input of other brain regions on the antennal lobe. Each receptor is associated with

Parameter	Value
$D(t)$	$3 \cdot 10^{-5}$
$T$	$30^\circ\text{C}$

**Table 4.1:** Parameters used for the temperature-dependent white noise.

#### 4.1. BEHAVIOR OF THE COMPONENTS

---

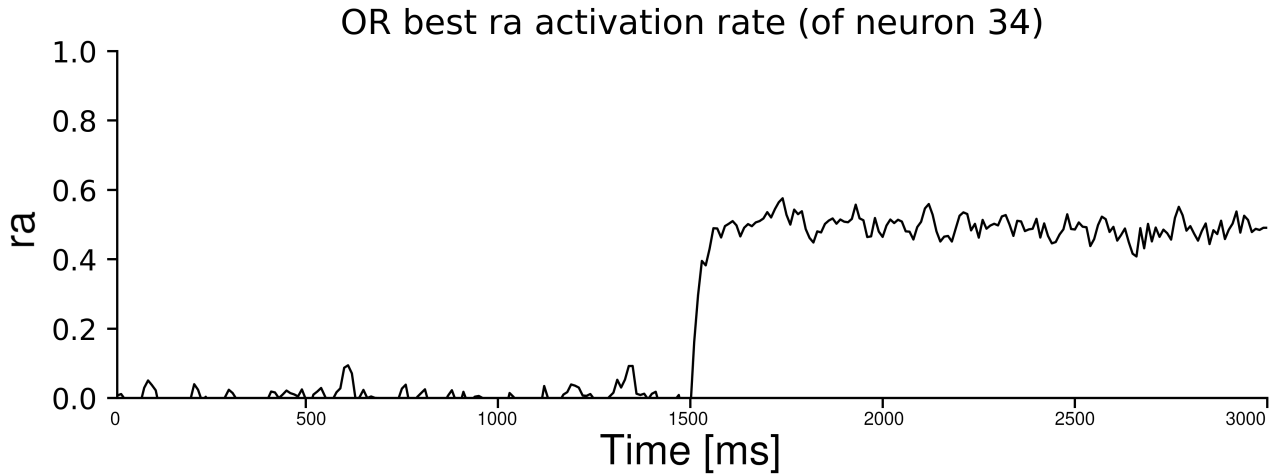


**Figure 4.1:** Behavior of an olfactory receptor without the poisson train time [ms] on the  $x$ -axis and  $r_{active}$  on the  $y$ -axis. An increase in the rate can be seen when an odor is presented.

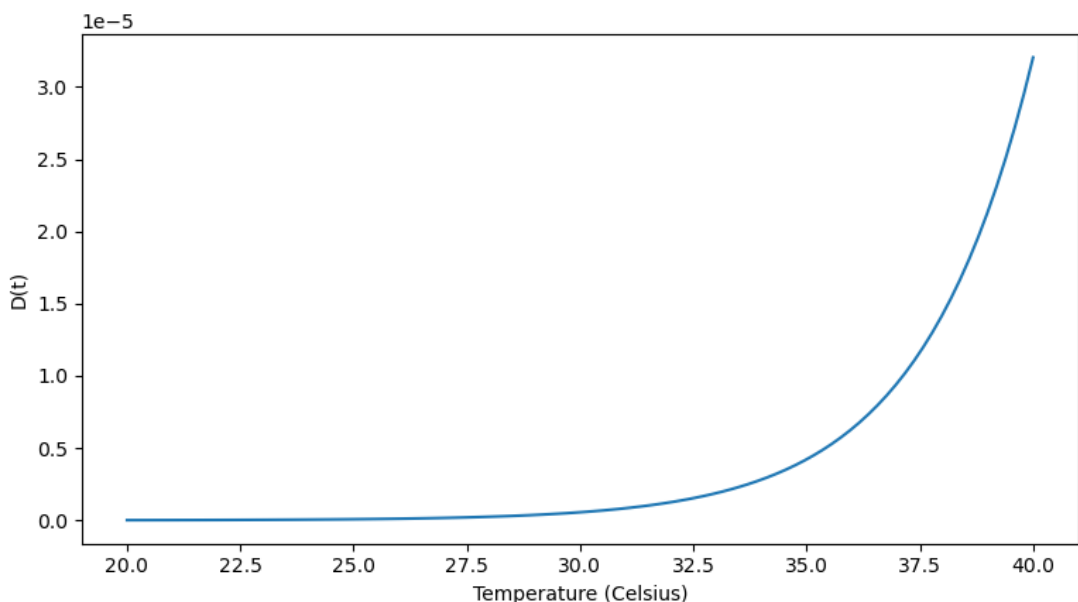


**Figure 4.2:** Effect of the  $Q_{10}$  formalism on the scaling coefficient  $D(t)$  of the white noise. The increase in temperature causes an exponential increase in the scaling factor  $D(t)$ , which in turn causes an increase in the fluctuations of the receptors, increasing the average firing rate of the network.

## 4.1. BEHAVIOR OF THE COMPONENTS

---

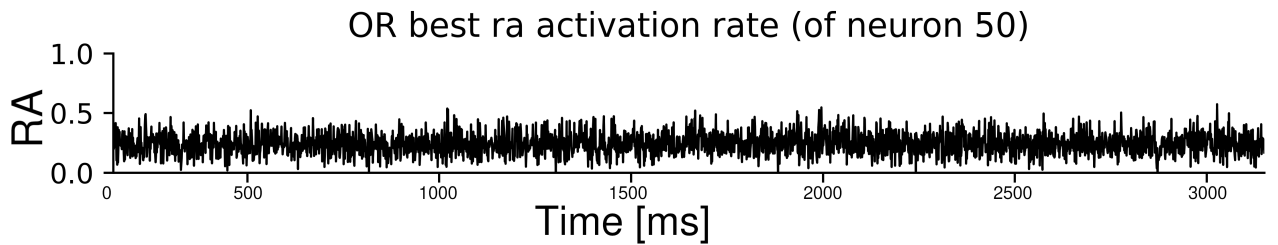


**Figure 4.3:** Behavior of an olfactory receptor with the Poisson train, time [ms] on the  $x$ -axis and  $r_{active}$  on the  $y$ -axis.

Parameter	Value
$A$	$1.8 \times 10^{-2}$ mV
$l$	0.5
$c$	0.7
$\sigma$	5
$\tau$	2 ms

**Table 4.2:** Parameters used for generating the Poisson trains.

a Poisson train with a given rate, as described in section 3.1.2.3.

The effect of the Poisson trains for 6 second of the simulation is shown in figure 4.3. The long-term effect cannot be fully appreciated with this plot, but it can be seen how the Poisson train causes an increase in the equilibrium  $r_{active}$  and at the same time an increase in the fluctuations.

The parameters for the Poisson trains were found performing simulation varying one parameter at a time and keeping fixed the others (shown in figure 4.4), and are shown in table 4.2.

In particular:

- $A$  is the amplitude of the Poisson trainn.
- $l$  is the propensity for a spike event to be generated.
- $c$  is the probability for an event in the template to be added to each Poisson train or for an event in the Poisson train to be removed.
- $\sigma$  is the length of the exponential kernel.
- $\tau$  is the time constant of the exponential kernel.

The correlated input has to be balanced with the white noise. It is their interplay that generates the desired correlation in the populations. In particular looking at figure 4.5, it can be seen how if the white noise is too strong, the effect of the correlated input becomes negligible and it isn't able to increase correlation anymore.

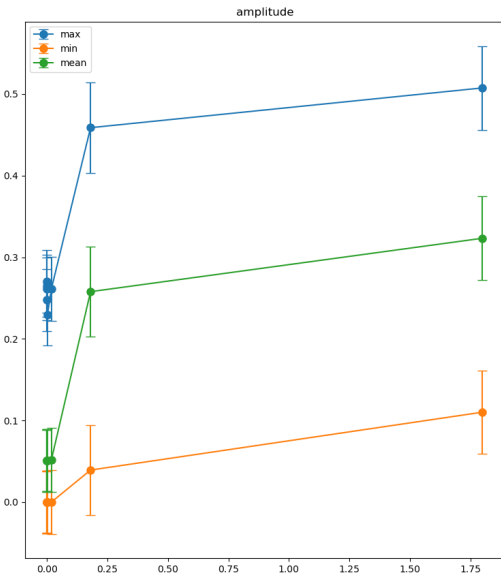
### 4.1.2 Neurons

The membrane potential of neurons evolves according to equation 3.16.

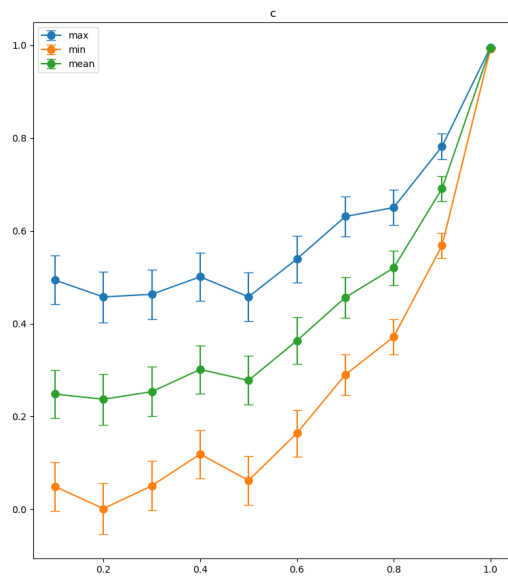
In figure 4.6 the behavior of the neurons is shown for 60 seconds of spontaneous activity. The spikes do not show in the membrane potential because of how GeNN saves the data. In fact, a spike is not saved as a change in the membrane potential, but as a separate event in a different memory buffer. This figure shows how the membrane potential of the neurons is affected by the activity of the olfactory receptors: an increase in their

#### 4.1. BEHAVIOR OF THE COMPONENTS

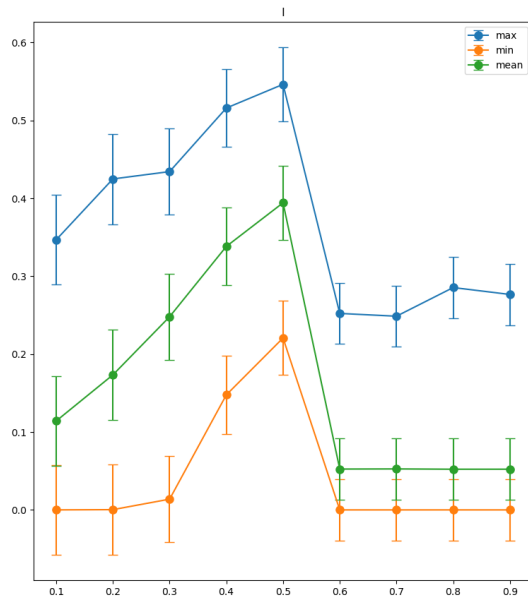
---



(a) Effect of the amplitude of the Poisson trains on the average (green), maximum (blue), and minimum (orange) correlation in the projection neurons. Amplitude [mV] on the  $x$ -axis and correlation on the  $y$ -axis.



(b) Effect of the probability to add events from a template or remove them from the Poisson trains on the average (green), maximum (blue), and minimum (orange) correlation in the projection neurons. Probability on the  $x$ -axis and correlation on the  $y$ -axis.

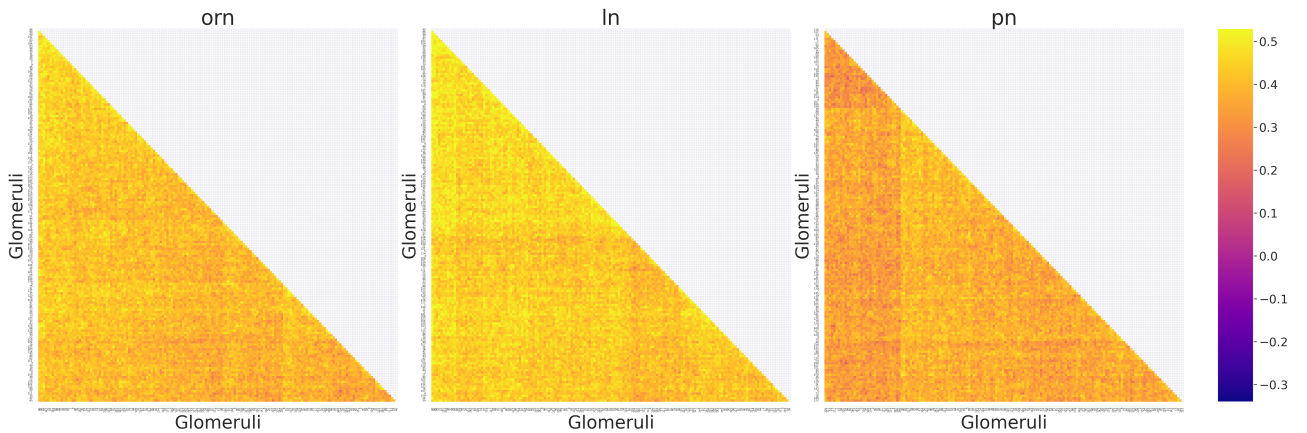


(c) Effect of the propensity to generate a spike event in the Poisson trains on the average (green), maximum (blue), and minimum (orange) correlation in the projection neurons. Propensity on the  $x$ -axis and correlation on the  $y$ -axis.

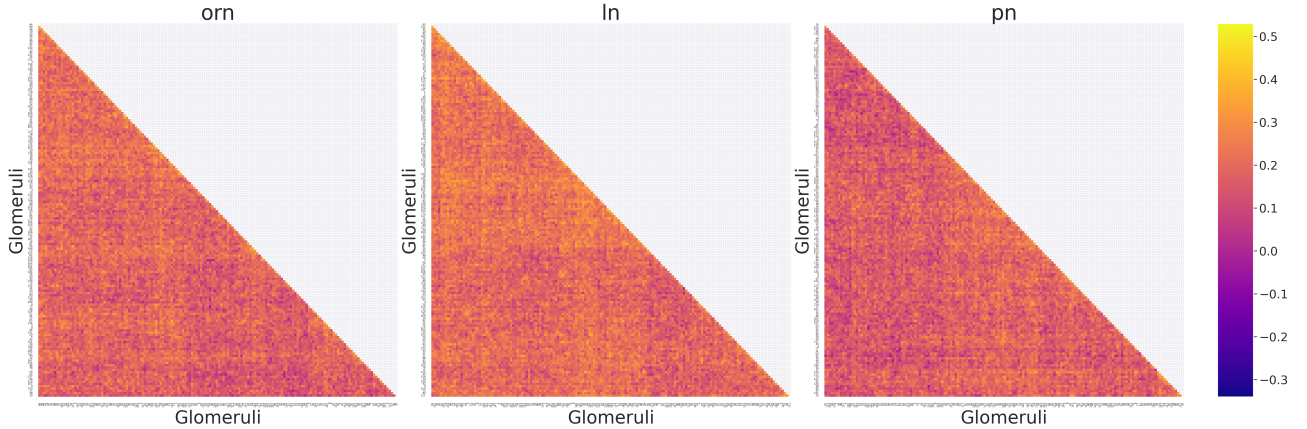
**Figure 4.4:** Effect of the parameters of the Poisson trains on the average (green), maximum (blue), and minimum (orange) correlation in the projection neurons. A simulation is performed for every value of each parameter that is being explored, while the others are being kept fixed.

## 4.1. BEHAVIOR OF THE COMPONENTS

---



**(a)** Correlation between different neuron population with the optimal white noise intensity ( $D(t) = 3 \cdot 10^{-5}$ ). Average correlation per population  $\overline{Corr}_{ORN} = 0.35$ ,  $\overline{Corr}_{LN} = 0.32$ ,  $\overline{Corr}_{PN} = 0.32$



**(b)** Correlation between different neuron population with a tenfold increase in white noise intensity ( $D(t) = 3 \cdot 10^{-4}$ ). Average correlation per population  $\overline{Corr}_{ORN} = 0.13$ ,  $\overline{Corr}_{LN} = 0.10$ ,  $\overline{Corr}_{PN} = 0.11$

**Figure 4.5:** Effect of the interplay between white noise and correlated input on the correlation between different neuron populations. Inhibitory synapses are reduced by a factor of 100 so that they have a negligible effect on correlation.

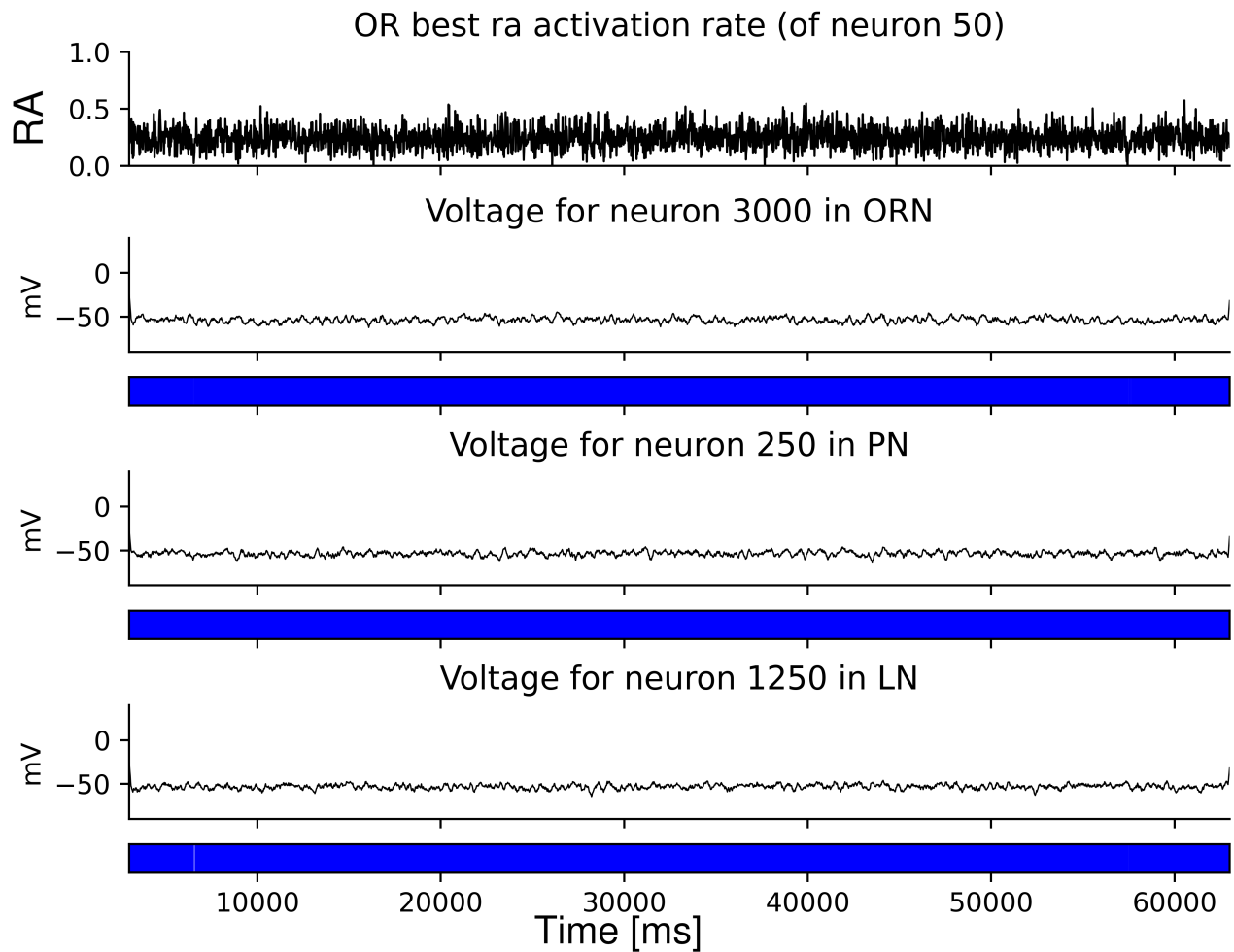


**Figure 4.6:** 60 seconds of spontaneous activity of neurons with no odor input. From top to bottom: activation rate for an olfactory receptor, membrane potential of a random olfactory receptor neuron connected to the olfactory receptor, time series of the spike for the ORN, membrane potential of a random projection neuron and the spike train for the corresponding neuron, membrane potential for a local neuron and its spike train. Time [ms] on the x-axis.

#### 4.1. BEHAVIOR OF THE COMPONENTS

---

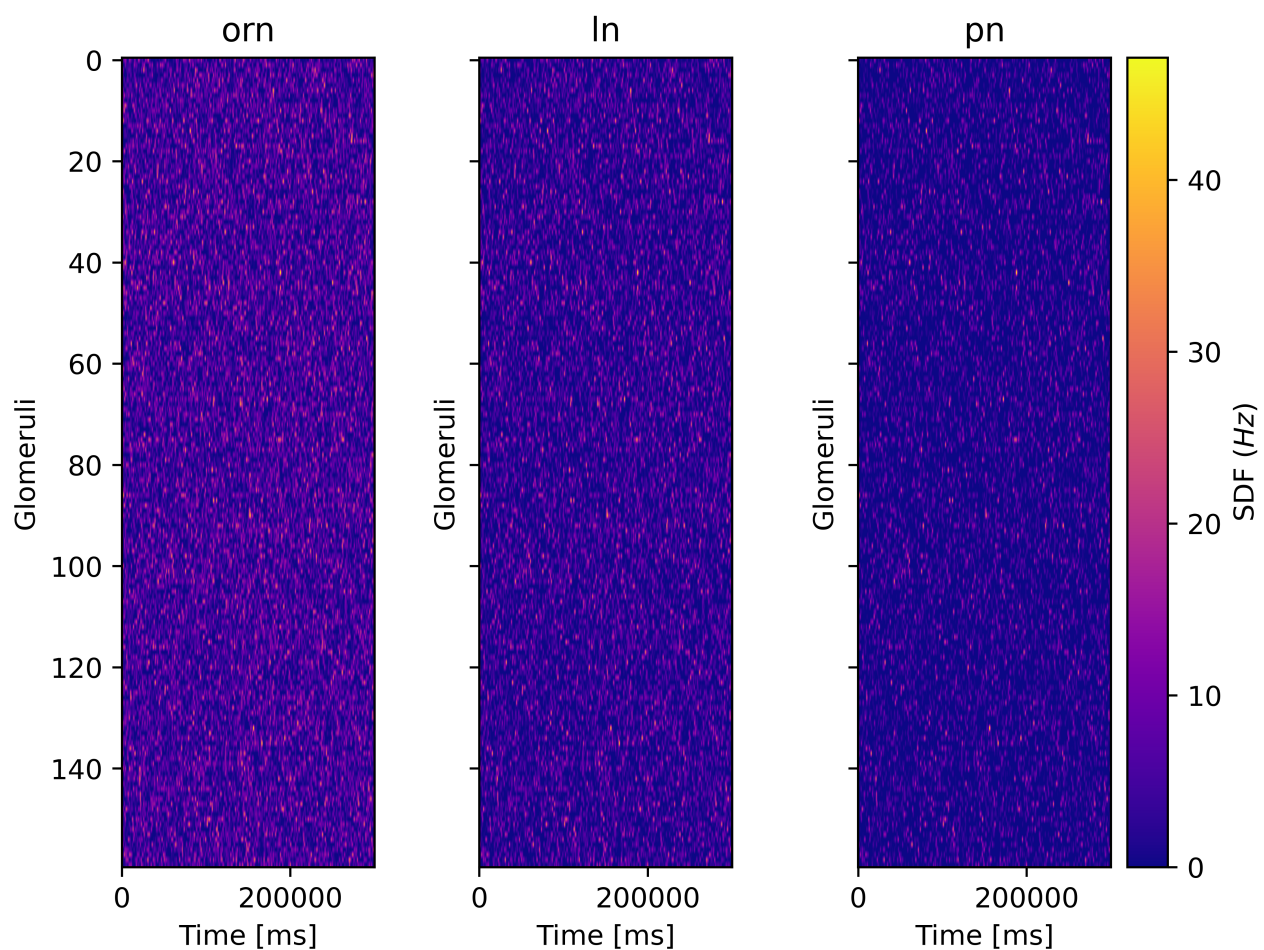


**Figure 4.7:** 60 seconds of spontaneous activity of neurons with no odor input. From left to right spike density matrix for olfactory receptor neurons, local neurons and projection neurons averaged over glomeruli.

#### 4.1. BEHAVIOR OF THE COMPONENTS

---

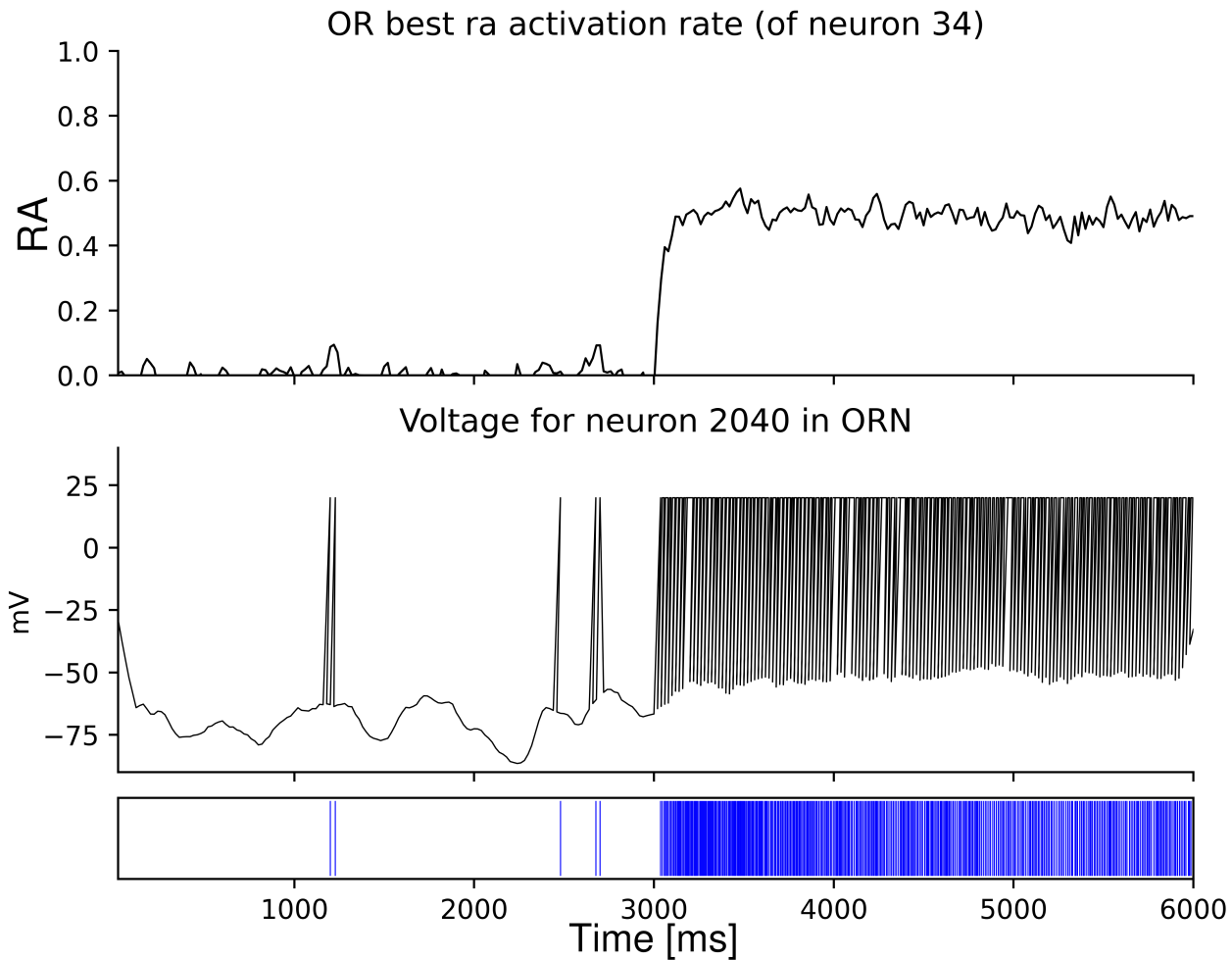


**Figure 4.8:** 6 seconds of activity of neurons with an odor presented to the network at 3 second. From top to bottom: activation rate for an olfactory receptor, membrane potential of a random olfactory receptor neuron connected to the olfactory receptor, time series of the spike for the ORN. Time [ms] on the  $x$ -axis

activity is directly related to an increase in the firing rate of the neurons downstream in the network.

A better way to visualize this is through the spike density matrix, as in figure 4.7. This figure shows the average firing rate of a glomerulus divided by neuron population. It can be seen how the firing rate is similar across glomeruli since no olfactory receptor is activated by an odor.

The fact that the firing rate increases with the activity of the olfactory receptor can be better appreciated in figure 4.8: when the odor is presented at second 3 the activity of the corresponding ORN increases significantly.

This can be further noticed by looking at the spike density matrix (figure 4.9). The figure shows how the glomerulus activated by this particular odor is much more active than the other. The activity of the network shows an initial increase in firing rate before it reaches an equilibrium.

The parameters for the neurons are shown in table 4.3.

#### 4.1.3 Synapses

The model has two types of synapses:

#### 4.1. BEHAVIOR OF THE COMPONENTS

---

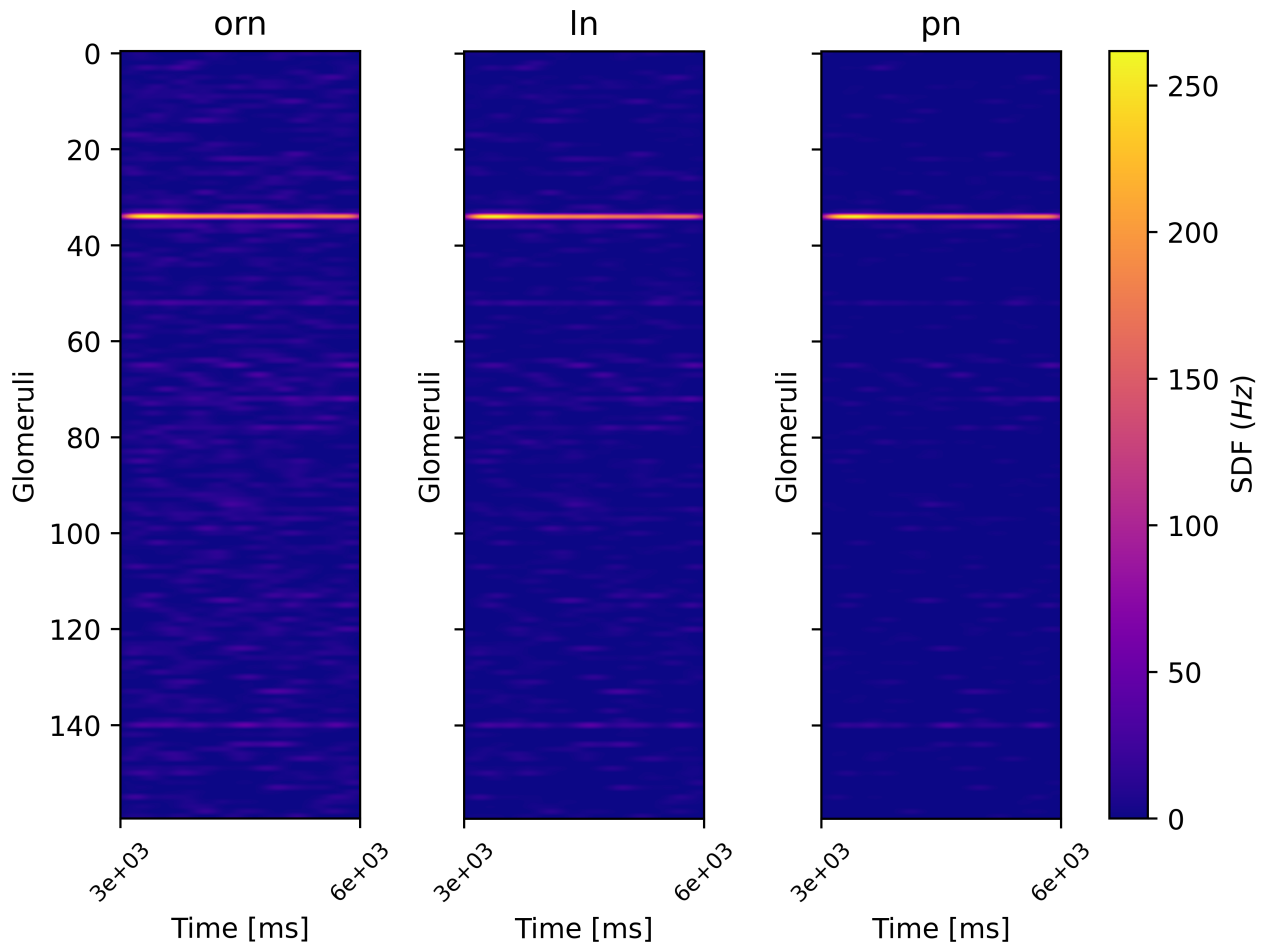


**Figure 4.9:** 3 seconds of activity of neurons with an odor presented to the network during all the 3 seconds.

Olfactory receptor neurons		Projection neurons		Local neurons	
Parameter	Value	Parameter	Value	Parameter	Value
$C$	1 mF	$C$	1 mF	$C$	1 mF
$V_{reset}$	-70 mV	$V_{reset}$	-70 mV	$V_{reset}$	-70 mV
$V_{thresh}$	-40 mV	$V_{thresh}$	-40 mV	$V_{thresh}$	-40 mV
$V_{leak}$	-60 mV	$V_{leak}$	-60 mV	$V_{leak}$	-60 mV
$V_{adapt}$	-70 mV	$V_{adapt}$	-70 mV	$V_{adapt}$	-70 mV
$g_{leak\ 0}$	0.01 S	$g_{leak\ 0}$	0.01 S	$g_{leak\ 0}$	0.01 S
$g_{adapt\ 0}$	0.0015 S	$g_{adapt\ 0}$	0.0015 S	$g_{adapt\ 0}$	0.0015 S
$r_{scale}$	10	$r_{scale}$	10	$r_{scale}$	10
$\tau_{adapt}$	1000 ms	$\tau_{adapt}$	1000 ms	$\tau_{adapt}$	1000 ms
$T_{ref}$	36 °C	$T_{ref}$	36 °C	$T_{ref}$	36 °C
$T$	30 °C	$T$	30 °C	$T$	30 °C
$Q$	1.1	$Q$	1.1	$Q$	1.1
$\sigma$	$\frac{1.4}{\sqrt{dt}}$	$\sigma$	$\frac{1.4}{\sqrt{dt}}$	$\sigma$	$\frac{1.4}{\sqrt{dt}}$

**Table 4.3:** Parameters for the neurons.

## 4.1. BEHAVIOR OF THE COMPONENTS

---

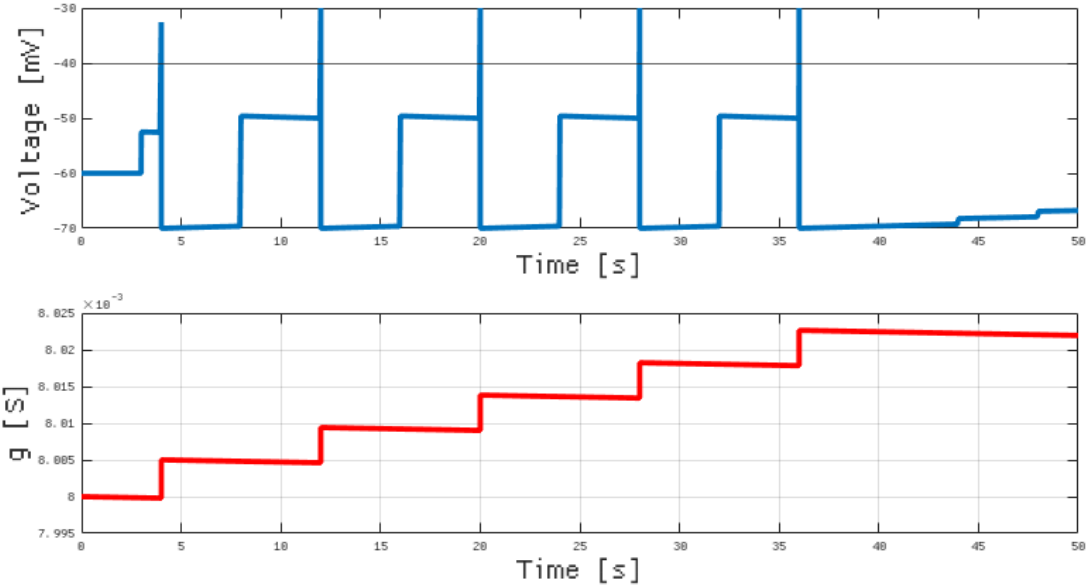


**Figure 4.10:** Behavior of the conductance of an excitatory synapse (bottom) in relation to the activity of the presynaptic neuron (top).

- Excitatory.
- Inhibitory.

Both are modeled as conductance-based synapses according to the static pulse model with an exponential decay as in equations 3.21 and 3.22. There are two differences in how the inhibitory and excitatory synapses are modeled.

### 4.1.3.1 Excitatory synapses

Excitatory synapses form sparse directional connections between:

- Olfactory receptor neurons and projection neurons.
- Olfactory receptor neurons and local neurons.
- Projection neurons and local neurons.

Where each neuron of the source population is connected with a random neuron of the target population.

The behavior of the model on the changes in conductance in relation to the activity of the presynaptic neuron can be seen in figure 4.10. It can be seen how the more the presynaptic neuron spikes the faster this conductance increases, facilitating the ability of the postsynaptic neuron to spike.

The parameters for the excitatory conductances are found in table 4.4.

### 4.1.3.2 Inhibitory synapses

Inhibitory synapses form dense directional connections between:

- Local neurons and projection neurons.

## 4.2. RESPONSE TO ODOURS

ORN to PN		ORN to LN		PN to LN	
Parameter	Value	Parameter	Value	Parameter	Value
$g$	0.008 S	$g$	0.008 S	$g$	0.001 S
$E$	0 mV	$E$	0 mV	$E$	0 mV
$\tau$	10 ms	$\tau$	10 ms	$\tau$	10 ms

**Table 4.4:** Parameters for the excitatory synapses.

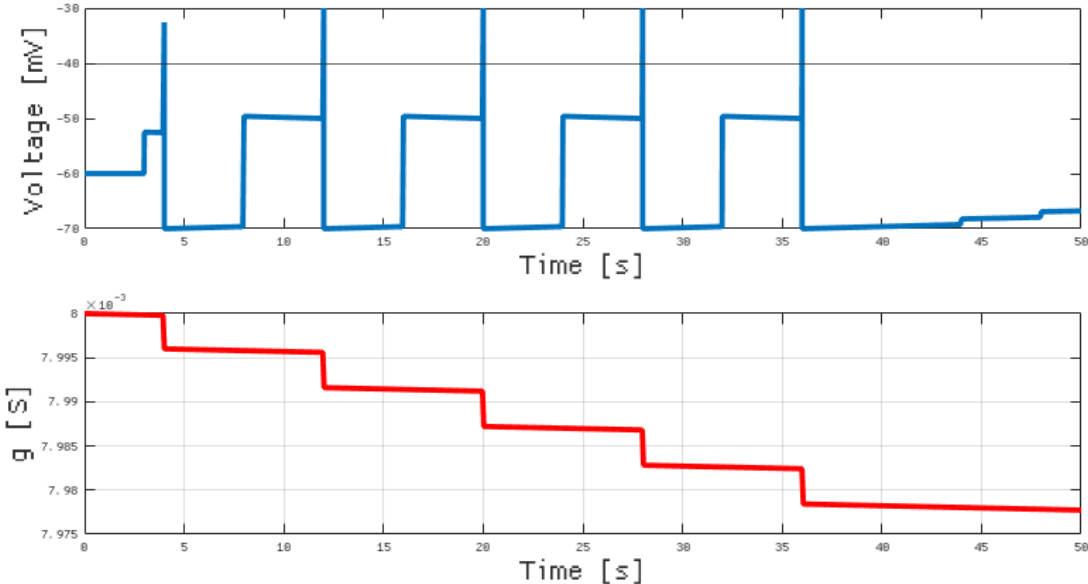


**Figure 4.11:** Behavior of the conductance of an inhibitory synapse (bottom) in relation to the activity of the presynaptic neuron (top).

- Local neurons and local neurons.

Where each neuron of the source population is connected with all the neurons of the target population.

The behavior of the model on the changes in conductance in relation to the activity of the presynaptic neuron can be seen in figure 4.11. It can be seen how the more the presynaptic neuron spikes the faster the conductance decreases, making it harder for the postsynaptic neuron to spike.

The parameters for the inhibitory conductances are found in table 4.5.

## 4.2 Response to odours

As described in section 3.1.2.1, the odors are described as Gaussian profiles, determining the ability of the molecule to bind each of the 160 olfactory receptors. Because of these odors are described by four parameters:

LN to PN		LN to LN	
Parameter	Value	Parameter	Value
$g$	$5.5 \times 10^{-5}$ S	$g$	$2.0 \times 10^{-5}$ S
$E$	-80 mV	$E$	-80 mV
$\tau$	20 ms	$\tau$	20 ms

**Table 4.5:** Parameters for the inhibitory synapses.

	$A$	$\sigma$
Isoamyl acetate	0.8	3
Geosmin	4.4	10
Other	$x \sim \mathcal{N}(1.5, 0.5) : x \in [0, 4.0]$	$x \sim \mathcal{N}(3, 0.5) : x \in [1.5, \infty[$

**Table 4.6:** Parameters for the odors.

- $c$ : the concentration of the odor.
- $x$  or the midpoint: the olfactory receptor where the mean of the Gaussian profile is located.
- $A$ : the amplitude of the profile, determining the maximum value of the profile.
- $\sigma$ : the standard deviation of the profile, determining the width of the profile.

Besides two odors for which this Gaussian profile was already determined in [39],  $A$  and  $\sigma$  are sampled from bounded Gaussian distributions.

A full list of odor parameters can be found in table 4.6. It can be noted that the isoamyl acetate (IAA) has a lower standard deviation than geosmin, meaning that it will tend to activate less olfactory receptors than geosmin.

The response of the network to IAA and geosmin can be seen respectively in figures 4.12 and 4.13. It can be noted how geosmin, thanks to its higher  $\sigma$  activates more glomeruli, while IAA activates fewer glomeruli, but with a higher firing rate. It is important to note that in this case both the temperature-dependent white noise and the Poisson trains were not included in the model, as done in [48]. They were excluded from this simulation as their impact on the firing rate of the neurons was not significant, and they were not necessary to reproduce the biological behavior with enough accuracy.

## 4.3 Awake state

The awake state is represented by the model described in section 4.1. The parameters for the neurons are the ones in 4.3, while the parameters for the synapses are the ones in 4.4 and in 4.5. The model is left to evolve without any odor input, with only the temperature-dependent white noise.

Figure 4.14 shows the activity of the glomeruli in the awake state without the Poisson trains. It is visible the effect of the inhibitory synapses on the projection neurons, as the average firing rate of the projection neurons is lower than the one of the olfactory receptor neurons.

Figure 4.15 shows the correlation between the glomeruli in the awake state without the Poisson trains. It can be seen how the correlation in the projection neurons tends to be lower than the one in the olfactory receptor neurons, due to the inhibitory synapses that decouple the projection neurons from the input in the olfactory receptor neurons.

### 4.3.1 Adding the Poisson trains

The Poisson trains are added to the model, to explore what is the effect of a correlated input on the activity of the antennal lobe.

The Poisson trains have a strong effect on the activity of the antennal lobe, as shown in figure 4.16. It can be seen that when Poisson trains are added, although the firing rate of the olfactory receptor neurons doesn't change, the activity of the projection neurons goes almost completely to zero.

This is due to the strong synaptic inhibition that the projection neurons receive from the local neurons: the

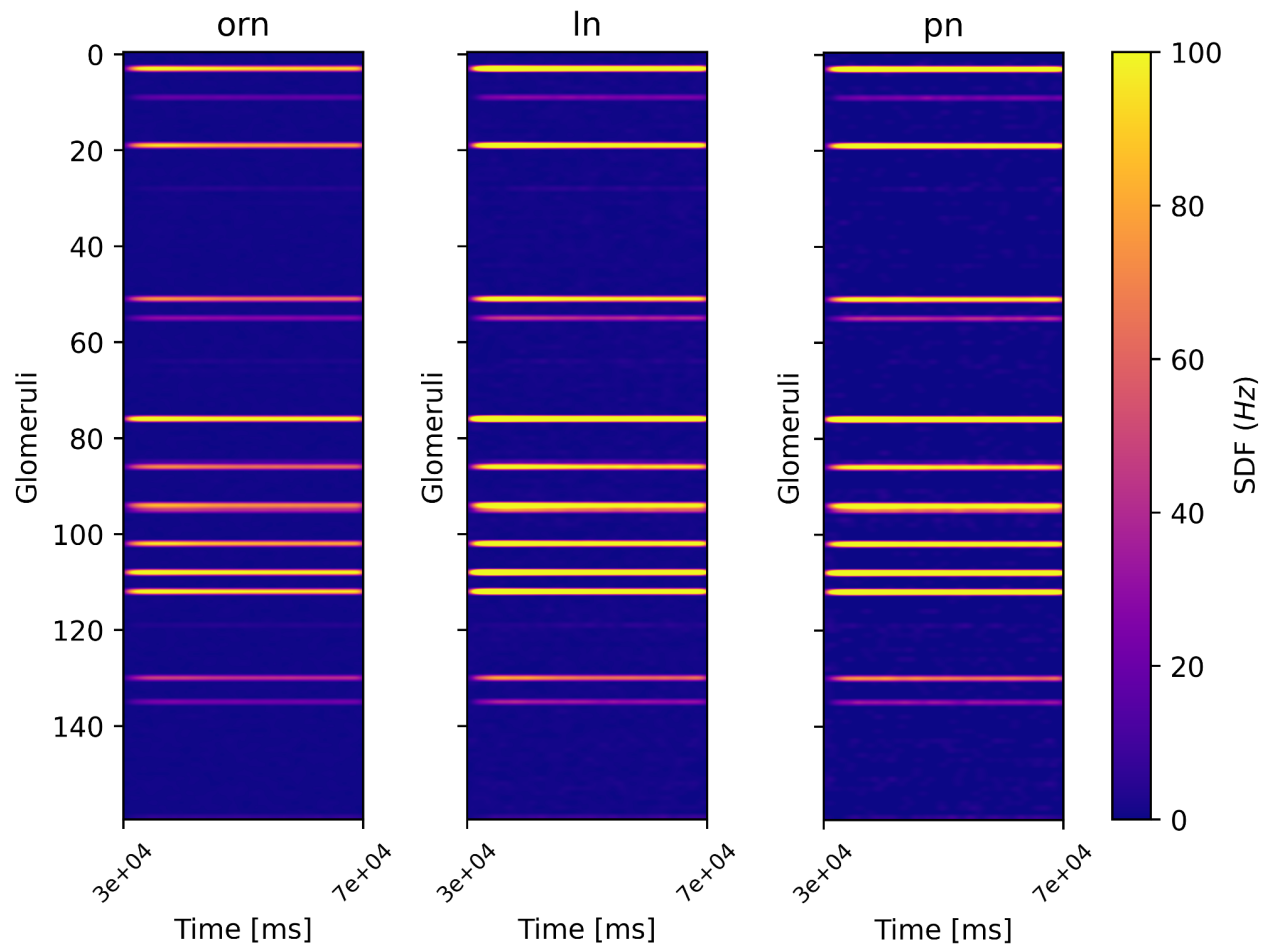


**Figure 4.12:** Spike density matrix of the antennal lobe in response to isoamyl acetate (concentration  $10^{-3} \text{ mol L}^{-1}$ ). 3 s of simulation.

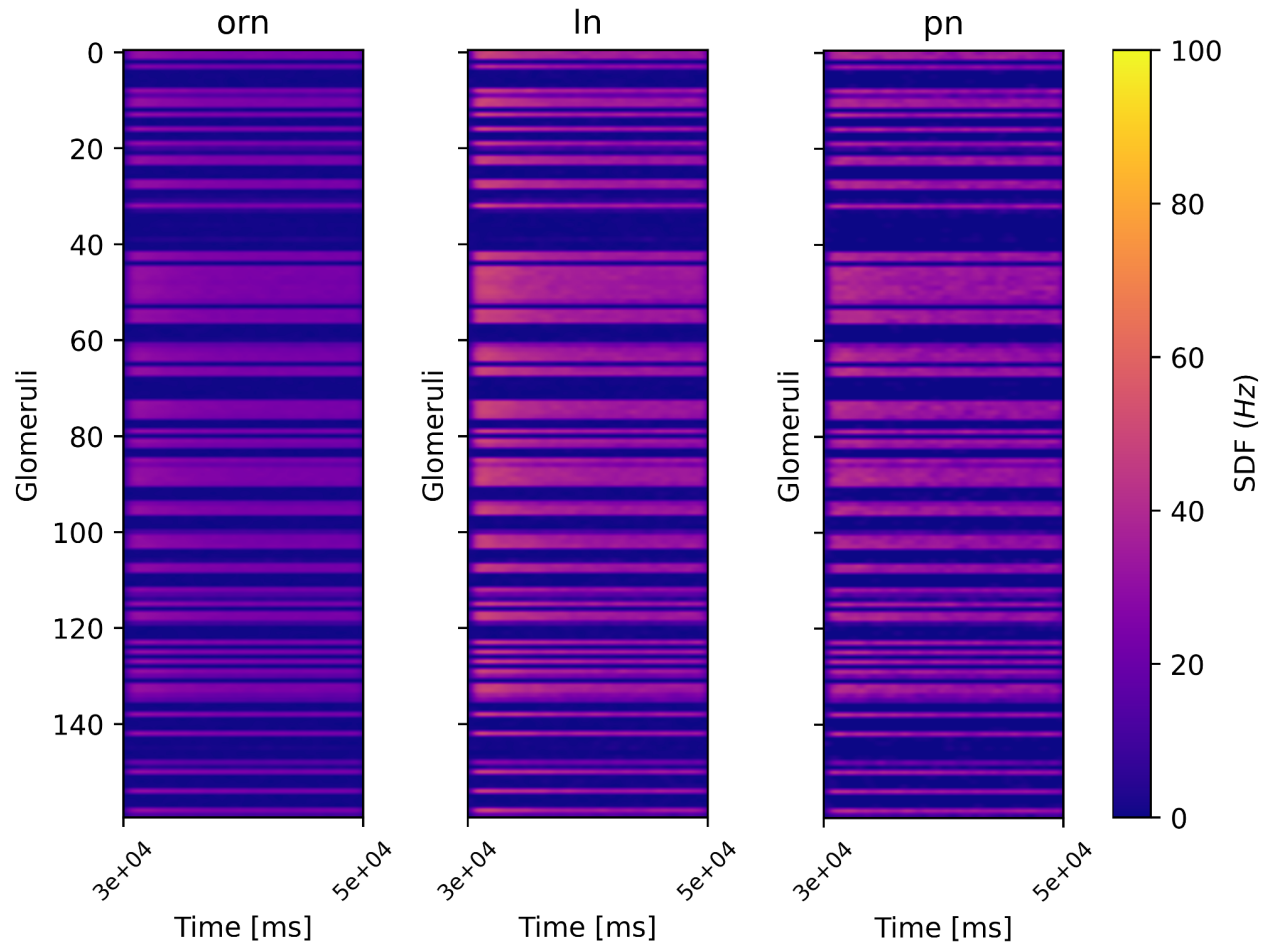


**Figure 4.13:** Spike density matrix of the antennal lobe in response to geosmin (concentration  $10^{-3} \text{ mol L}^{-1}$ ). 3 s of simulation.

### 4.3. AWAKE STATE

---

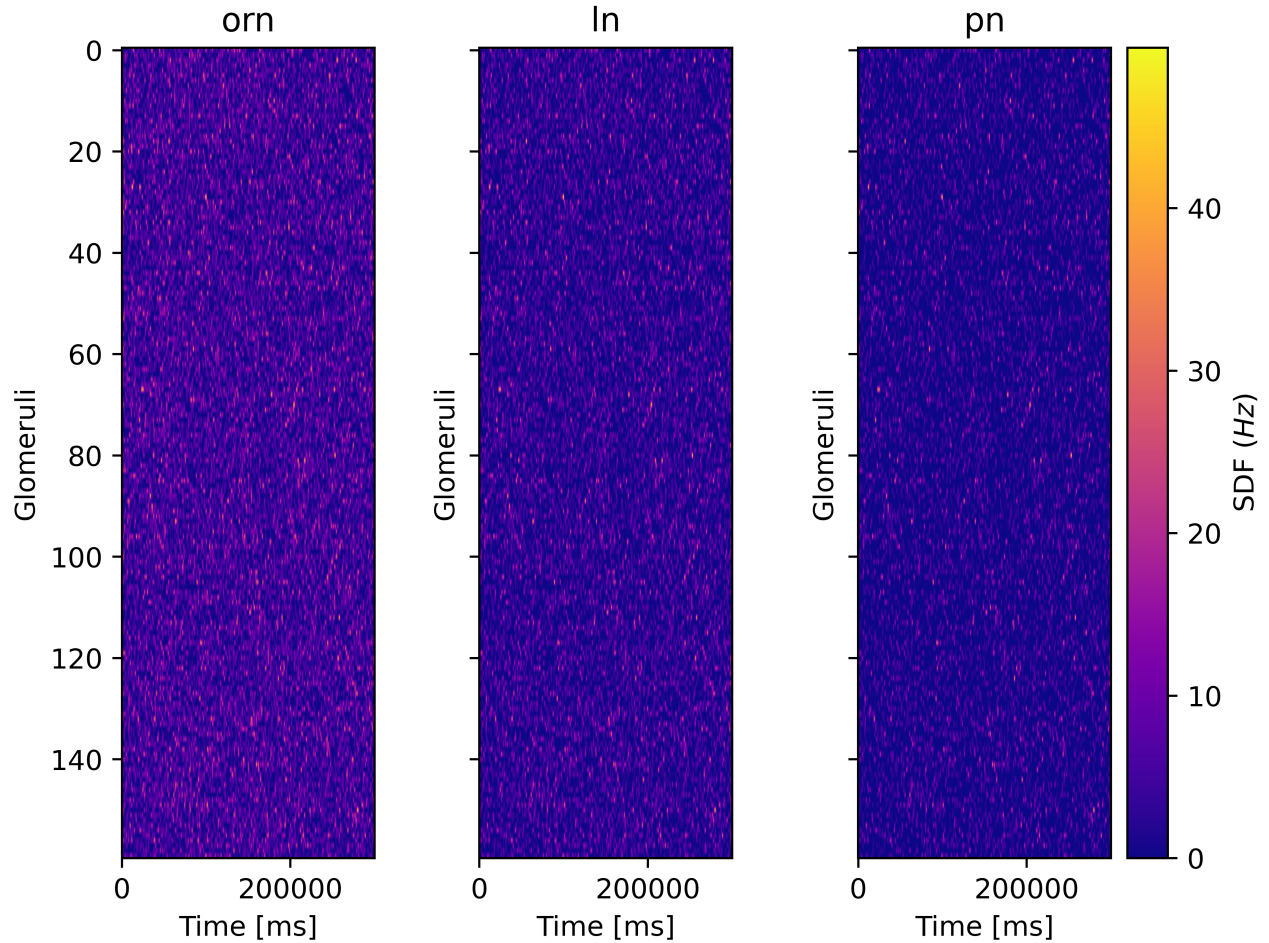


**Figure 4.14:** Spike density matrix of the spontaneous activity of the antennal lobe without the Poisson trains. 60 s of simulation.

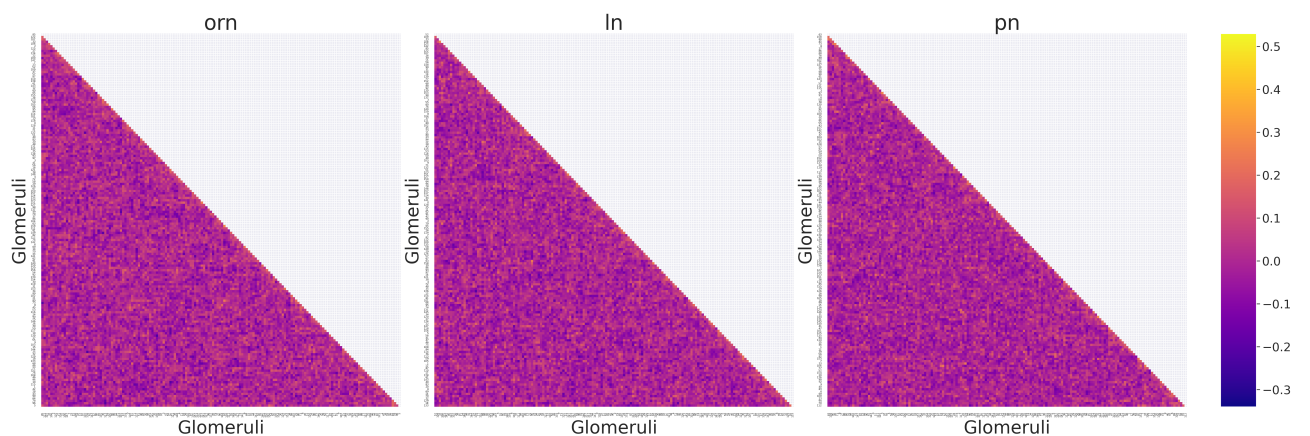


**Figure 4.15:** Correlation of the spontaneous activity of the antennal lobe without the Poisson trains. 60 s of simulation. Average correlation per population  $\overline{Corr}_{ORN} = 0.007$ ,  $\overline{Corr}_{LN} = 0.003$ ,  $\overline{Corr}_{PN} = 0.001$ .

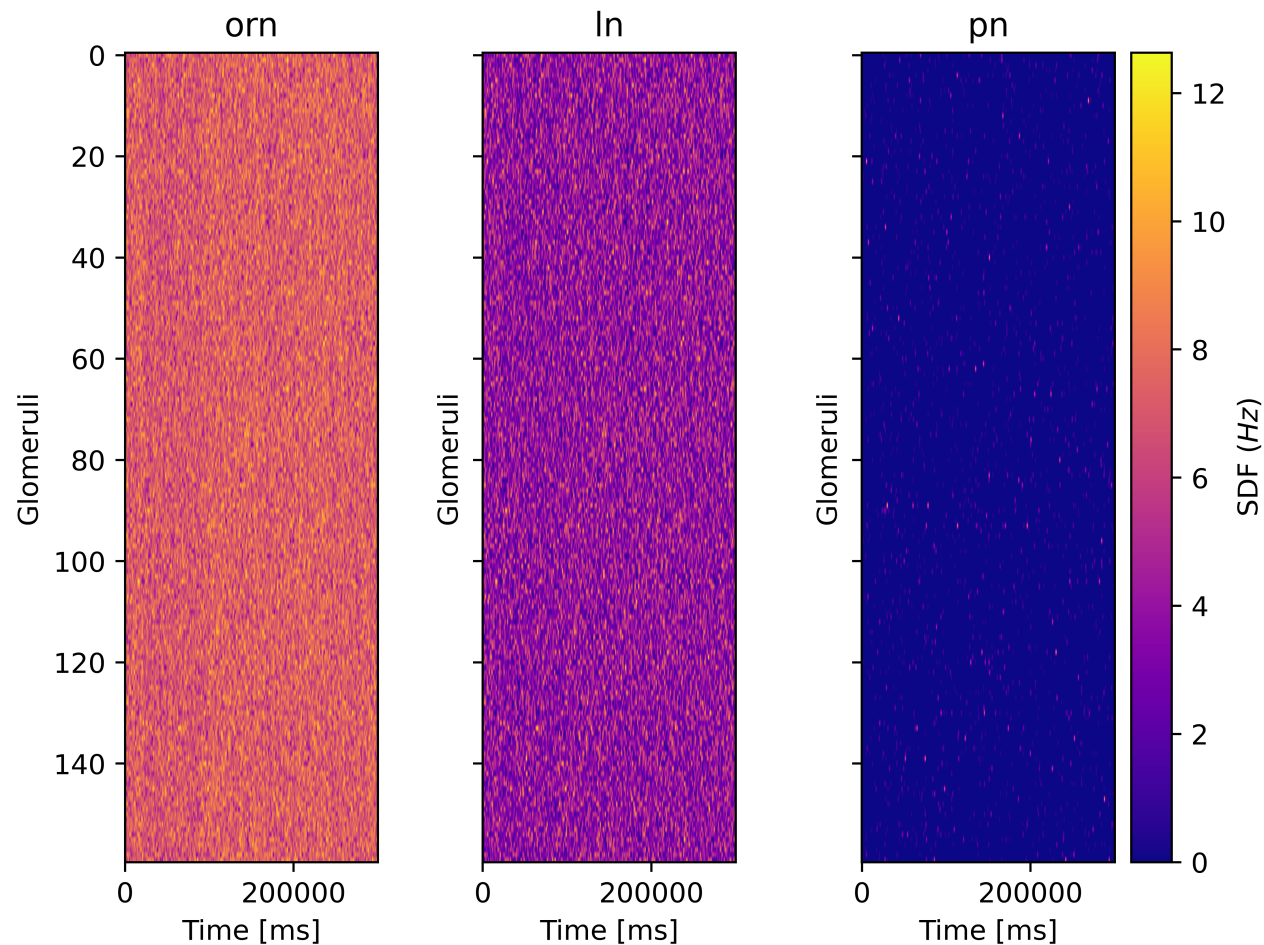


**Figure 4.16:** Spike density matrix of the spontaneous activity of the antennal lobe with the Poisson trains. 60 s of simulation.

#### 4.4. ASLEEP STATE

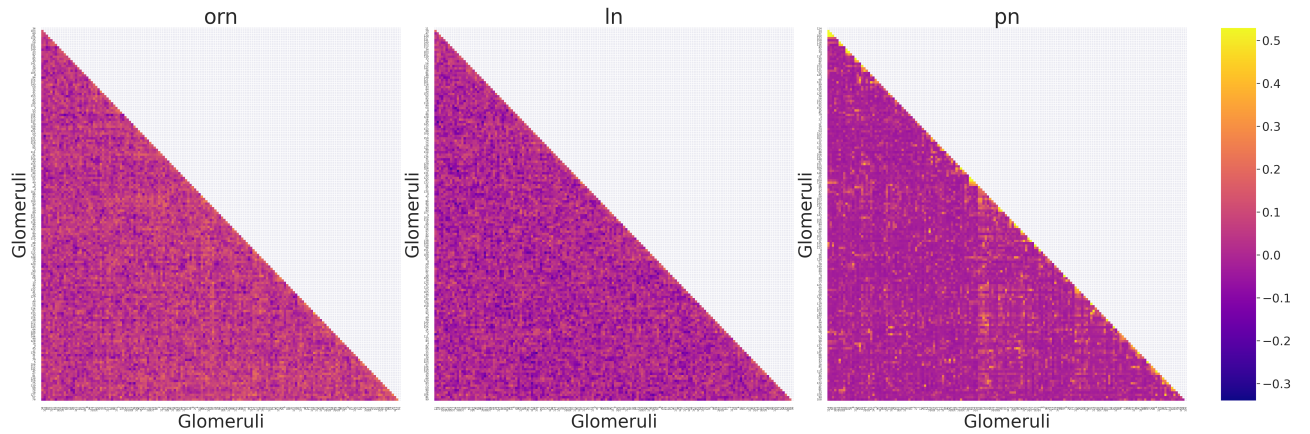


**Figure 4.17:** Correlation of the spontaneous activity of the antennal lobe with the Poisson trains. 60 s of simulation. Average correlation per population  $\text{Corr}_{ORN} = 0.04$ ,  $\text{Corr}_{LN} = 0.006$ ,  $\text{Corr}_{PN} = 0.007$

	Awake	Halved	Quarter	Tenth	Hundredth
Reducing factor	1	0.5	0.25	0.1	0.01
$g_{LN \rightarrow LN}$	$2.0 \times 10^{-5}$ S	$1.0 \times 10^{-5}$ S	$5.0 \times 10^{-6}$ S	$2.0 \times 10^{-6}$ S	$2.0 \times 10^{-7}$ S
$g_{LN \rightarrow PN}$	$5.5 \times 10^{-5}$ S	$2.75 \times 10^{-5}$ S	$1.375 \times 10^{-5}$ S	$5.5 \times 10^{-6}$ S	$5.5 \times 10^{-7}$ S

**Table 4.7:** Reduction of the inhibitory synapses to find the asleep state

decoupling effect of the inhibitory part of the system is too strong to allow for activity in the projection neurons and seems to have a much greater effect when the output coming from the olfactory receptor neurons is correlated.

At the same time due to the inhibitory effect of the local neurons, the correlation between the projection neurons across glomeruli is higher than the system without the correlated input. This is not due to the correlation present in the input, but rather due to the fact that the activity of the projection neurons becomes so inhibited that its correlation increases: neurons that never fire have a completely correlated activity. This is further supported by the fact that this is the only simulation where the correlation of the projection neurons is higher than the one of the olfactory receptor neurons. Another evidence of this is the increased variability in the correlation of the Projection neurons (figure 4.17), suggesting that the activity of the projection neurons per glomerulus is more inhibited for those glomeruli that tend to receive as input more correlated Poisson trains.

Moreover, this suggests that there is no correlated input in the awake state and that it can be found only in the asleep state.

## 4.4 Asleep state

Finding the correct parameters that describe the asleep state required two modifications from the awake state:

- Introducing a correlated input in the form of Poisson trains.
- Reducing the strength of the inhibitory synapses.

The optimal Poisson trains were already found in 4.1.1.2, so the only thing left to explore is the effect of the inhibitory synapses on the coupling of the system. To do so several simulations have been run with different reducing factors for the inhibitory synapses. The new simulations with the corresponding value of the inhibitory synapses are shown in table 4.7.

#### 4.4. ASLEEP STATE

---

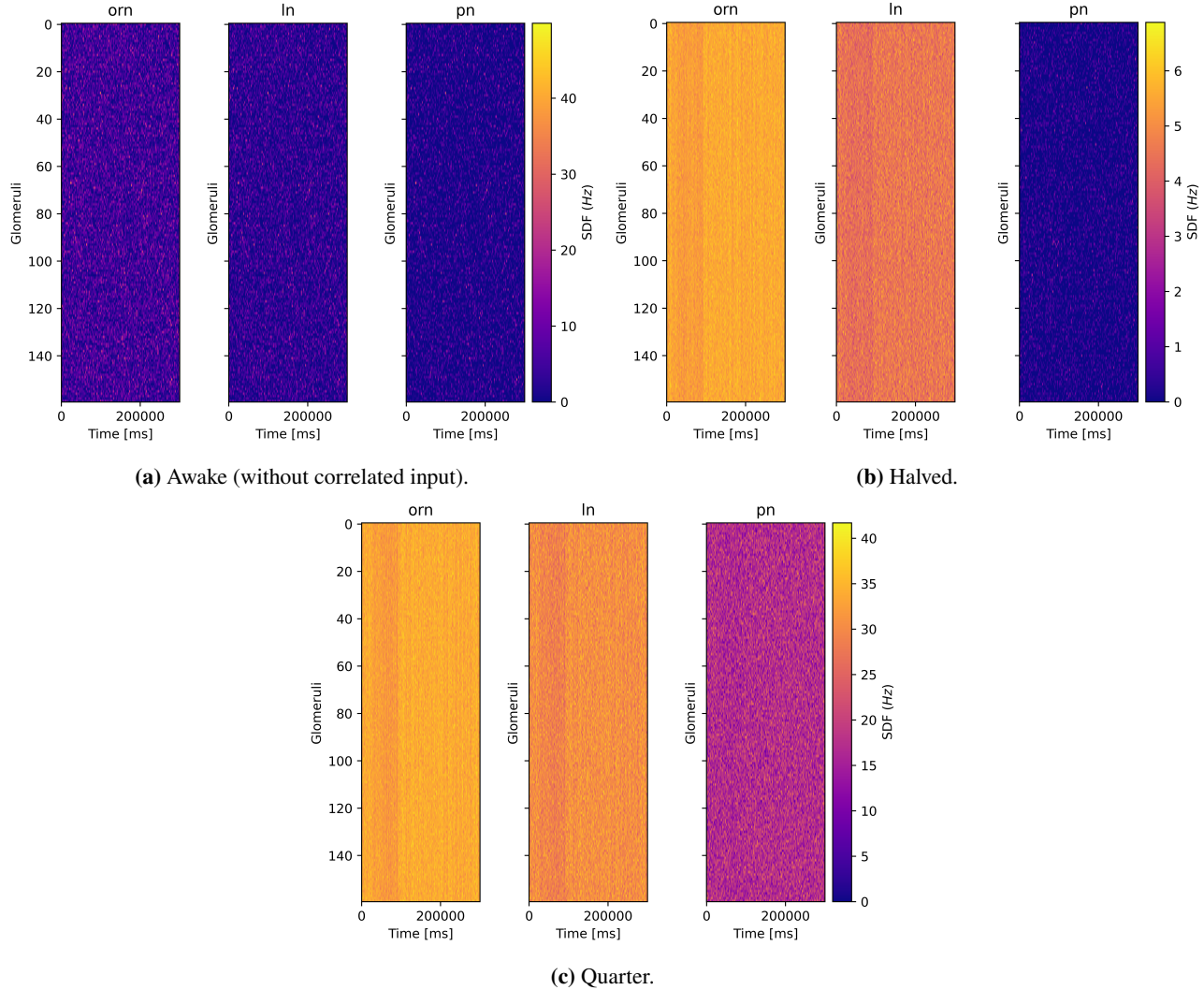


**Figure 4.18:** Spike density matrix of the spontaneous activity of the antennal lobe with the Poisson trains and different reduction of the inhibitory synapses. 60 s of simulation.

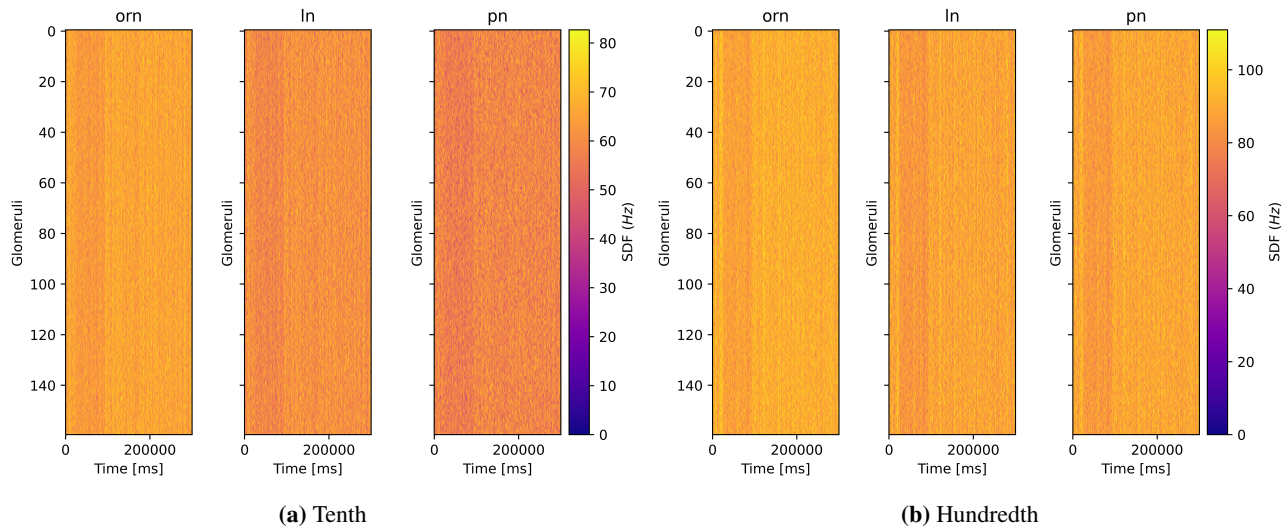


**Figure 4.19:** Spike density matrix of the spontaneous activity of the antennal lobe with the Poisson trains and different reduction of the inhibitory synapses. 60 s of simulation.

## 4.5. COMPARISON BETWEEN AWAKE AND ASLEEP STATES

---

The resulting spike density matrices are shown in figures 4.18 and 4.19. It can be noted how the coupling of the network increases as the inhibitory synapses are reduced. In particular, it can be seen how the activity of the projection neurons increases and becomes increasingly similar to the one of the olfactory receptor neurons as the inhibitory synapses are reduced and becomes almost the same in the “Hundredth” simulation, suggesting that reducing the inhibitory synapses by a factor of 100 makes their effect on the network negligible.

The same effect can be seen in the correlation matrices, shown in figures 4.20 and 4.21.

From the correlation figures (4.20 and 4.21), it can be seen how the difference between the correlation of the olfactory receptor neurons and the projection neurons reduces with the inhibitory synapses strength (figure 4.22).

Figure 4.23 shows the correlation between glomeruli in the projection neurons, averaged over several simulations. It can be seen that there is a small decrease in correlation between the “Halved” and the “Quarter” simulation that can be ascribed to statistical error, while a kink is found in the “Tenth” simulation, suggesting that the inhibitory synapses stop to have a significant impact on the network already at a reduction factor of 10.

Looking instead at figure 4.22, the amount of correlation that it is lost due to the effect of the inhibitory synapses can be seen. In particular, in the awake condition and in the “Hundredth” simulation almost no correlation is lost. This is due to two different reason: in the awake condition there is no correlated input, while in the “Hundredth” the inhibitory synapses have stopped having an impact on the activity of the network. Moreover it can be observed that this correlation difference decreases from the “Halved” to the Hundredth”, suggesting that the weaker the inhibitory synapses are, the less able the network is to filter out correlated input coming into the synapses. From this it can be inferred that the inhibitory synapses decouple the activity of the olfactory receptor neurons and the projection neurons, and their effect is particularly significant when the input of the network presents a level of correlation. The correlation change between the populations approaches zero in the “Hundredth” simulation, again supporting the fact that the inhibitory synapses are negligible in this condition.

## 4.5 Comparison between awake and asleep states

To find which of the different inhibitory synapses reduction is the best to simulate the asleep state, the features described in section 3.2.5 are extracted from the different simulations and compared. These features can be classified into two categories: one set of features will regard the distribution of the activity of the projection neurons, while the other set will regard the functional connectivity of the network.

Experimental results (shown in figure 4.24) suggest a shift in the distribution of the different features between the awake and the asleep state. In particular, the different distributions of the features extracted from the asleep state suggest that the asleep state is characterized by a more strongly functionally connected network with greater variability.

The same features are extracted from the different simulations and compared with the ones extracted from the awake state (figures 4.25, 4.26, 4.27 and 4.28). The best fit to experimental data seems to be the one between the awake state and the “Quarter” simulation.

Something interesting that can be seen from the figures is that the difference in features between the different values of inhibitory synapses doesn’t seem to change linearly with the change in inhibition. This behavior is explored in figures 4.29, 4.30, 4.31, 4.32. It can be seen how for all the features beside standard deviation (plot 4.29a), skewness (plot 4.29b) and kurtosis (plot 4.29c) there is a change in directionality of the mean of the feature. This non-linear effect suggests that, as expected, the inhibitory synapses perform a non-linear function in the network, changing how the input is represented. Furthermore, there is no significant difference in features’ means between the “Tenth” and “Hundredth” simulations, suggesting that the inhibitory synapses reduction by a factor of 10 is great enough to make the local neurons unable to perform their function.

#### 4.5. COMPARISON BETWEEN AWAKE AND ASLEEP STATES

---

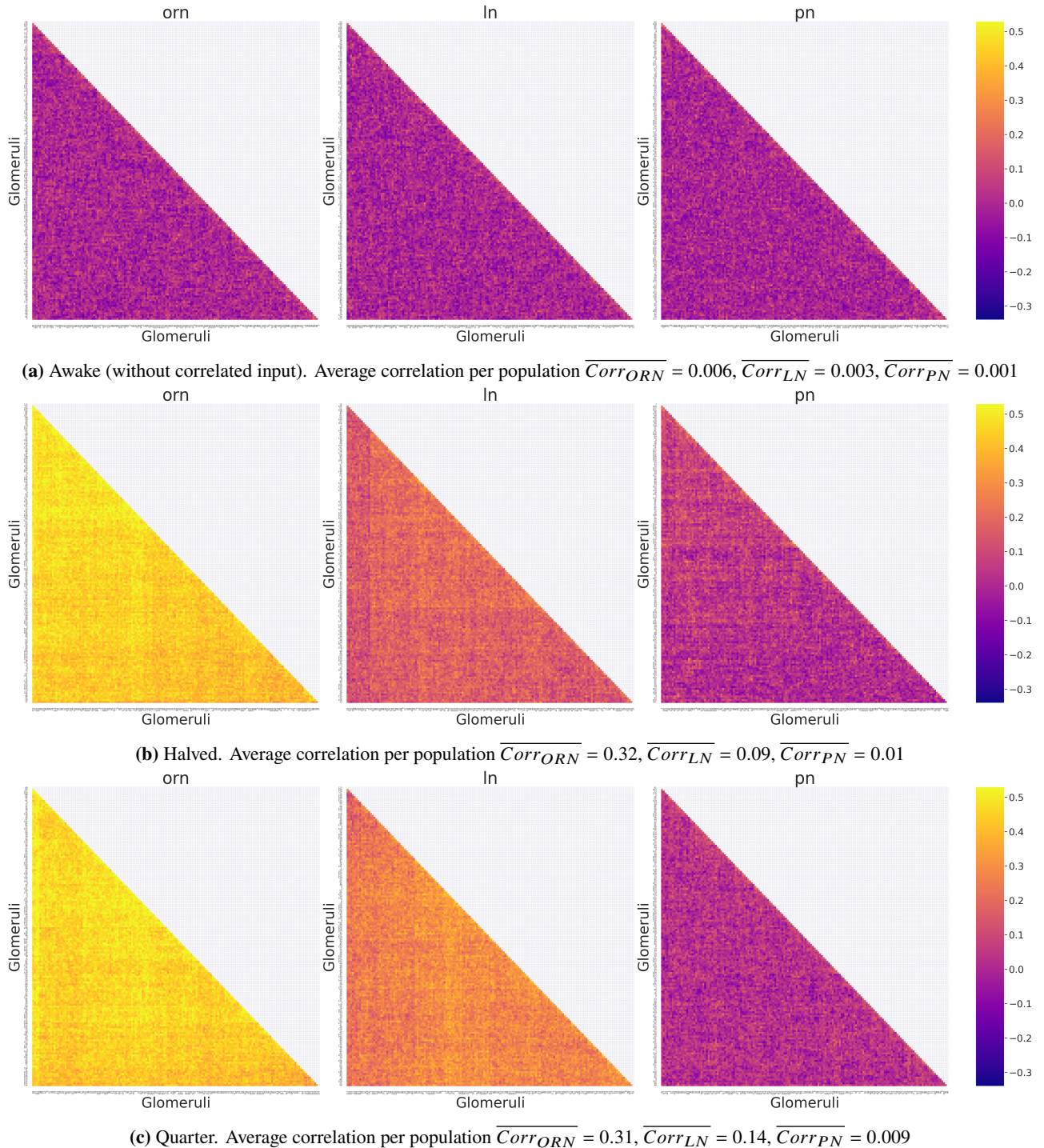


**Figure 4.20:** Correlation of the spontaneous activity between glomeruli of the antennal lobe with the Poisson trains and different reduction of the inhibitory synapses. 60 s of simulation.

## 4.5. COMPARISON BETWEEN AWAKE AND ASLEEP STATES

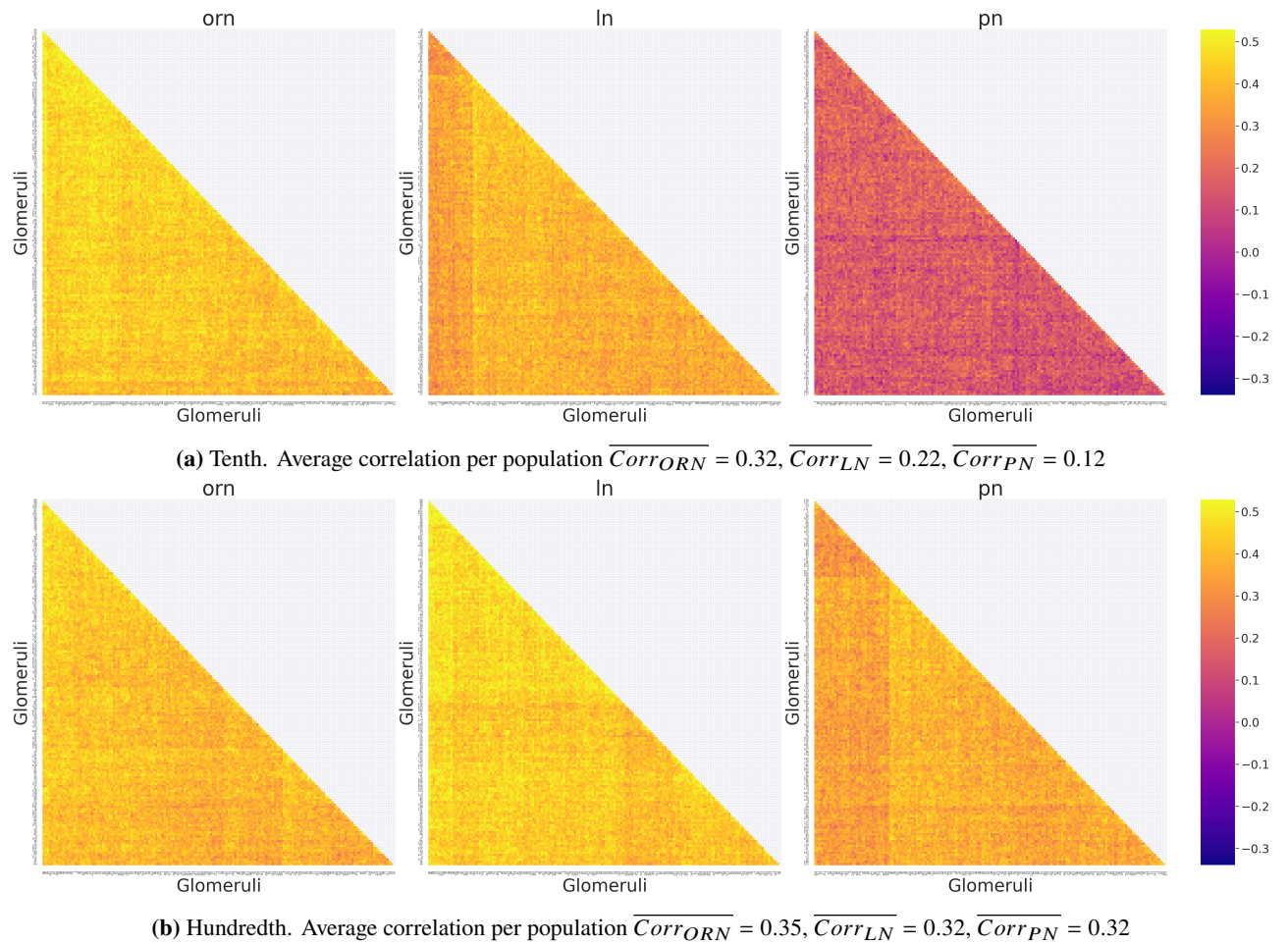


**Figure 4.21:** Correlation of the spontaneous activity between glomeruli of the antennal lobe with the Poisson trains and different reduction of the inhibitory synapses. 60 s of simulation.

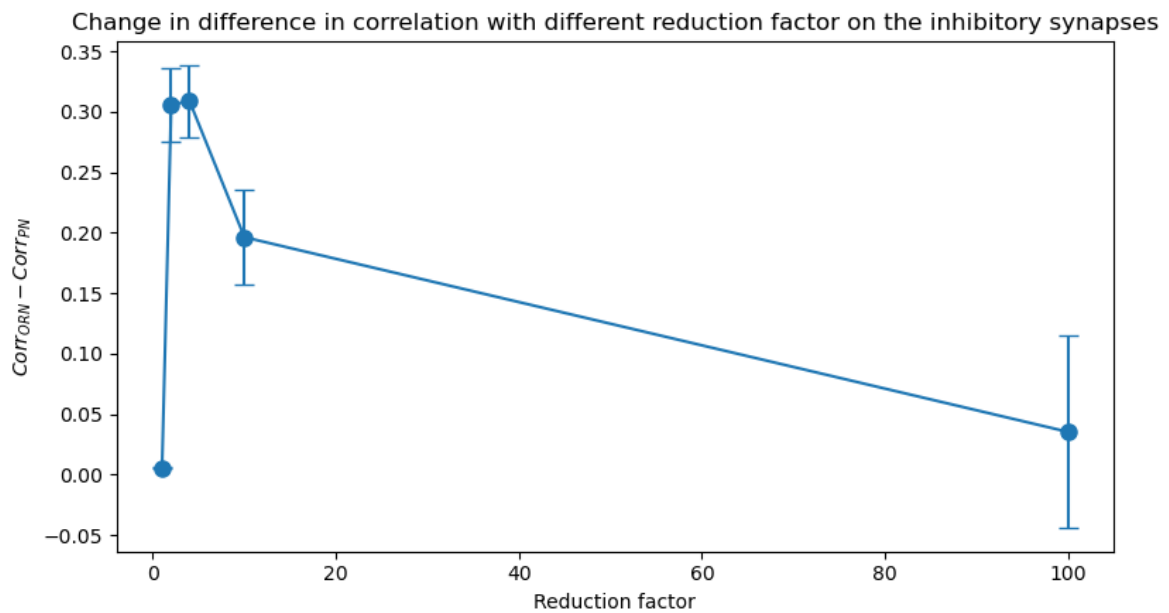


**Figure 4.22:** Change in the difference in the correlation between olfactory receptor neurons and projection neurons in the different reduced synapses strength conditions.

#### 4.5. COMPARISON BETWEEN AWAKE AND ASLEEP STATES

---

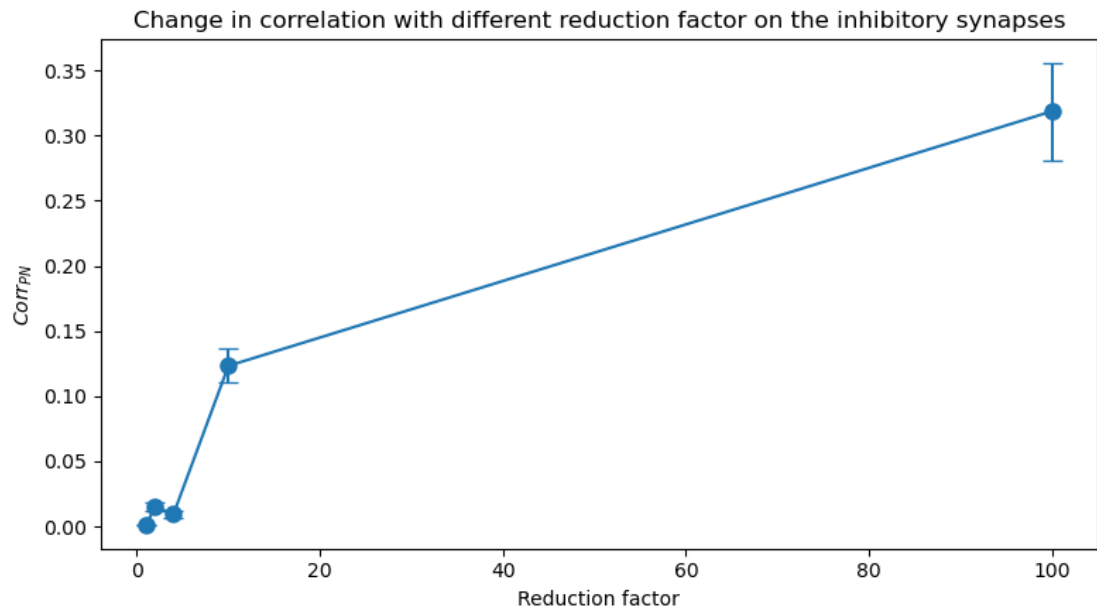


**Figure 4.23:** Change in the correlation of projection neurons in the different reduced synapses strength conditions.

Beside betweenness and transitivity the non-linearity of the features seems to derive from the introduction of the correlated input in the simulations with reduced inhibitory synapses strength.

#### 4.5. COMPARISON BETWEEN AWAKE AND ASLEEP STATES

---

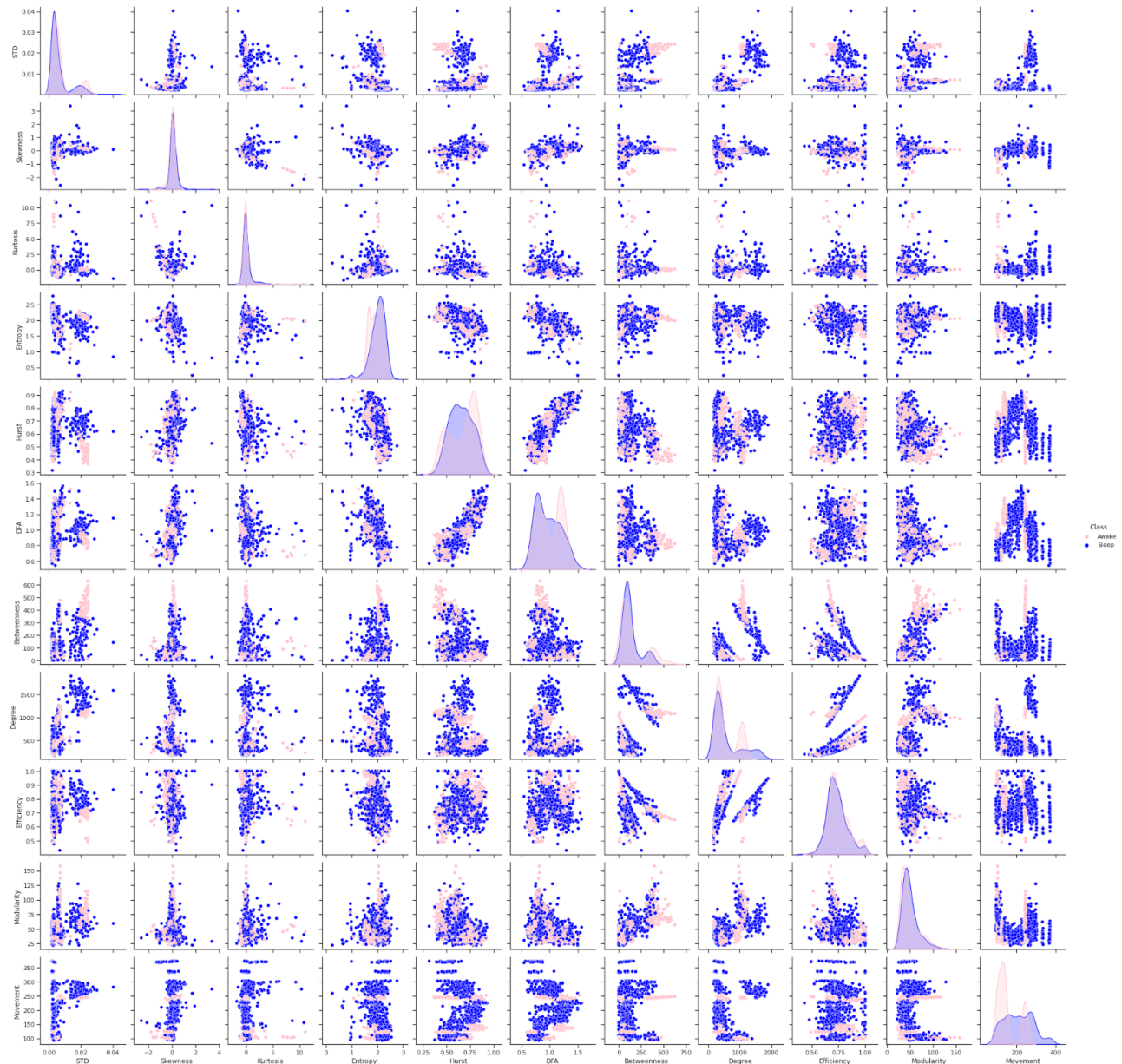


**Figure 4.24:** Distribution of the different features extracted from the awake and the asleep state, image from [24].

## 4.5. COMPARISON BETWEEN AWAKE AND ASLEEP STATES

---

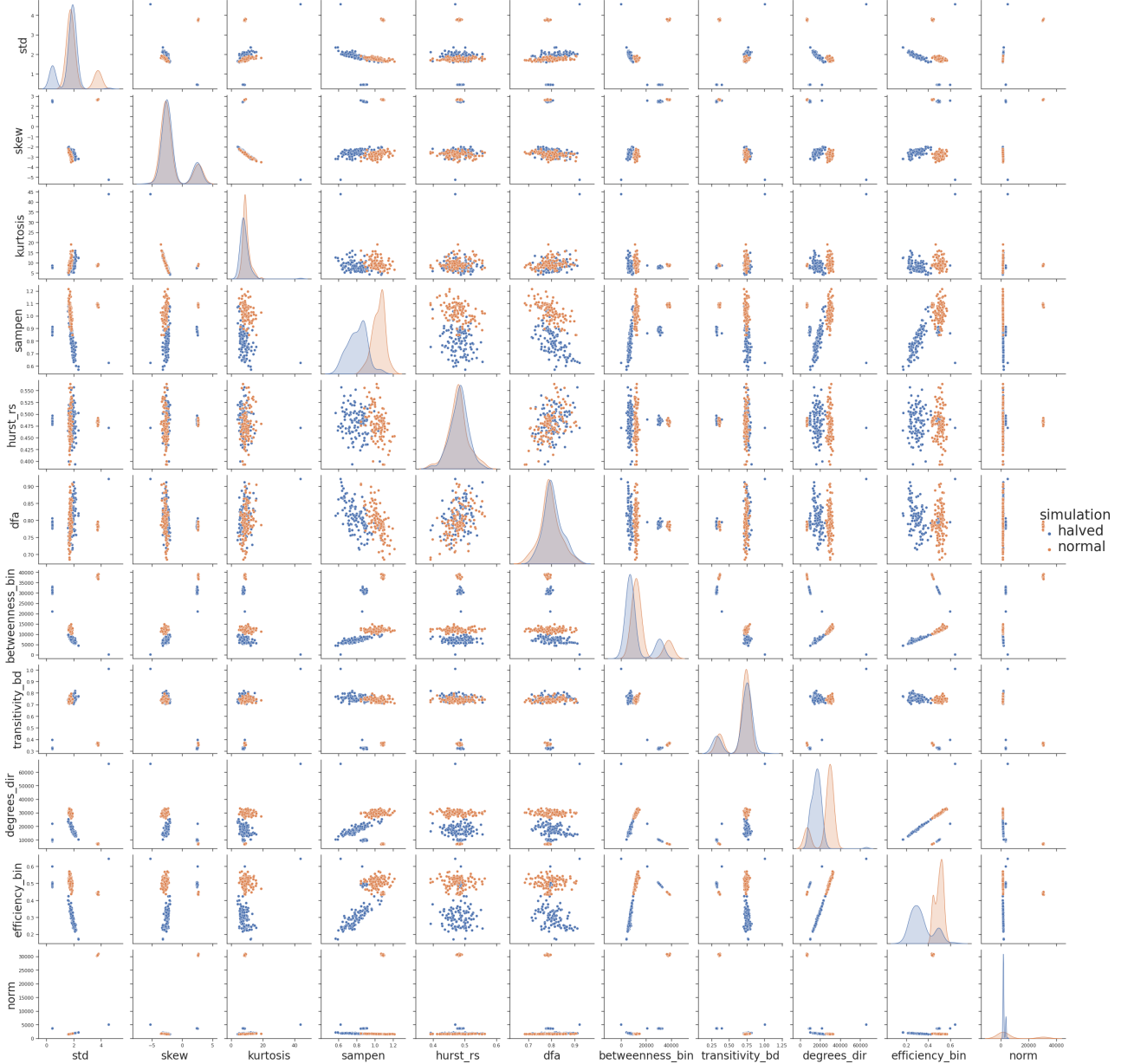


**Figure 4.25:** Distribution of the different features extracted from the normal and the halved simulation. Each point is extracted from a second of simulation.

## 4.5. COMPARISON BETWEEN AWAKE AND ASLEEP STATES

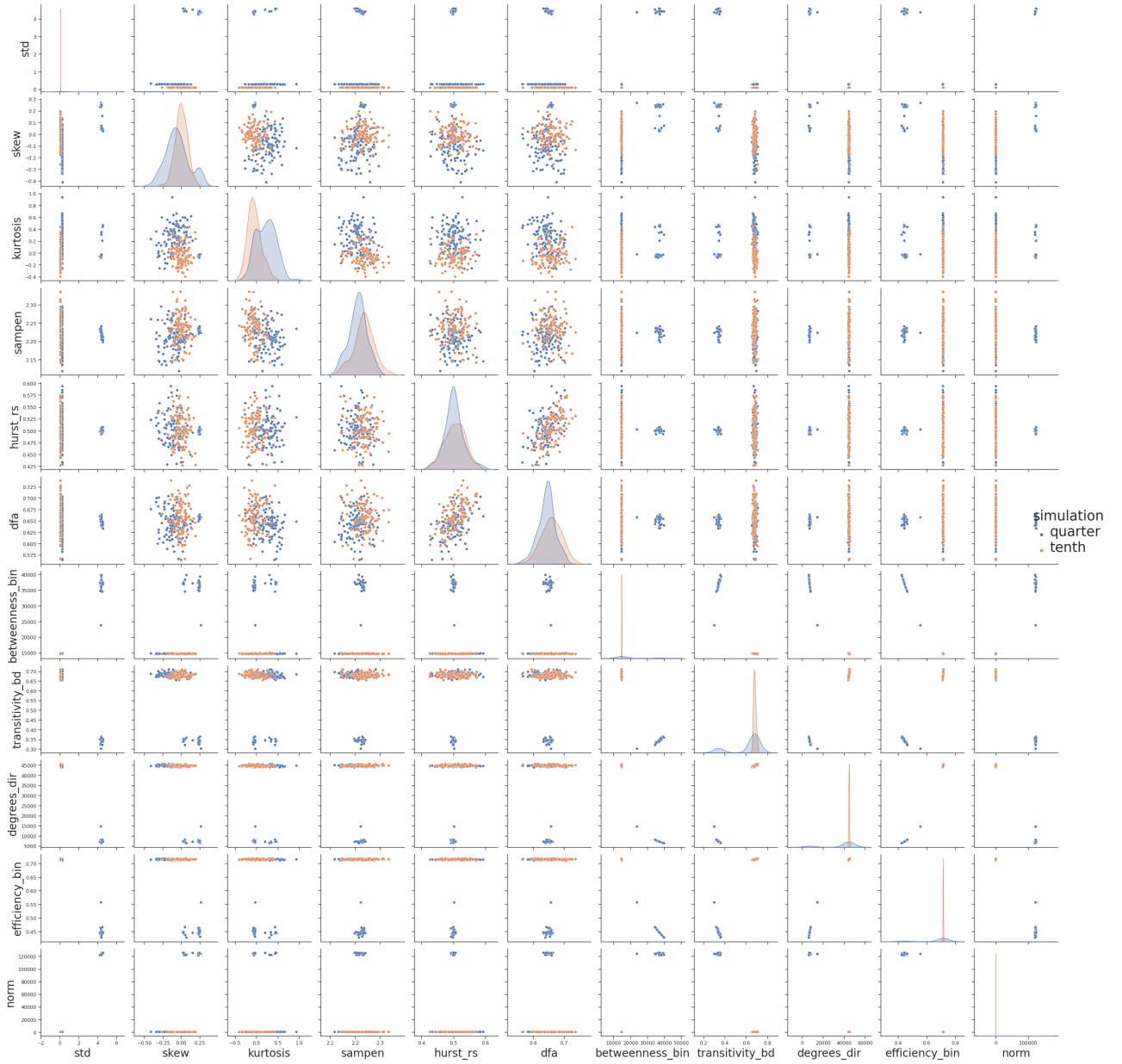


**Figure 4.26:** Distribution of the different features extracted from the normal and the quarter simulation. Each point is extracted from a second of simulation.

## 4.5. COMPARISON BETWEEN AWAKE AND ASLEEP STATES

---

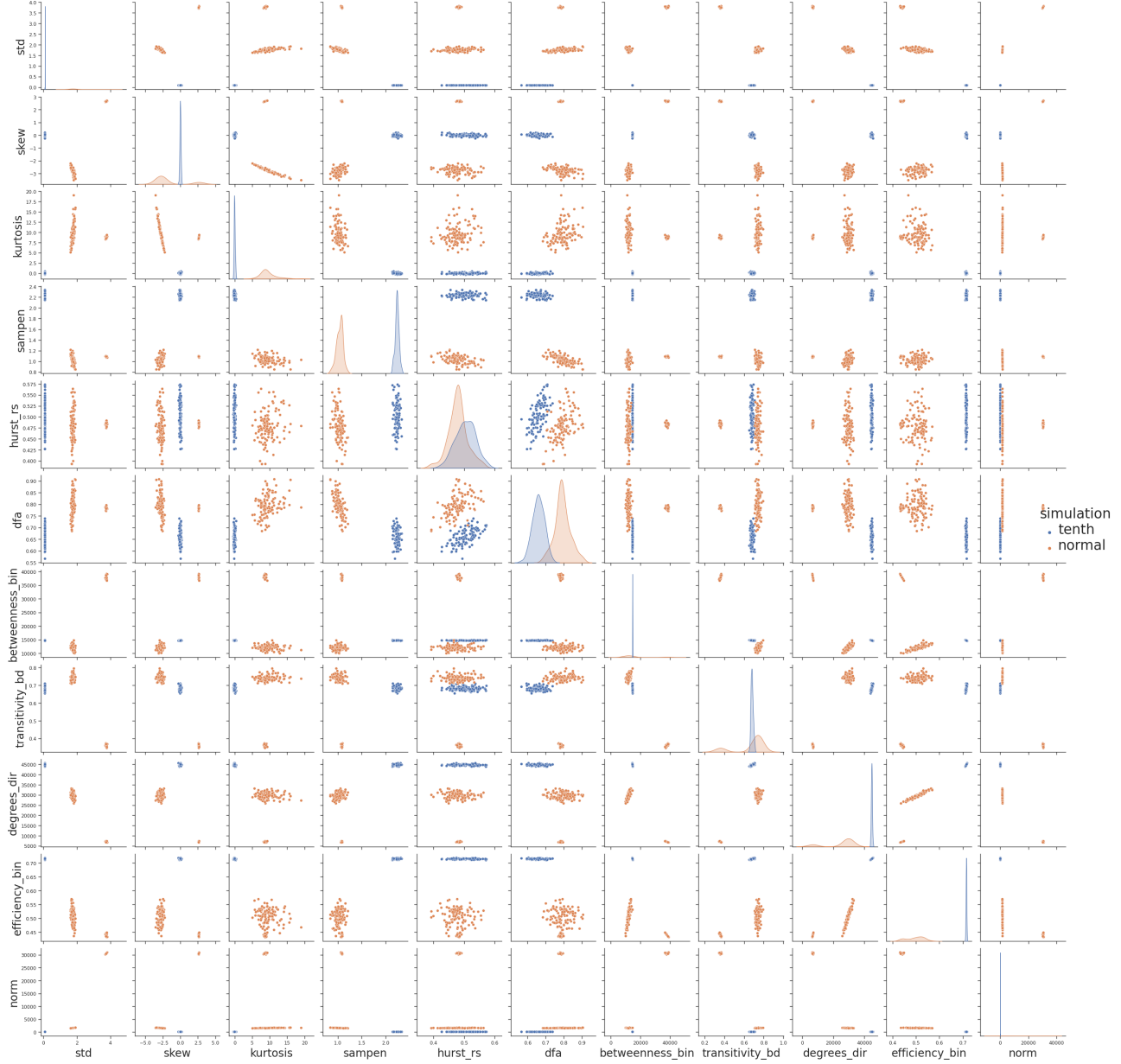


**Figure 4.27:** Distribution of the different features extracted from the normal and the tenth simulation. Each point is extracted from a second of simulation.

## 4.5. COMPARISON BETWEEN AWAKE AND ASLEEP STATES

---

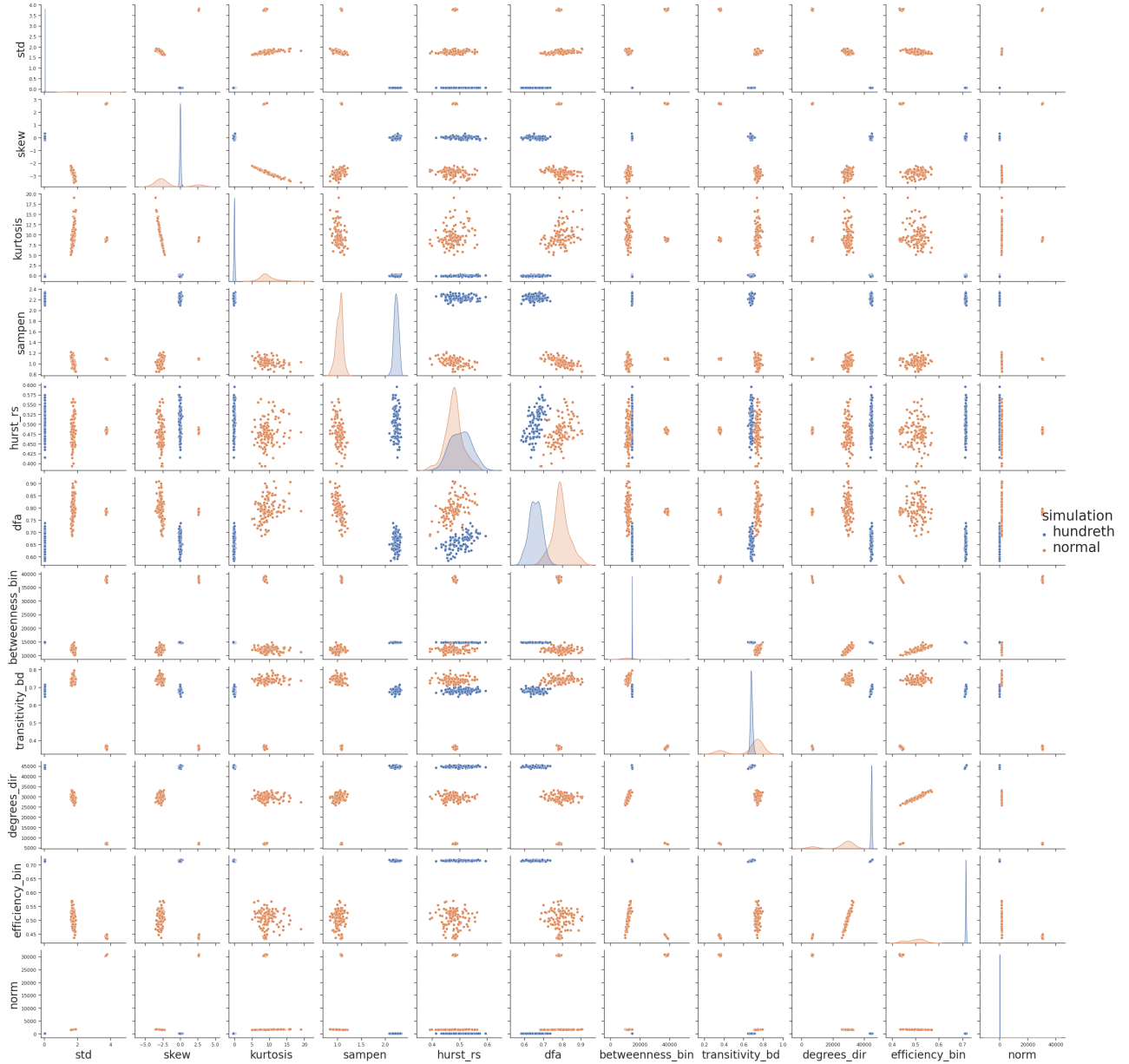
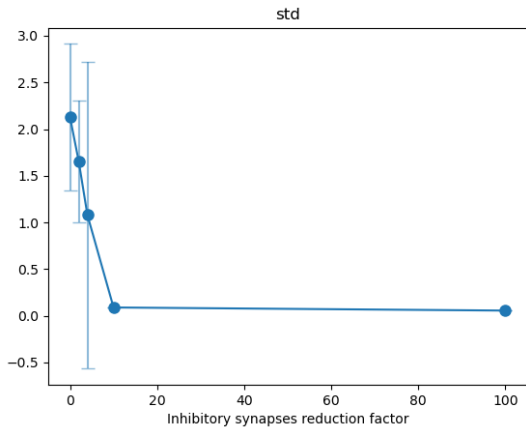


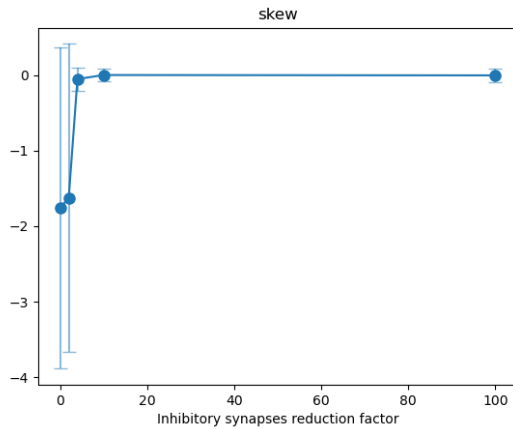
**Figure 4.28:** Distribution of the different features extracted from the normal and the hundredth simulation. Each point is extracted from a second of simulation.

#### 4.5. COMPARISON BETWEEN AWAKE AND ASLEEP STATES

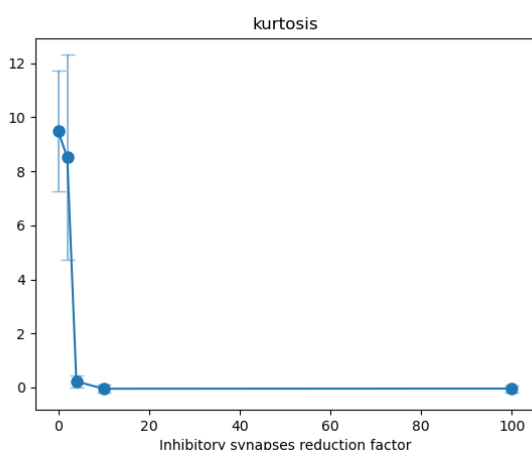
---



(a) Behavior of the standard deviation during the simulation of the different inhibitory synapses reduction. Reduction factor on the *x*-axis



(b) Behavior of the skewness during the simulation of the different inhibitory synapses reduction. Reduction factor on the *x*-axis

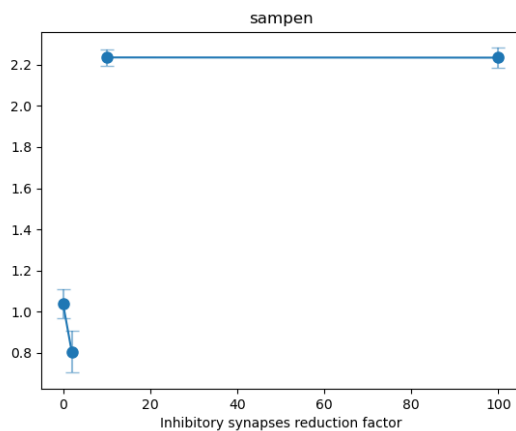


(c) Behavior of the kurtosis during the simulation of the different inhibitory synapses reduction. Reduction factor on the *x*-axis

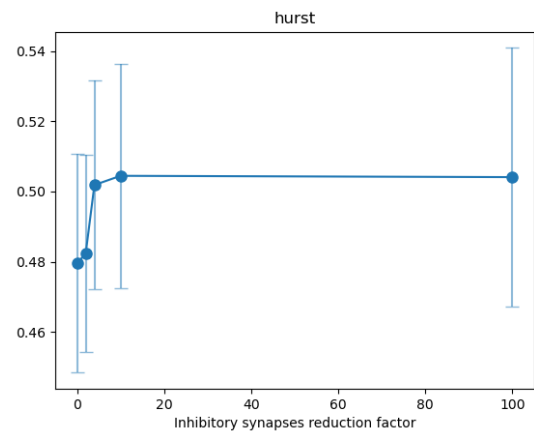
**Figure 4.29:** Behavior of standard deviation, skewness and kurtosis during the simulation of the different inhibitory synapses reduction.

#### 4.5. COMPARISON BETWEEN AWAKE AND ASLEEP STATES

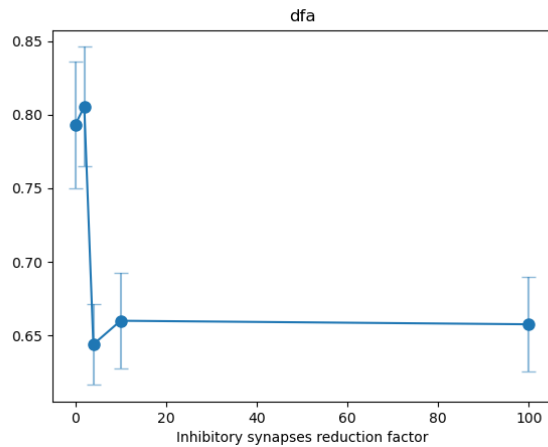
---



(a) Behavior of sample entropy during the simulation of the different inhibitory synapses reduction. Reduction factor on the  $x$ -axis



(b) Behavior of the Hurst during the simulation of the different inhibitory synapses reduction. Reduction factor on the  $x$ -axis

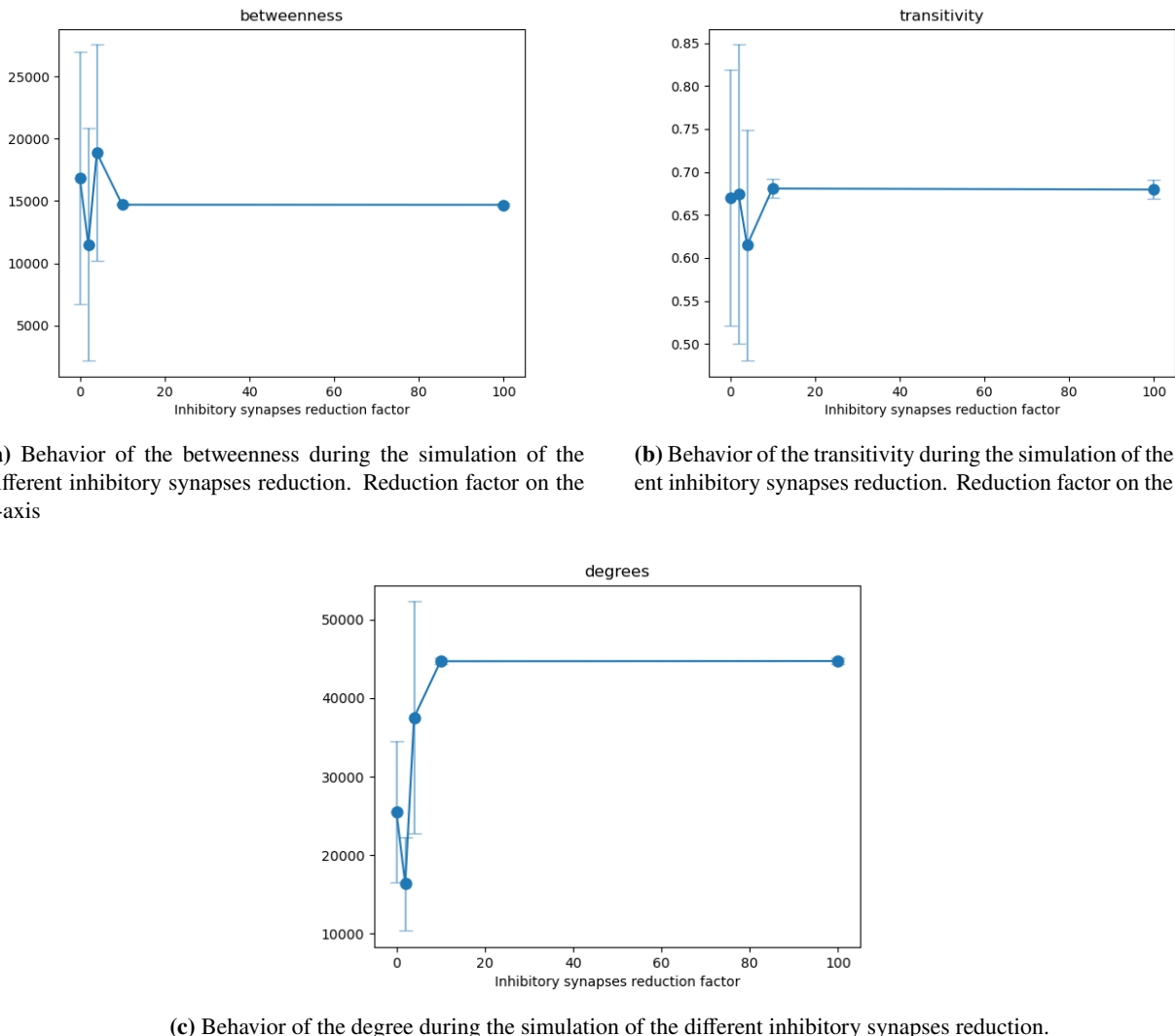


(c) Behavior of the DFA during the simulation of the different inhibitory synapses reduction. Reduction factor on the  $x$ -axis

**Figure 4.30:** Behavior of sample entropy, Hurst and DFA during the simulation of the different inhibitory synapses reduction.

#### 4.5. COMPARISON BETWEEN AWAKE AND ASLEEP STATES

---



**(a)** Behavior of the betweenness during the simulation of the different inhibitory synapses reduction. Reduction factor on the *x*-axis

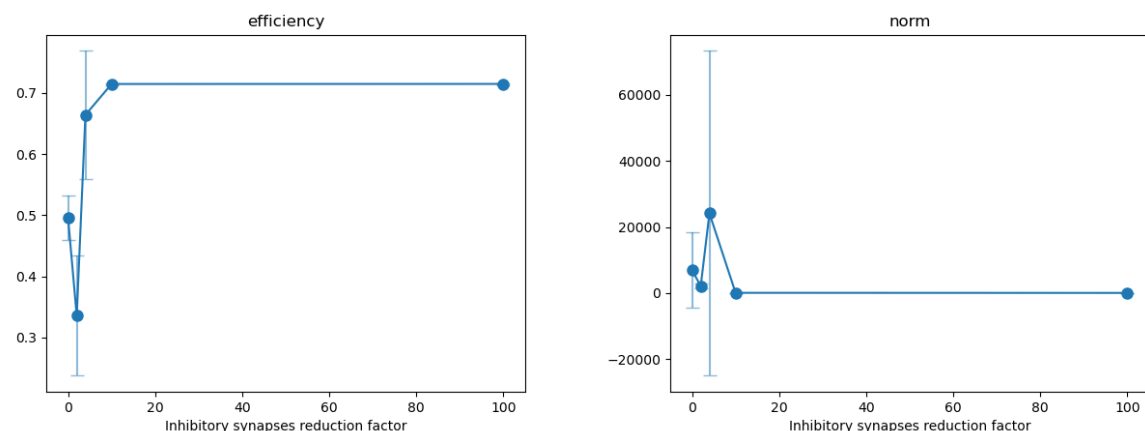
**(b)** Behavior of the transitivity during the simulation of the different inhibitory synapses reduction. Reduction factor on the *x*-axis

**(c)** Behavior of the degree during the simulation of the different inhibitory synapses reduction.

**Figure 4.31:** Behavior of betweenness, transitivity and degree during the simulation of the different inhibitory synapses reduction.

#### 4.5. COMPARISON BETWEEN AWAKE AND ASLEEP STATES

---



(a) Behavior of the efficiency during the simulation of the different inhibitory synapses reduction. Reduction factor on the  $x$ -axis  
(b) Behavior of the Frobenius norm during the simulation of the different inhibitory synapses reduction. Reduction factor on the  $x$ -axis

**Figure 4.32:** Behavior of efficiency and Frobenius norm during the simulation of the different inhibitory synapses reduction.

#### 4.5. COMPARISON BETWEEN AWAKE AND ASLEEP STATES

---

# **Chapter 5**

## **Discussion**

### **5.1 Deep learning in neuroscience**

Recent advances in neuroscience and computing technologies have caused a burst of interest in deep learning as a basis for brain function [9]. Several circuits in the brain have been modeled as deep learning networks, such as vision [63], audition [30], motor control [37], navigation [59] and cognitive control [10].

However, there is still no conclusive model for the olfactory system. This is because the olfactory system offers several unique challenges that are not present in other sensory systems [6]. First of all the number of possible combinations by which chemical features are encoded creates an incredibly large search space, especially because they are not continuous but discrete. This suggests that there might not be a clear-cut correspondence in properties and structure between the odor model and the system response. Because of this obtaining the generalizable structure-odor rules that can reduce the chemical complexity of the stimulus is a difficult task. Moreover, the olfactory system contains a high stimulus-response variation based on a genetically highly heterogeneous population of receptors, resulting in divergent perceptual responses to physicochemical information. These challenges, and the centrality of the antennal lobe in memory formation and learning in the honey bee, make this system an ideal candidate for the type of exploratory analysis performed here. Because of the difficulties of abstracting the olfactory system into a deep learning model, the neurobiological structure of the olfactory system is replicated as closely as possible in the model. This requires the use of spiking neural networks, which are more biologically plausible than the more common rate-based neural networks, but require a larger number of parameters to be tuned and are more computationally intensive to both train and run.

#### **5.1.1 Spiking neural networks**

Spiking neural networks have been proven to be successful in several fields, proving to be able to solve problems that are difficult for other types of neural networks [62]. In particular, they have been a driving factor in the development of many modern computer vision and signal processing techniques. This is because they excel in encoding and decoding data consisting of temporal information. Another important application of spiking neural networks is in robotic control, where they have been used as the controller of robots to provide perception and action to mimic the behaviors captured in nature. Most commonly they are used to hand-craft and tune for the specific task of interest, but their deployment as a locomotion controller has become more and more common. Another advantage of spiking neural networks for robotics is the fact that task-specific neuromorphic computer hardware has been developed, reducing the energy consumption and increasing the speed of the network [46].

### 5.1.2 Spiking neural networks in neuroscience

Spiking neural networks have seen an increase in interest as a tool to analyze neurobiological networks because they offer a major advantage over classical artificial neural networks: they mimic more closely the biology of a brain. This offers the opportunity to study the dynamics of the network in an *in silico* setting with a single-neuron resolution. Moreover, they can be trained directly on spiking biological data, offering a one-to-one correspondence between the model and the data. This allows to understand the contribution of the components on the network on the task the system is supposed to perform, for example, evaluating the contribution of different brain regions on the current activity of another observed brain region [43].

They offer several advantages over classical data analysis techniques in neuroscience, in particular over methods that rely on correlative analysis of neural data. In particular, correlative analysis methods cannot distinguish between correlations that arise from common inputs and those that arise from other types of interactions. Moreover, directionality cannot be accounted for and they are difficult to describe interactions between more than two brain regions.

Spiking neural networks address these problems, providing a system that is able to replicate the dynamics of the biological system and that can be used to test hypotheses about the role of different components of the system. Data collection is also improved, as there are no physical limits that constrain the number of neurons that can be recorded and the frequency at which they can be recorded. At the same time, the *in silico* nature of the network allows to perform experiments that would be impossible in a biological system, such as the removal of a specific component of the network or the addition of a new one simply by modifying the network's parameter or its architecture.

Taken together these characteristics make spiking neural networks an ideal tool to study the dynamics of the brain and to test hypotheses about the role of different components of the system, providing a tool to experimentalists for performing exploratory experiments to test hypotheses more quickly and without the need to set up expensive experimental apparatuses or the limits of having to deal with an animal model.

## 5.2 The honey bee as a model for human sleep

Although the spiking neural network presented here is a model of the antennal lobe, the part of the olfactory system responsible for the first processing of the olfactory information, the focus of this work is not on the capability of the network to code for different odors, but rather on what happens to it during sleep. In this setting, the antennal lobe does not receive any input, but rather it is left alone, allowing it to evolve spontaneously.

As said before insects, and in particular the honey bee, are increasingly used as a model for human sleep. The brain of the honey bee has proven to be an ideal system to study in experimental settings and this has extended to computational pipelines. In particular, the small number of neurons in the honey bee brain allows to perform long simulations that include a large part of the neuronal circuitry, allowing to investigate large-scale effects in a reasonable amount of time.

The antennal lobe has proven to be an ideal system to study in this exploratory pipeline, as it is the first processing unit of the olfactory system, with a well-understood anatomy and physiology, while still missing a definitive model on how it is able to code for different odors and their interactions. Spiking neural networks have proven to be an ideal candidate to model the antennal lobe, as they are able to reproduce with a high degree of accuracy the activity of the antennal lobe, both in response to different odors and without any input. The flexibility in how the neural network is built and works have been crucial during this exploration, as it has allowed to test quickly different hypotheses about the role of different components of the antennal lobe, while not requiring a domain-specific model of how odor information is coded.

#### 5.2.1 Sleep in the antennal lobe

As described before, sleep is fundamental for the consolidation of memories and the formation of new ones. The antennal lobe has been chosen as the region of study, besides the fact that it is the first processing unit of the olfactory system because it has been shown to be involved in the formation of memories for the honey bee. Sleep is a fascinating process to study, and it has been shown to be linked to memory formation in the honey bee [7] and many other species [5].

There are differences in sleep between humans and honey bees such as the fact that there is no EEG signal in the latter, but the similarities are striking. Previous experimental results [29] and [24] show how the honey bee exhibits a circadian rhythm in its sleep, with a higher amount of sleep during the night and a lower amount during the day. Moreover, there are differences in activity in the antennal lobe between the awake and asleep states. These differences cannot be completely ascribed to a different average firing rate, but rather to changes in the pattern of the activity of the antennal lobe. The objective of this work has been to explore what the biological cause of this activity could be by building a spiking neural network model of the antennal lobe able to replicate the behavior both in the awake state and when fed an odor input and modify its parameter until it replicates the asleep state.

### 5.3 Neuronal correlates of sleep

The model proposed in this work has been able to reproduce the change in correlation in the projection neurons of different glomeruli that happens in the asleep and awake state of the honey bee (figure 5.1). This has been achieved by changing two components of the network, namely:

- The strength of the inhibitory synapses between local neurons and projection neurons and between local neurons and themselves.
- Introducing a correlated input to the system.

From this information, it can be proposed that there are two major mechanisms at play in the antennal lobe during sleep. The reduction of inhibitory synapses' strength is a mechanism that is localized in the antennal lobe. The added correlated input suggests that global changes in regions of the brain of the honey bee that are not modeled here cause a change in the pattern of the input current to the antennal lobe.

These two mechanisms contribute to the change in the correlation of the projection neurons in two different ways. The correlated input or Poisson train current increases the correlation upstream of the network, in the olfactory receptor neurons. This increase in correlation in the olfactory receptor neurons causes the local neurons to have a much stronger inhibitory effect on the projection neurons. Introducing correlated Poisson trains without changing the strength of the inhibitory synapses causes the correlation to increase (figure 5.1b), but this effect is due to the fact that the activity of the projection neurons drop near to zero (figure 4.16), which doesn't agree with experimental results. This is a property of how the local neurons work, as they are able to synchronize the activity of the projection neurons by inhibiting them. If the activity of the neurons afferent to the local neuron is already correlated, their inhibitory power increases drastically, causing the projection neurons' firing rate to drop near to zero.

The inhibitory synapses control the coupling of the system: the stronger the inhibitory synapses, the more the activity of the projection neurons is coupled. It can be seen how reducing the strength of the synapses causes the activity of the projection neurons to become more correlated until it reaches the level of the olfactory receptor neurons. This synchronization property of the inhibitory synapses is fundamental for the coding of odors in the antennal lobe, allowing to have response patterns that vary non-monotonically with odor concentration, or when odors are mixed together with varying concentration [48]. The inhibitory potential of the local neuron is then tightly related to the pattern of activity of the olfactory receptor neurons, rather than their firing rate.

From this, it can be seen how the resulting pattern of correlation in the projection neurons of the asleep state is a

### 5.3. NEURONAL CORRELATES OF SLEEP

---

careful balance of two components of the network that work in opposing ways. By carefully tuning the strength of the inhibitory synapses and the amount of correlated input it is possible to obtain a network that replicates the correlation of the projection neurons in the asleep state.

#### 5.3.1 Features of the system

To further investigate the differences between the awake and asleep state, and to understand what functional properties of the network change in them, several features have been extracted from simulations with different parameters.

These features can be divided into two categories:

- Features related to the spiking activity of the network.
- Functional connectivity features.

Comparing the change in features obtained from simulating the system at different inhibitory synaptic strengths with the feature extracted from an experimental run, further supported the hypothesis that the introduction of a correlated input together with the reduction in inhibitory strength are the mechanisms that contribute to the different pattern of activity between the two states. In particular, the simulation that best replicated experimental results is the “Quarter” one, where the inhibitory synapses have been reduced by a factor of four.

Interestingly, not all the features change monotonically with the decrease in inhibitory synapses’ strength. Features concerned with the statistical distribution of the spiking activity of the network, such as:

- Standard deviation (section 3.2.5.1.1).
- Skewness (section 3.2.5.1.2).
- Kurtosis (section 3.2.5.1.3).
- Hurst exponent (section 3.2.5.1.5).

Tend to be the only ones that change monotonically. All the other features, concerning the functional connectivity of the network tend to show local minima when inhibitory synapses strength is reduced by a factor of two (“Halted” simulation, figure 5.1c):

- Efficiency (section 3.2.5.2.4).
- Sample entropy (section 3.2.5.1.4).
- Degree (section 3.2.5.2.3).

Or when they are reduced by a factor of four (“Quarter” simulation, figure 5.1d):

- Transitivity (section 3.2.5.2.2).
- DFA (section 3.2.5.1.6).

Local maxima can be found for a reduction factor of four, together with local minima for a reduction factor of two for:

- Frobenius norm (section 3.2.5.2.5).

### 5.3. NEURONAL CORRELATES OF SLEEP

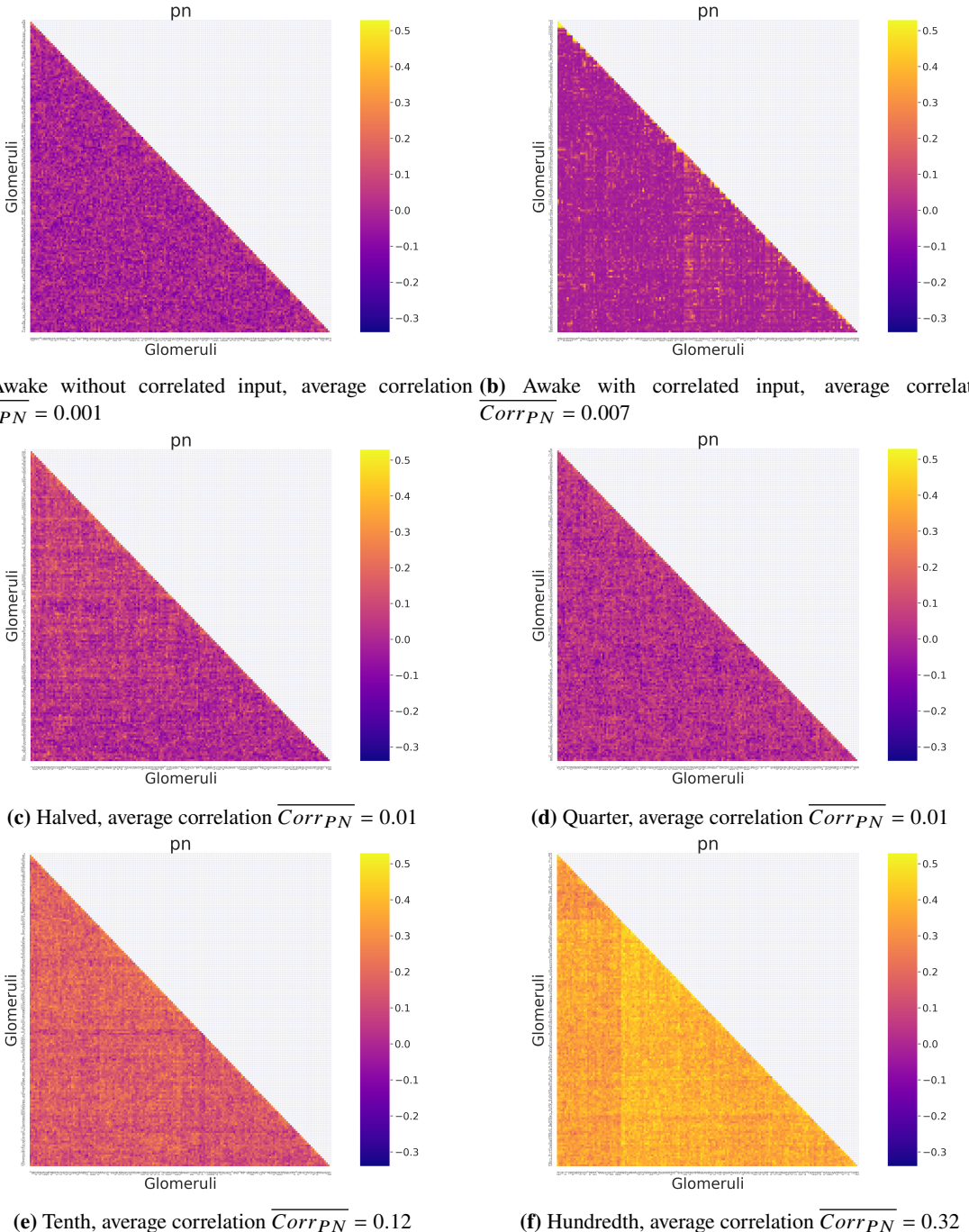


**Figure 5.1:** Correlation between the activity of the projection neurons of the antennal lobe averaged over glomeruli in different conditions. The first row represents the awake state, with and without a correlated input. The successive plots (from left to right and top to bottom) are the same correlation matrices of simulations with increasingly reduced strength of the inhibitory synapses, respectively by a factor of 2, 4, 10 and 100.

## 5.4. PUTATIVE BIOLOGICAL MECHANISMS

---

- Betweenness (section 3.2.5.2.1).

All features remain almost unchanged when the reduction factor goes from 10 to 100, suggesting that the inhibitory synapse's function is not significant anymore and the reduction is too strong.

The local minima in the “Halved” simulation can be explained by the fact that the inhibitory synapses are still strong enough to synchronize the activity of the projection neurons and the introduction of the correlated input changes drastically the inhibition pattern, causing in turn a different conformation of functional connections. Local minima in the “Quarter” simulation are found in measures that involve the interconnection of the network, suggesting an increase in functional connection for these measures. They could be explained by the slight increase in the average correlation neurons in this condition, which even though it could be ascribed to statistical error, has this effect on the measures.

All these measures suggest that the sleep state can be found in a region of the parameter space where the inhibitory synapses are not strong enough to synchronize the activity of the projection neurons, but still strong enough to have a significant effect on the functional connectivity of the network. This can be reconduted to a close range around the “Quarter” simulation in the parameter space (figure 5.2).

## 5.4 Putative biological mechanisms

The results presented here suggest that the differences in activity patterns between the asleep and awake states are due to two major putative mechanisms:

- The reduction of inhibitory synapses' strength.
- The introduction of a correlated input.

Both of these processes can be linked to biological mechanisms that happen both in the honeybee and in the human brain.

### 5.4.1 Reduction of inhibitory synapses' strength

The reduction of inhibitory synapses' strength is a process that happens in the honeybee brain during sleep, and it is thought to have an important role in humans. In particular, GABAergic synapses in hippocampal CA1 pyramidal neurons in mice, neurons involved in the memory consolidation and integration processes, undergo daily rhythmic alteration. Consistently with electrophysiological data, wake decreased the synaptic expression of  $\alpha_1/\alpha_2$ -GABA<sub>ARs</sub> but increased surface expression of  $\alpha_4/\alpha_5$ -GABA<sub>ARs</sub> in the hippocampus, causing a net decrease in inhibitory synapses' strength. This implies a profound difference in the control of neuronal network function across the asleep and awake states. Moreover, in human disorders in the GABAergic inhibition mechanisms are linked with insomnia [61]. Wakefulness is increased when the ventral midbrain/pons area is chemogenetically inhibited [52], suggesting that GABAergic neurons have a fundamental role in sleep regulation in mammals. Chemogenetic activation of ventral midbrain/pons GABAergic neurons induces slow-wave-sleep. Consistently with the results presented here this process in mice is thought to contribute to the increase in correlation of network activity, which is speculated to facilitate memory consolidation during sleep.

### 5.4.2 Introduction of a correlated input

Although no characteristic EEG trace is recorded in the honey bee [5], global oscillation and neuron grouping are common in humans and mice during slow wave sleep [8]. During slow wave sleep the brain is characterized by a slow oscillation in the range of 0.5 Hz, with a high amplitude and a low frequency. The neocortex and the

## 5.4. PUTATIVE BIOLOGICAL MECHANISMS

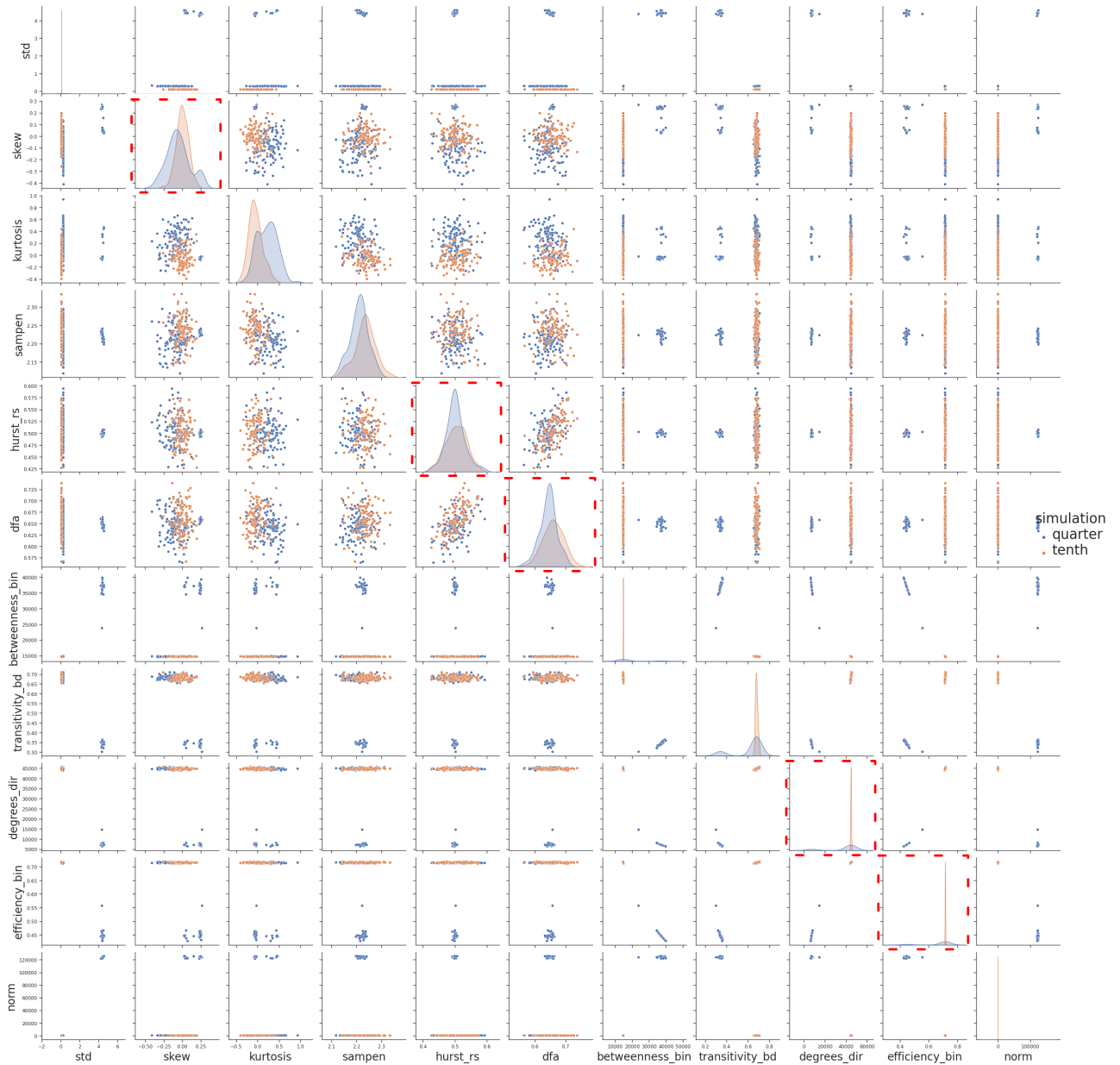


**Figure 5.2:** Comparison between the extracted features of the awake condition (in orange) and the putative sleep condition (in blue), features that best fit experimental results are highlighted in red.

#### 5.4. PUTATIVE BIOLOGICAL MECHANISMS

---

hippocampus interact such that neocortical slow oscillations drive the repeated reactivation of newly encoded memories in the hippocampus, driving these representations to become long-term.

The origin of this correlated input is not clear and has not been observed in the antennal lobe of the honey bee, but it is a feature that is able to reproduce observed behavior and is akin to mammals' EEG traces. This suggests a global factor that drives the antennal lobe behavior during sleep, without being able to pinpoint its exact origin. Putative mechanisms for the increase in spiking synchronization could be attributed to several processes [53]. Firstly chemical synaptic transmission of not modelled feedback connections analogous to the mammalian cortico-thalamo-cortical feedback loop, as it has been modeled for the *Drosophila* antenna [33]. Gap junctions, or electrical synapses, allow direct flux of ions between connected cells, providing a mechanism of communication that is action potential independent: changes of membrane voltage could in one neuron would trigger current flow between coupled neurons leading to corresponding changes of membrane cells, acting as low-pass filters. In cortical networks groups of GABA-releasing interneurons and glial cells are interconnected via gap junctions, suggesting that electrical coupling may occur between axons of pyramidal neurons. Lastly, extracellular currents produced by other brain regions constituting local field potentials may directly influence the electrical properties of neurons, causing changes in excitability with a global influence.

# Chapter 6

## Conclusions and future perspectives

### 6.1 Conclusions

The work presented here involved building a spiking neural network to model part of the olfactory system of the honeybee. The antennal lobe is fundamental in the processing of olfactory information and the formation of memories in the honeybee. Because of its role in memory formation, its behavior during sleep has been explored. Starting from a model of the waking antennal lobe, capable of coding correctly for odors, a new model for the sleeping state has been built by tweaking the parameters of the component of the awake system.

The resulting system has been compared with a set of experimental results to assess its validity. The model provides several advantages over the experimental results, not being constrained by physical limitation, the whole antennal lobe could be simulated and the activity of the projection neurons could be recorded at any arbitrary frequency. The two drivers for the validity assessment of the model have been:

- The correlation matrices of projection neurons activity averaged across glomeruli.
- The connectivity and activity distribution features extracted from a time series simulated of the model.

The model's parameters have been tuned to match these two sets of measures.

This has led to the identification of two major drivers of the increased correlation and coupling in the sleeping antennal lobe:

- A decrease in the inhibitory synapses' strength.
- An introduction of a correlated input to the system, in the form of Poisson trains of spikes.

The role of the correlated input was to increase the overall correlation of the activity of projection neurons. Its effect on the waking system is remarkable: without reducing the inhibitory synapses' strength, this type of correlated input pattern causes the inhibitory ability of the local neurons to completely shut off the activity of the projection neurons. Reducing inhibitory synapses reduced the effect of the local interneuron on the activity of the projection neurons, making it more similar to the one observed in the olfactory receptor neuron population. If the reduction of the inhibitory synapses' strength during sleep is well documented in the literature, the origin of the correlated input still needs to be further explored. This input could be due to global effects which are well documented in mice and humans ([8] and [53]) but not yet in insects or to components not considered for this model, such as gap junctions or local field potentials. Another putative mechanism that could provide this level

## 6.2. FUTURE PERSPECTIVES

---

of correlated input is a feedback loop in the system, as it has been done in [33] in *Drosophila*. The parameters of the correlated input used in the model have been found by manual exploration, such as to maximize their effect on the correlation of the activity of the projection neurons. Several simulations have been run at different reduction factors of the inhibitory synapses' strength, identifying the sleep state as the one having features distribution separation from the awake state most similar to the experimental data. This state corresponded to the one where inhibitory synapses' strength has been reduced by a factor of 4, with the most similar features being:

- Skewness.
- Hurst exponent.
- Detrended fluctuation analysis.
- Degree.
- Efficiency.

The match is not perfect, suggesting that the actual reduction factor lies between 4 and 10.

## 6.2 Future perspectives

The model presented here is a first step in the exploration of the sleeping state of the antennal lobe and can be expanded in a number of directions. The first one is to explore if the sleep state is still able to code for odors: it has been documented that context odor presentation during sleep enhances memory in honeybees [64]. This suggests that the antennal lobe is still able to code for odors during sleep, but this has not been explored in the model. Some changes in the coding capabilities are expected, but the system should still be able to produce a response for certain odor stimuli, even if with a weaker activity pattern.

Even though the model has been able to reproduce the correlation matrices of the experimental data, the exploratory nature of the work has not allowed to explore in detail the parameter space. This could be done by training a classification algorithm such as random forest as done in [24] to gauge the performance of the model.

Automatic learning could be introduced using the trained classification algorithm as a fitness function for the parameters of the model. This learning could be performed using classical machine learning techniques such as gradient descent or more biologically plausible ones [57] such as spike timing dependent plasticity (STDP).

## **6.2. FUTURE PERSPECTIVES**

---

# Chapter 7

## Bibliography

- [1] Static pulse model. [https://genn-team.github.io/genn/documentation/4/html/d9/d74/classWeightUpdateModels\\_1\\_1StaticPulse.html](https://genn-team.github.io/genn/documentation/4/html/d9/d74/classWeightUpdateModels_1_1StaticPulse.html). Accessed: 2023-04-06.
- [2] Neuron anatomy. <https://askabiologist.asu.edu/neuron-anatomy>, 2011. Accessed: 2023-04-06.
- [3] ABEL, T., HAVEKES, R., SALETIN, J. M., AND WALKER, M. P. Sleep, plasticity and memory from molecules to whole-brain networks. *Current Biology* 23, 17 (Sept. 2013), R774–R788.
- [4] AESTRIVEX. Bctpy. <https://github.com/aestrivex/bctpy>, 2023.
- [5] ALBRECHT P. VORSTER, AND JAN BORN. sleep and memory in mammals, birds and invertebrates. *neuroscience & biobehavioral reviews* 50 (Mar. 2015), 103–119.
- [6] BARWICH, A.-S., AND LLOYD, E. A. More than meets the AI: The possibilities and limits of machine learning in olfaction. *Frontiers in Neuroscience* 16 (Sept. 2022).
- [7] BEYAERT, L., GREGGERS, U., AND MENZEL, R. Honeybees consolidate navigation memory during sleep. *Journal of Experimental Biology* 215, 22 (Nov. 2012), 3981–3988.
- [8] BORN, J. Slow-wave sleep and the consolidation of long-term memory. *The World Journal of Biological Psychiatry* 11, sup1 (Jan. 2010), 16–21.
- [9] BOTVINICK, M., WANG, J. X., DABNEY, W., MILLER, K. J., AND KURTH-NELSON, Z. Deep reinforcement learning and its neuroscientific implications. *Neuron* 107, 4 (Aug. 2020), 603–616.
- [10] BOTVINICK, M. M., AND COHEN, J. D. The computational and neural basis of cognitive control: Charted territory and new frontiers. *Cognitive Science* 38, 6 (July 2014), 1249–1285.
- [11] BRILL, M. F., MEYER, A., AND RÖSSLER, W. It takes two—coincidence coding within the dual olfactory pathway of the honeybee. *Frontiers in Physiology* 6 (July 2015).
- [12] BURKITT, A. N. A review of the integrate-and-fire neuron model: I. homogeneous synaptic input. *Biological Cybernetics* 95, 1 (Apr. 2006), 1–19.
- [13] DIJK, D.-J. Regulation and functional correlates of slow wave sleep. *J. Clin. Sleep Med.* 5, 2 Suppl (Apr. 2009), S6–15.
- [14] E., Y., J., T., AND NOWOTNY, T. Genn: a code generation framework for accelerated brain simulations, 2016.
- [15] FACEBOOK. Zstd. <https://github.com/facebook/zstd>, 2023.

- 
- [16] FALUP-PECURARIU, C., ȘTEFANIA DIACONU, TÎNT, D., AND FALUP-PECURARIU, O. Neurobiology of sleep (review). *Experimental and Therapeutic Medicine* 21, 3 (Jan. 2021).
- [17] FLANAGAN, D., AND MERCER, A. R. An atlas and 3-d reconstruction of the antennal lobes in the worker honey bee, apis mellifera l. (hymenoptera : Apidae). *International Journal of Insect Morphology and Embryology* 18, 2-3 (Jan. 1989), 145–159.
- [18] FONTA, C., SUN, X.-J., AND MASSON, C. Morphology and spatial distribution of bee antennal lobe interneurones responsive to odours. *Chemical Senses* 18, 2 (1993), 101–119.
- [19] GALÁN, R. F., FOURCAUD-TROCMÉ, N., ERMENTROUT, G. B., AND URBAN, N. N. Correlation-induced synchronization of oscillations in olfactory bulb neurons. *The Journal of Neuroscience* 26, 14 (Apr. 2006), 3646–3655.
- [20] GALIZIA, C. G. Olfactory coding in the insect brain: data and conjectures. *European Journal of Neuroscience* 39, 11 (Apr. 2014), 1784–1795.
- [21] GERSTNER, W., KISTLER, W. M., NAUD, R., AND PANINSKI, L. *Neuronal dynamics*. Cambridge University Press, Cambridge, England, July 2014.
- [22] GIURFA, M. Cognitive neuroethology: dissecting non-elemental learning in a honeybee brain. *Current Opinion in Neurobiology* 13, 6 (Dec. 2003), 726–735.
- [23] GUO, D., THOMAS, R. J., LIU, Y., SHEA, S. A., LU, J., AND PENG, C.-K. Slow wave synchronization and sleep state transitions. *Scientific Reports* 12, 1 (May 2022).
- [24] HAASE, S. M. L. D. T. U. H. A. Neuronal correlates of sleep in the olfactory system of the honey bee.
- [25] HARRIS, C. R., MILLMAN, K. J., VAN DER WALT, S. J., GOMMERS, R., VIRTANEN, P., COURNAPEAU, D., WIESER, E., TAYLOR, J., BERG, S., SMITH, N. J., KERN, R., PICUS, M., HOYER, S., VAN KERWIJK, M. H., BRETT, M., HALDANE, A., DEL RÍO, J. F., WIEBE, M., PETERSON, P., GÉRARD-MARCHANT, P., SHEPPARD, K., REDDY, T., WECKESSER, W., ABBASI, H., GOHLKE, C., AND OLIPHANT, T. E. Array programming with NumPy. *Nature* 585, 7825 (Sept. 2020), 357–362.
- [26] HOBSON, J. A., AND PACE-SCHOTT, E. F. The cognitive neuroscience of sleep: neuronal systems, consciousness and learning. *Nature Reviews Neuroscience* 3, 9 (Sept. 2002), 679–693.
- [27] HUNTER, J. D. Matplotlib: A 2d graphics environment. *Computing in Science & Engineering* 9, 3 (2007), 90–95.
- [28] HUSSAINI, S. A., BOGUSCH, L., LANDGRAF, T., AND MENZEL, R. Sleep deprivation affects extinction but not acquisition memory in honeybees. *Learning & Memory* 16, 11 (Oct. 2009), 698–705.
- [29] KAISER, W., AND STEINER-KAISER, J. Neuronal correlates of sleep, wakefulness and arousal in a diurnal insect. *Nature* 301, 5902 (Feb. 1983), 707–709.
- [30] KELL, A. J., YAMINS, D. L., SHOOK, E. N., NORMAN-HAIGNERE, S. V., AND McDERMOTT, J. H. A task-optimized neural network replicates human auditory behavior, predicts brain responses, and reveals a cortical processing hierarchy. *Neuron* 98, 3 (May 2018), 630–644.e16.
- [31] KINTALI, S. Betweenness centrality : Algorithms and lower bounds, 2008.
- [32] KLEIN, B. A., KLEIN, A., WRAY, M. K., MUELLER, U. G., AND SEELEY, T. D. Sleep deprivation impairs precision of waggle dance signaling in honey bees. *Proceedings of the National Academy of Sciences* 107, 52 (Dec. 2010), 22705–22709.

## CHAPTER 7. BIBLIOGRAPHY

- 
- [33] LAZAR, A. A., LIU, T., AND YEH, C.-H. The functional logic of odor information processing in the drosophila antennal lobe. *PLOS Computational Biology* 19, 4 (Apr. 2023), e1011043.
  - [34] MALCOLM, K., AND CASCO-RODRIGUEZ, J. A comprehensive review of spiking neural networks: Interpretation, optimization, efficiency, and best practices.
  - [35] MARCHETTI, L., PRIAMI, C., AND THANH, V. H. *Simulation Algorithms for Computational Systems Biology*. Springer International Publishing, 2017.
  - [36] MATLAB. *version 9.13.0 (R2022b)*. The MathWorks Inc., Natick, Massachusetts, 2022.
  - [37] MEREL, J., BOTVINICK, M., AND WAYNE, G. Hierarchical motor control in mammals and machines. *Nature Communications* 10, 1 (Dec. 2019).
  - [38] MERKEL, D. Docker: lightweight linux containers for consistent development and deployment. *Linux journal* 2014, 239 (2014), 2.
  - [39] NOWOTNY, T., STIERLE, J. S., GALIZIA, C. G., AND SZYSZKA, P. Data-driven honeybee antennal lobe model suggests how stimulus-onset asynchrony can aid odour segregation. *Brain Research* 1536 (Nov. 2013), 119–134.
  - [40] NVIDIA, VINGELMANN, P., AND FITZEK, F. H. Cuda, release: 10.2.89, 2020.
  - [41] PANDAS DEVELOPMENT TEAM, T. pandas-dev/pandas: Pandas, Feb. 2020.
  - [42] PAOLI, M., AND GALIZIA, G. C. Olfactory coding in honeybees. *Cell and Tissue Research* 383, 1 (Jan. 2021), 35–58.
  - [43] PERICH, M. G., ARLT, C., SOARES, S., YOUNG, M. E., MOSHER, C. P., MINXHA, J., CARTER, E., RUTISHAUSER, U., RUDEBECK, P. H., HARVEY, C. D., AND RAJAN, K. Inferring brain-wide interactions using data-constrained recurrent neural network models.
  - [44] POE, G. R., WALSH, C. M., AND BJORNES, T. E. Cognitive neuroscience of sleep. In *Progress in Brain Research*. Elsevier, 2010, pp. 1–19.
  - [45] ROZENBERG, M. J., SCHNEEGANS, O., AND STOLIAR, P. An ultra-compact leaky-integrate-and-fire model for building spiking neural networks. *Scientific Reports* 9, 1 (July 2019).
  - [46] SANDAMIRSKAYA, Y., KABOLI, M., CONRADT, J., AND CELIKEL, T. Neuromorphic computing hardware and neural architectures for robotics. *Science Robotics* 7, 67 (June 2022).
  - [47] SAUER, S., KINKELIN, M., HERRMANN, E., AND KAISER, W. The dynamics of sleep-like behaviour in honey bees. *Journal of Comparative Physiology A: Sensory, Neural, and Behavioral Physiology* 189, 8 (Aug. 2003), 599–607.
  - [48] SCARANO, F., SURESH, M. D., TIRABOSCHI, E., CABIROL, A., NOUVIAN, M., NOWOTNY, T., AND HAASE, A. Geosmin suppresses defensive behaviour and elicits unusual neural responses in honey bees. *Scientific Reports* 13, 1 (Mar. 2023).
  - [49] SCHÖLZEL, C. Nonlinear measures for dynamical systems, 2019.
  - [50] SIEGEL, J. M. Sleep viewed as a state of adaptive inactivity. *Nature Reviews Neuroscience* 10, 10 (Aug. 2009), 747–753.
  - [51] STERRATT, D. C. Q10: The effect of temperature on ion channel kinetics. In *Encyclopedia of Computational Neuroscience*. Springer New York, 2014, pp. 1–3.

- 
- [52] TAKATA, Y., OISHI, Y., ZHOU, X.-Z., HASEGAWA, E., TAKAHASHI, K., CHERASSE, Y., SAKURAI, T., AND LAZARUS, M. Sleep and wakefulness are controlled by ventral medial midbrain/pons GABAergic neurons in mice. *The Journal of Neuroscience* 38, 47 (Oct. 2018), 10080–10092.
- [53] TIMOFEEV, I., BAZHENOV, M., SEIGNEUR, J., AND SEJNOWSKI, T. Neuronal synchronization and thalamocortical rhythms in sleep, wake and epilepsy.
- [54] VIRTANEN, P., GOMMERS, R., OLIPHANT, T. E., HABERLAND, M., REDDY, T., COURNAPEAU, D., BUROVSKI, E., PETERSON, P., WECKESSER, W., BRIGHT, J., VAN DER WALT, S. J., BRETT, M., WILSON, J., MILLMAN, K. J., MAYOROV, N., NELSON, A. R. J., JONES, E., KERN, R., LARSON, E., CAREY, C. J., POLAT, İ., FENG, Y., MOORE, E. W., VANDERPLAS, J., LAXALDE, D., PERKTOLD, J., CIMRMAN, R., HENRIKSEN, I., QUINTERO, E. A., HARRIS, C. R., ARCHIBALD, A. M., RIBEIRO, A. H., PEDREGOSA, F., VAN MULBREGT, P., AND SCIPY 1.0 CONTRIBUTORS. SciPy 1.0: Fundamental Algorithms for Scientific Computing in Python. *Nature Methods* 17 (2020), 261–272.
- [55] VOORHEES, E. M. Implementing agglomerative hierachic clustering algorithms for use in document retrieval. *Information Processing & Management* 22, 6 (Jan. 1986), 465–476.
- [56] WANG, X., LIN, X., AND DANG, X. Supervised learning in spiking neural networks: A review of algorithms and evaluations. *Neural Networks* 125 (May 2020), 258–280.
- [57] WANG, X., LIN, X., AND DANG, X. Supervised learning in spiking neural networks: A review of algorithms and evaluations. *Neural Networks* 125 (May 2020), 258–280.
- [58] WASKOM, M. L. seaborn: statistical data visualization. *Journal of Open Source Software* 6, 60 (2021), 3021.
- [59] WHITTINGTON, J. C., MULLER, T. H., MARK, S., CHEN, G., BARRY, C., BURGESS, N., AND BEHRENS, T. E. The tolman-eichenbaum machine: Unifying space and relational memory through generalisation in the hippocampal formation.
- [60] WU, K., AND LU, W. GABAergic synaptic transmission and plasticity oscillate across sleep and wake. *Neural Regeneration Research* 18, 12 (Apr. 2023), 2647–2648.
- [61] XIANG, T., LIAO, J., CAI, Y., FAN, M., LI, C., ZHANG, X., LI, H., CHEN, Y., AND PAN, J. Impairment of GABA inhibition in insomnia disorders: Evidence from the peripheral blood system. *Frontiers in Psychiatry* 14 (Feb. 2023).
- [62] YAMAZAKI, K., Vo-Ho, V.-K., BULSARA, D., AND LE, N. Spiking neural networks and their applications: A review. *Brain Sciences* 12, 7 (June 2022), 863.
- [63] YAMINS, D. L. K., AND DiCARLO, J. J. Using goal-driven deep learning models to understand sensory cortex. *Nature Neuroscience* 19, 3 (Feb. 2016), 356–365.
- [64] ZWAKA, H., BARTELS, R., GORA, J., FRANCK, V., CULO, A., GöTSCH, M., AND MENZEL, R. Context odor presentation during sleep enhances memory in honeybees. *Current Biology* 25, 21 (Nov. 2015), 2869–2874.